Review Article

Sterilization/disinfection of medical devices using plasma: the flowing afterglow of the reduced-pressure N₂-O₂ discharge as the inactivating medium

Michel Moisan[1,a], Karim Boudam[1], Denis Carignan[1], Danielle Kéroack[1], Pierre Levif[1], Jean Barbeau[2], Jacynthe Séguin[2], Kinga Kutasi[3], Benaïssa Elmoualij[4], Olivier Thellin[4], and Willy Zorzi[4]

[1] Groupe de Physique des Plasmas, Université de Montréal, Montréal, Québec, Canada
[2] Laboratoire de Microbiologie et d'Immunologie, Faculté de Médecine Dentaire, Université de Montréal, Montréal, Québec, Canada
[3] Institute for Solid State Physics and Optics, Wigner Research Centre for Physics, Hungarian Academy of Sciences, Budapest, Hungary
[4] Centre de Recherche sur les Protéines Prions (CRPP), Service d'Histologie Humaine, Université de Liège, Liège, Belgium

Abstract. Potential sterilization/disinfection of medical devices (MDs) is investigated using a specific plasma process developed at the Université de Montréal over the last decade. The inactivating medium of the microorganisms is the flowing afterglow of a reduced-pressure N₂-O₂ discharge, which provides, as the main biocidal agent, photons over a broad ultraviolet (UV) wavelength range. The flowing afterglow is considered less damaging to MDs than the discharge itself. Working at gas pressures in the 400–700 Pa range (a few torr) ensures, through species diffusion, the uniform filling of large volume chambers with the species outflowing from the discharge, possibly allowing batch processing within them. As a rule, bacterial endospores are used as bio-indicators (BI) to validate sterilization processes. Under the present operating conditions, *Bacillus atrophaeus* is found to be the most resistant one and is therefore utilized as BI. The current paper reviews the main experimental results concerning the operation and characterization of this sterilizer/disinfector, updating and completing some of our previously published papers. It uses modeling results as guidelines, which are particularly useful when the corresponding experimental data are not (yet) available, hopefully leading to more insight into this plasma afterglow system. The species flowing out of the N₂-O₂ discharge can be divided into two groups, depending on the time elapsed after they left the discharge zone as they move toward the chamber, namely the early afterglow and the late afterglow. The early flowing afterglow from a pure N₂ discharge (also called pink afterglow) is known to be comprised of N_2^+ and N_4^+ ions. In the present N₂-O₂ mixture discharge, NO^+ ions are additionally generated, with a lifetime that extends over a longer period than that of the nitrogen molecular ions. We shall suppose that the disappearance of the NO^+ ions marks the end of the early afterglow regime, thereby stressing our intent to work in an ion-free process chamber to minimize damage to MDs. Therefore, operating conditions should be set such that the sterilizer/disinfector chamber is predominantly filled by N and O atoms, possibly together with long-lived metastable-state $O_2(^1\Delta_g)$ (singlet-delta) molecules. Various aspects related to the observed survival curves are examined: the actual existence of two "phases" in the inactivation rate, the notion of UV irradiation dose (fluence) and its implications, the UV photon best wavelength range in terms of inactivation efficiency, the influence of substrate temperature and the reduction of UV intensity through surface recombination of N and O atoms on the object/packaging being processed. To preserve their on-shelf sterility, MDs are sealed/wrapped in packaging material. Porous packaging materials utilized in conventional sterilization systems (where MDs are packaged before being subjected to sterilization) were tested and found inadequate for the N₂-O₂ afterglow system in contrast to a (non-porous) polyolefin polymer. Because the latter is non-porous, its corresponding pouch must be kept unsealed until the end of the process. Even though it is unsealed, but because the opening is very small,

[a] e-mail: michel.moisan@umontreal.ca

the $O_2(^1\Delta_g)$ metastable-state molecules are expected to be strongly quenched by the pouch material as they try to enter it and, as a result, only N and O atoms, together with UV photons, are significantly present within it. Therefore, by examining a given process under pouch and no-pouch conditions, it is possible to determine what are the inactivating agents operating: (i) when packaged, these are predominantly UV photons, (ii) when unpackaged, $O_2(^1\Delta_g)$ molecules together with UV photons can be acting, (iii) comparing the inactivation efficiency under both packaged and unpackaged conditions allows the determination of the relative contribution of UV photons (if any) and $O_2(^1\Delta_g)$ metastable-state molecules. Such a method is applied to pyrogenic molecules and to the enzymatic activity of lysozyme proteins once exposed to the N_2-O_2 flowing afterglow. Finally, the activity of the infectious prion protein is shown to be reduced when exposed to the present flowing afterglow, as demonstrated by both in vitro and in vivo experiments.

1 Introduction

1.1 Sterility/disinfection and available conventional methods

Sterilization is the complete and definitive inactivation of all forms of life. The accepted international standard for processes claiming "sterility" is a 6-$\log_{10}$ reduction in bacterial endospores (*Bacillus atrophaeus* (*subtilis*) or *Geobacillus stearothermophilus*), the most resistant form of microorganisms. This criterion is known as the safety assurance level (SAL). It relates to the probability of finding a single medical device (MD) being non-sterile in a batch of 1 million similar devices subjected to the sterilization process. High-level disinfection is less demanding, implying the complete inactivation of all microorganisms with the exception of bacterial endospores. The food and drug administration (FDA, USA) definition of high-level disinfection is a sterilant (an agent able to inactivate spores) used for a shorter contact time to achieve a 6-$\log_{10}$ kill of an appropriate *Mycobacterium* species. Cleaning followed by high-level disinfection should eliminate enough pathogens to prevent transmission of infection [1]. While SAL is required for critical use, i.e. for MDs in direct contact with blood vessels or sterile tissues, for instance a scalpel, high-level disinfection is considered satisfactory for semi-critical use such as contact of the MD with mucous membranes, for example as is the case for endoscopes (Spaulding's classification 1968 [2]).

The inactivation of a microorganism signifies its definitive inability to replicate. Inactivation must be distinguished from dormancy or growth inhibition. Bacteria in their sporulated form[1] are in a state of dormancy, meaning that under favorable conditions, they can revert to their vegetative state (through germination) and start replicating again. Growth inhibition exists when the microorganisms appear inactivated but are actually inhibited in their growth by an agent (of chemical/physical nature), while they can resume proliferation whenever the antimicrobial stimulus is removed or the damage repaired.

The action of sterilization/disinfection involves damaging the microorganisms to the point that they become irreversibly inactivated: this can be achieved, generally speaking, in three ways, namely through:

(i) Intense heat (>120 °C). Until now, the most effective and accepted method of this kind relies on moist heat (autoclaving). It leads to the destruction of key molecules and structures involved in metabolism (e.g., enzymes, RNA), replication (DNA) and preservation of integrity (proteins, lipids) of the microorganism, but at the same time can severely damage thermosensitive polymer-based MDs affecting, for example, their mechanical properties and appearance. It may also create oxidative damage to simple items such as surgical scissors. It has been a general regulatory recommendation that autoclaving be used whenever it is possible for critical items, preferentially to all other methods. Typical processing time is less than an hour, excluding loading, unloading and heating/cooling.

(ii) Chemical action, using molecules such as ozone, ethylene oxide, glutaraldehyde or hydrogen peroxide. For improved efficiency, chemical sterilization is better achieved at temperatures higher than ambient but typically below 65 °C in order to be considered as a low-temperature process (chemiclaves are an exception, which operate above 100 °C). Drawbacks to chemical methods are their long processing times: up to 4 h with ozone and 10 h with glutaraldehyde while, with chemicals that impregnate MD materials such as those exposed to ethylene oxide, long ventilation periods are required before they can be utilized.[2]

(iii) Ionizing and molecular-damaging irradiation, respectively gamma and UV photons. Such processes can be conducted at, or close to, ambient temperature. This approach, in contrast to the two previously mentioned methods, aims at creating lesions in the DNA of microorganisms yielding, as a rule, little apparent morphological damage to spores. Nonetheless, some polymers are adversely affected by gamma rays and vacuum UV (VUV) (10–180 nm) photons, to a lesser extent by UV (180–400 nm) photons. The action of UV photons, in contrast to that of gamma rays, is hindered by their limited penetration depth in matter. UV photons supplied by *germicidal* lamps are used in

---

[1] Vegetative bacteria (i.e., capable of undergoing replication) of the *Bacillus* and *Clostridium* types can transform into spores whenever they feel "stressed" as a result, for instance, of too high an ambient temperature, excessive dryness and lack of nutrients. At the end of the sporulation process, there remain only the bacterial DNA (genetic material) and some proteins, surrounded by "coats" protecting it from heat, radiation and chemicals.

[2] Two processing temperatures are commonly used with ethylene oxide: 37 °C, which requires a 3 h exposure, or 55 °C with only 1 h exposure time, followed by 20 and 12 h vent times, respectively.

some disinfection processes, but not for sterilization purposes: this is because irradiation with a lamp ensures only a limited access of photons to the microorganisms since they are emitted at a given fixed angle from the lamp, providing line-of-sight radiation. As a result, such UV photons cannot fully sweep the interior of crevices or reach some parts of morphologically complex objects. This situation can be avoided with gaseous plasmas as long as the species, bound to emit photons, have time to diffuse throughout complex objects and crevices before they come into the excited state from which a photon is released.

All the above methods can achieve sterility provided conditions as well as contact times between spores and the biocidal agent are adequate, but they can also be used to decontaminate or disinfect items of all sorts. As already indicated, disinfection is less exacting than sterilization and it actually uses a larger variety of chemicals, such as alcohols, chlorine, phenolics or quaternary ammoniums. In contrast, quaternary ammoniums can achieve low-level disinfection in 10 min but are unable to sterilize, no matter how long is the contact time.

In summary, appraising a given sterilization/disinfection technique requires considering its inactivation efficiency with respect to the type and level of damage it induces into materials, which determines the more or less rapid renewal of the MDs at use. Processing time is also of economical concern: the quicker the process, the greater the usage rotation of the MDs.

1.2 Bio-burden, infectious prions and pyrogens

The preceding paragraph considered microorganisms while assuming implicitly that they stand alone: Figure 1a shows that, in fact, they can be aggregated and stacked. Furthermore, in actual life, these microorganisms can be embedded in a bio-burden (bio-products), as in Figure 1b (which originates, for example, from coagulated blood), thereby reducing or even preventing their contact with the biocidal agents. Some bio-products, including proteins[3] and various organic molecules, can furthermore have an infectious or pyrogenic action: this is the case, respectively, of the Creutzfeldt-Jakob pathogenic prion proteins and of some pyrogenic molecules, the latter stemming mostly from the membranes of Gram-negative and Gram-positive bacteria.[4] The bottom line is that: (i) bio-products, in principle, should not be found on MDs once the latter have gone through an appropriate cleaning procedure (e.g., agitation, brushing, washing and sonicating, followed by visual inspection) prior to their submission to the sterilization process; (ii) nonetheless, low-level infectious loads can

---

[3] Strictly speaking it should not be said that proteins are inactivated but rather denatured (loss of three-dimensional structure without rupture of covalent bonds) or damaged (rupture of covalent bonds), which implies, for instance, a reduction/loss of their enzymatic properties.

[4] Gram-positive and Gram-negative bacteria have similar internal, but very different external structures (membranes).
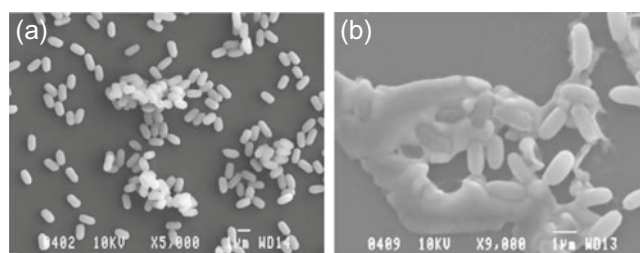

Fig. 1. Scanning electron microscopy (SEM) images of: (a) "clean" isolated as well as stacked spores [3]; (b) spores embedded in a bio-product [4].

still remain after the cleaning and subsequent sterilization procedures, the action of which on people depends on the intended use of the MDs, namely critical or semi-critical as previously defined.

The paper is structured as follows: in the coming Section 2, we consider the use of plasma as an alternative to conventional sterilization/disinfection methods, which includes its possible biocidal agents and operating conditions. Then, in Section 3, we examine how UV radiation is generated in the flowing afterglow of the N_2-O_2 discharge and show the corresponding spectral domain over which its efficiency is the greatest for inactivating, for instance, *Bacillus atrophaeus* spores. Further on, Section 4 describes the experimental arrangement for achieving and diagnosing the N_2-O_2 discharge flowing afterglow together with the optimization of its operating conditions, followed by the microbiology protocols used in the various assays. Next comes Section 5 presenting the results characterizing the N_2-O_2 flowing afterglow operation when used specifically for inactivating bacterial endospores: corresponding survival curves, damage to materials and spores, influence of heat on their inactivation rate, surface recombination of N and O atoms on various materials because of the ensuing reduction in intensity of the UV emission and, last, the behavior of some packaging materials in the flowing afterglow and the election of a pouch material withstanding its action. Section 6 shows that the activity of pyrogenic molecules can be reduced by the N_2-O_2 flowing afterglow system; it also illustrates the possibility of using it to decrease, even eliminate, the enzymatic properties of proteins as well as to inactivate infectious prion proteins. Finally, Section 7 comprises a commented summary of the paper and some perspectives.

2 The use of plasma as an alternative to conventional methods of sterilization/disinfection

Gaseous "cold plasma" sterilization is emerging as an ideal replacement solution to low-temperature chemical sterilization techniques because, in contrast, its biocidal agent(s), depending on the discharge gas(es) used for producing plasma, can be non-polluting, non-toxic and not requiring aeration of the treated objects once processed [5].

2.1 Nature of the biocidal agents possibly provided by plasma and their mode of action

Plasma biocidal agents are essentially of two kinds:

(i) Chemically reactive radicals (e.g., O, OH), with or without the assistance of ions, and metastable-state atoms and molecules. Chemically active species operate by inflicting more or less severe structural damage affecting vital metabolic functions of the microorganisms, mostly through erosion (etching);

(ii) UV photons, which in the end induce irreversible lesions on the genetic material (DNA, RNA), with little or no apparent damage to the morphology of the bacterial spores used as biological indicators.

The respective contribution of these biocidal agents depends on the plasma operating conditions.

Bacterial endospores as biological indicators (BI). Bacterial endospores are considered the most resistant form of microorganisms, implying that their successful inactivation ensures that lesser resistant microorganisms, such as vegetative bacteria, molds and viruses, would all be easily inactivated. A spore is comprised of a central core containing the DNA double-helix, i.e. the genetic material, surrounded by protective coats; as mentioned, spores are in a state of dormancy, waiting for a possible "external signal" (referred to as germinants) to inform them that the environment has become favorable for their germination (i.e., that nutrients are available, temperature and humidity are satisfactory) and transform into vegetative bacteria, which can replicate, divide, grow. *Bacillus* (genus) *atrophaeus* (species) and *Geobacillus stearothermophilus* both being non-pathogenic endospores, are generally used as BI. Under our operating conditions, *B. atrophaeus* ATCC® 9372 was found to be the most resistant spore (Sect. 5.1.5).

2.2 Achievable operating conditions for a plasma sterilizer/disinfector

Direct or indirect (remote) exposure of MDs to plasma species. There are two main ways of putting plasma to work for sterilization/disinfection purposes:

Direct contact with the discharge plasma.[5] In this case, the MDs are either located between the electrodes producing the gas discharge or in the vessel within which the discharge (plasma) is being sustained (by a microwave field, for example) or, alternatively, subjected to the flame of a plasma torch.

Remote discharge plasma. Owing to a high flow rate of the discharge gas, the species from the discharge zone outflow into a remotely located region, the afterglow chamber

Fig. 2. "Artist's view" representation of the discharge flow of the long-lived species as they enter the sterilization/disinfection chamber after traveling a distance x_d from the microwave plasma source. This figure illustrates the case where x_d is relatively short (see text for detail).

(see Fig. 2 for a schematic representation of the system). This outflow is termed the *discharge flowing afterglow.* Relative to the species composition of the discharge, in the flowing afterglow there are fewer electrons and charged particles. Some of the neutral particles are chemically reactive radicals (e.g., O, OH depending on the discharge gas composition) and some others are possibly in a metastable state (a reservoir of energy for contributing to chemical reactions). All these species have a limited lifetime, which extends from a few to some tens of ms.

As a rule, the inactivation rate of microorganisms is much faster when MDs are in direct contact with the plasma (a few seconds to a few minutes for a 4–6 $\log_{10}$ reduction) than in the afterglow (30–60 min). When under direct-contact exposure, the gas temperature of the discharge can be lowered by pulsing it sufficiently (adequate on/off time) to minimize thermal damage to MDs.

2.2.1 Reduced pressure (typically below 1000 Pa ($\approx$8 torr)) or atmospheric pressure operation

Reduced pressure. The main advantage of working at low enough pressures over atmospheric pressure is to achieve, through particle diffusion [7], a more uniform plasma, hence a more similar processing of MDs within the whole chamber, and a lower gas temperature (creating less damage to MDs) than with some atmospheric pressure systems.

Atmospheric pressure.[6] A faster inactivation rate than at reduced pressure is obtained. However, as a rule, such discharges are more or less in an open configuration,[7] making the achievement (and upholding) of sterility more difficult than in a closed chamber, where it is preserved until

---

[5] The inactivation of endospores deposited on Petri dishes, dried and subsequently located within the discharge area itself (at 100 Pa ($\approx$0.8 torr) in argon) has also been examined by our team [6]. Noteworthy is that some viable spores were detached and released from their substrate, contaminating the processing chamber, a situation which does not occur with our flowing afterglow system.
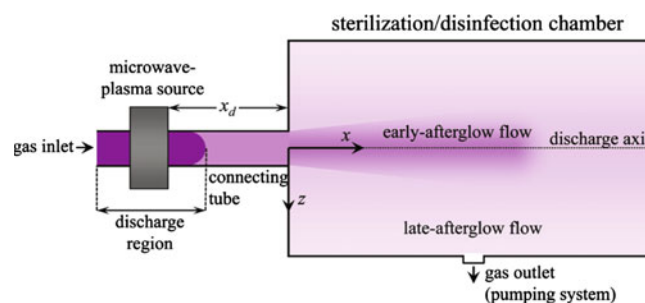
[6] Our team has obtained efficient survival curves for *B. subtilis* (renamed *atrophaeus*) endospores when put in direct contact with a N_2-N_2O uniform dielectric-barrier-discharge (DBD) at atmospheric pressure operated under maximum UV intensity conditions as obtained by tuning the concentration of N_2O in the N_2-N_2O mixture [8].

[7] An exception to this is with containment isolators or with systems with transfer ports.

it is opened. Nonetheless, it can provide high-level disinfection of practical interest (namely a reduction of 4–5 logs in the initial number of microorganisms) following a relatively short contact time, which minimizes damage to the treated objects: under such conditions, plasma-torch systems are worth considering since they allow devices to be processed rapidly by conveying them in front of the flame. A review of the various aspects of the reduced pressure and atmospheric pressure approaches can be found in [9] and [10], respectively.

2.3 Our strategic choice in designing an efficient plasma sterilizer/disinfector

To minimize damage to MDs during microorganism inactivation, it seems a priori better to rely on UV photons as the working biocidal agent rather than on chemically reactive species and ions: UV photons specifically act on the genetic material, eventually creating enough lesions on the DNA strands such that repair becomes impossible and, as already mentioned, leave the spore morphology, at first sight, unaffected. Such a feature suggests that damage to MDs should also be less than with chemical agents and/or chemically assisted etching (e.g., ions synergistically acting with O atoms), which heavily erode the spores when not completely destroying them. Then, since damage to material by UV photons is expected to be low, the question arises as to their ability to nonetheless denature proteins and pyrogenic molecules.

Sterilizing/disinfecting MDs in a batch process implies resorting to a sterilizer/disinfector vessel large enough to accommodate many (different) MDs and, further, ensuring that the biocidal agent(s) is (are) uniformly distributed within it: this last requirement is more easily attained with our technique when operating at low enough gas pressures, so as to benefit from diffusion, throughout the chamber of the species generating the UV photons.

UV radiation results in the present case from NO excited molecules stemming from the "collision", in the afterglow chamber, of N and O atoms, these atoms being supplied by the dissociation of N_2 and O_2 molecules in the discharge itself (Sect. 3.2).[8] UV intensity can be maximized by fine-tuning the amount of O_2 (<1%) added to N_2, the latter being the carrier (main) gas.

The current article reviews the work and publications mostly realized at the Université de Montréal, over a period of more than 12 years, in the quest for a low-temperature, low-damage and non-toxic plasma sterilizer/disinfector. Noteworthy is the contribution from the CRPP Liège laboratory (Belgium) concerning the infectious prion proteins. We believe that the work that we are reporting is by far more explanatory on many basic topics than what can be found in the literature for conventional sterilization systems. A final note is that this study, initiated by and mainly driven by physicists, but clearly with the essential assistance of microbiologists, emphasizes the importance of interdisciplinary collaboration in the present project.

3 Particle composition of the N₂-O₂ discharge flowing afterglow and wavelength range of the UV photons emitted with respect to the inactivation efficiency of bacterial endospores

3.1 The species present in the early afterglow and in the late afterglow

Figure 2 is an "artist's view" representation of the incoming flow from the discharge as it enters the sterilization/disinfection chamber. The species present in the chamber are termed long-lived species by contrast with the particles generated in the discharge that do not reach it.

As the gaseous outflow from the discharge moves toward the sterilization/disinfection chamber, its composition considerably changes since it actually varies with time. Figure 3 displays the calculated evolution of the species density in the afterglow flow as a function of the time elapsed after they flowed out of the discharge. Figure 3a shows the density variation of N_2^+, N_4^+ and NO^+ ions together with that of the O_2 ($^1\Delta_g$), $N_2(A)$ and $N_2(a')$ metastable-state molecules. The disappearance of the NO^+ ions, which live longer than N_2^+ and N_4^+ ions, is considered herein as the end of the early afterglow while the subsequent afterglow is referred to as the late afterglow. Figure 3b shows the time evolution of the (ground-state) densities of O and N atoms, indicating that these vary little with time up to 10 ms, their density starting to decrease significantly beyond 100 ms [12].

Figure 2 schematizes the situation where the distance x_d from the plasma source to the chamber entrance is not long enough (corresponding to an elapsed time <10 ms in Fig. 3) to ensure that only late afterglow species are present throughout the chamber. The early afterglow species coming in into the chamber in this case are represented as a slightly divergent cylindrical beam that dies out within the chamber, as functions of the axial distance x from the chamber entrance and distance z from the discharge axis down the chamber [12]. The late afterglow dominates outside this beam flow. This analysis is supported by the fact that polymer microspheres are strongly eroded in the beam region, but much less outside it (Sect. 5.2.1). In contrast, with long enough x_d distances, the chamber should be mostly filled with N and O atoms accompanied by $O_2(^1\Delta_g)$ metastable-state molecules [12].

Calculations indeed indicate (Fig. 3) that, among the metastable-state molecules present in the afterglow, it is the $O_2(^1\Delta_g)$ singlet species that survives longer because its quenching is much less efficient than that of $N_2(A)$. On the other hand, since in the late afterglow the $N_2(A)$ molecule (as well as the $N_2(a')$ one) has no creation source, this species is bound to decrease within the chamber

---

[8] An exhaustive review of the papers reporting the use, for sterilization purposes, of VUV/UV radiation stemming either from the gas discharge or from its afterglow can be found in [11].
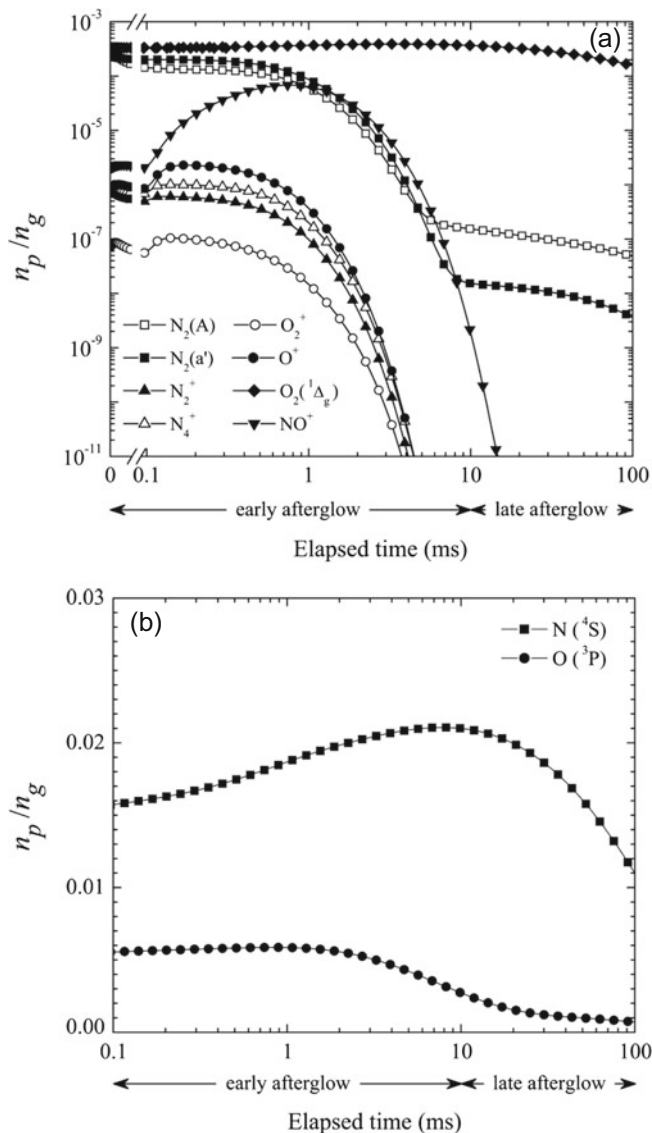
Fig. 3. Calculated time evolution of the particle densities (relative to the initial total gas density) of the different species after their outflow from the N_2-O_2 discharge (0.3% added O_2 to N_2) in a 28 mm diameter tube connecting to the afterglow chamber (at a 5 torr pressure ($\approx$670 Pa)): (a) relative densities of NO^+, N_2^+ and N_4^+ ions, and $N_2(A)$, $N_2(a')$ and $O_2(^1\Delta_g)$ metastable-state molecules; (b) relative densities of N and O atoms in their ground state (calculations after [12]).

(due to quenching in the gas phase: not accounted for in Fig. 3) while, in contrast, the singlet species can still be generated everywhere in the late afterglow through the (exothermal) three-body re-association reaction:

$$O(^3P) + O(^3P) + O_2 \rightarrow O_2(^1\Delta_g) + O_2, \qquad (1)$$
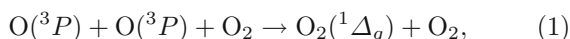
which ensures that its concentration remains high in the late afterglow.

The interaction, within the afterglow chamber volume, of N and O atoms (in the presence of N_2 when required as a 3rd-body, Sect. 3.5) leads to the formation of NO* excited molecules, which immediately emit UV photons.

An important remark at this point is that many of our experiments have been achieved with small x_d values ($x_d \simeq 200$ mm), such that the region close to the chamber axis ($z \approx 0$) comprises early afterglow species, whereas Petri dishes lying on the bottom of the chamber are subjected mostly to late afterglow species. It is only quite recently that experiments were conducted under conditions such that $x_d = 820$ mm, for which only late afterglow species are assumed to be present throughout the whole chamber volume.

3.2 Coverage of the UV spectral domain provided by the NO molecular systems

In the N_2-O_2 discharge flowing afterglows at reduced pressure, there are various NO molecular systems that can emit photons. The most commonly observed ones under our operating conditions are the NO_β ($B^2\Pi$-X) and NO_γ ($A^2\Sigma^+$-X) systems, where the parentheses indicate the upper and lower electronic energy levels of the radiative transition, X being the ground state. Figure 4 shows the spectral intensity of the NO_β and NO_γ emissions in the 200–400 nm range with identification of their main band heads as a function of wavelength: interestingly, these band heads ensure a rather uniform spectral coverage (with almost equal spacing) over the 180–380 nm domain. The emission spectrum recorded below 200 nm with a VUV spectrophotometer under similar operating conditions (see Fig. 6) shows two (neutral) N lines (149.0 and 174.3 nm)
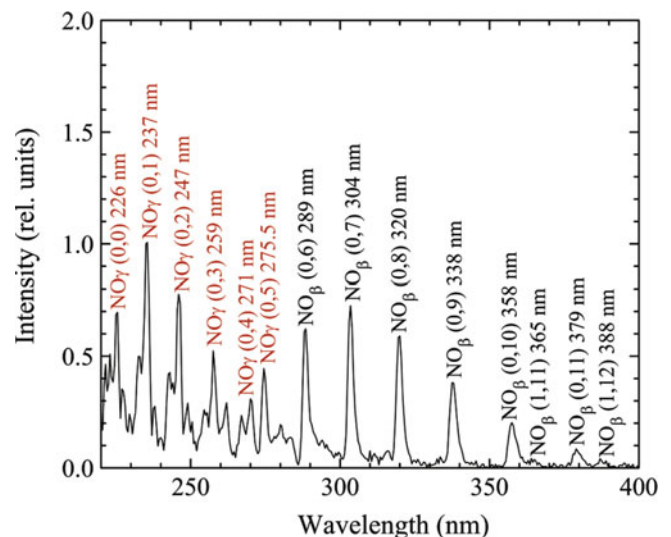

Fig. 4. Emission intensity recorded in the 200–400 nm spectral range from the flowing afterglow of the N_2-O_2 discharge sustained at 2450 MHz with 0.21% O_2 in the N_2-O_2 gas mixture and a 5 torr ($\approx$670 Pa) pressure in the 5.5 L chamber (Fig. 9): these operating conditions provide maximum intensity of the NO_γ molecular system. The lowest wavelength from the NO_β molecular system, in the present case, is at 289 nm. The number in parentheses refers to the transition upper and lower vibrational levels v' and v'', respectively, of the given molecular band.

and, with comparatively higher emission intensities, two band heads from the NO_δ molecular system (191 and 198 nm).

A broad and almost uniform spectral coverage such as the one observed as compared with a monochromatic emission (e.g., at 254 nm from the mercury (germicidal) lamp) increases the occurrence of different types of lesions, requiring different types of repair mechanisms. In that respect around 250 nm, the DNA of the bacterial spores is mainly affected by the generation of photoproducts, which can be eliminated during the germination process. In contrast, DNA simple and double strand breaks which occur at 250 nm and at wavelengths >290 nm necessitate different and more complex repair strategies,[9] as exemplified with solar radiation [15]. As will be shown in Section 5.1.6, the action spectra vary significantly among the three different types of *Bacillus* spores tested.

3.3 Inactivation efficiency of B. atrophaeus endospores by UV irradiation as a function of photon wavelength (action spectrum)

First, it has to be recalled that UV-induced inactivation of Bacillus endospores essentially results from DNA damage [16]. The inactivation efficiency of UV and VUV photons on a given type of spores depends upon its actual structure and composition. The action spectrum[10] of *B. atrophaeus* spores in the 50–300 nm range, reported in [17], is shown as an example in Figure 5. It has two domains of high inactivation efficiency, namely 100–180 nm and 210–290 nm, while photons with wavelengths above 300 nm, according to this plot, should have a much reduced effect on these spores.

Figure 6 shows that, for *B. atrophaeus* spores, the NO_γ (205–280 nm)[11] molecular system provides much more efficient UV photons than those due to the NO_β molecular system (289–380 nm). In contrast, *G. stearothermophilus* spores are found to respond to the lower-energy UV photons from the NO_β system (see Sect. 5.1.6 further on). An important feature of our inactivation technique is that the combined emission of the NO molecular systems offers an almost uniform spectral coverage over the 190–380 nm wavelength range, corresponding to the specific action spectrum of a large variety of microorganisms.

---

[9] The actual repair of a DNA strand is a function of the number of lesions inflicted and of the time needed for the repair process to be completed, which must be achieved before the replication process is over. Otherwise, when the DNA replication fork knocks on a dead end (a damage), the chemical injury results in biological death [13,14].

[10] The efficiency with which electromagnetic radiation produces a photochemical reaction plotted as a function of the wavelength of the radiation.

[11] At lower wavelengths, there is the NO_β molecular system with band heads at 191 and 198 nm having intensities comparable, for example, to that of the NO_γ band head at 205 nm. At atmospheric pressure, there is no NO_β emission, only that of the NO_γ molecular system [8].
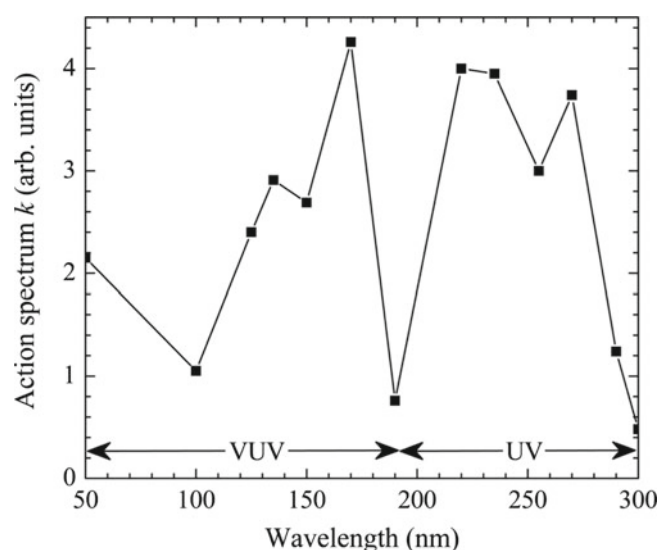

Fig. 5. Action spectrum of photons: relative inactivation and mutagenesis efficiency k from 50 to 300 nm of *Bacillus subtilis* spores as determined with synchrotron radiation (over 20 nm wide windows) emitted in vacuum [17].
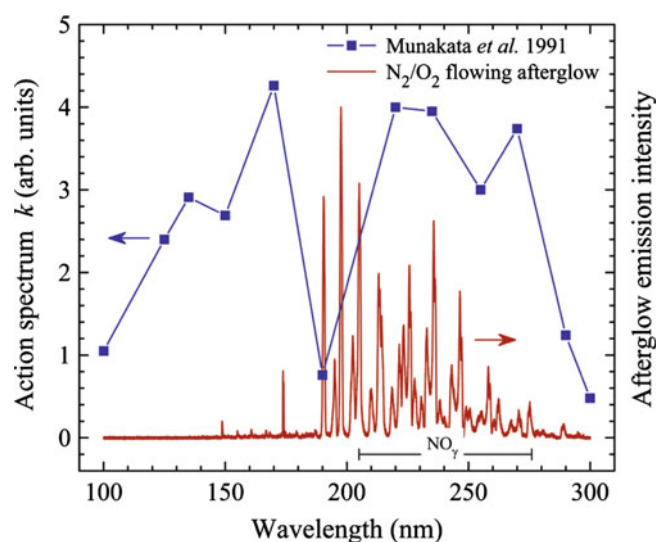

Fig. 6. The action spectrum of photons on *B. atrophaeus* spores presented in Figure 5 superposed on the emission intensity recorded with a vacuum UV (VUV) spectrophotometer in the 112–300 nm range, from the flowing afterglow of a 2450 MHz strip-line discharge [18] in a 1%O_2-N_2 mixture. Pressure in the chamber is set at 2 torr ($\approx$270 Pa) under a 0.5 standard liter per minute (sLm) N_2 gas flow. The emission spectrum (in red) comprises two (neutral) N lines (149.0 and 174.3 nm), two band heads from the NO_δ molecular system (191 and 198 nm) and essentially the NO_γ molecular system (205–280 nm). The emission intensities are not corrected for the spectral response of the spectrophotometer, which is optimized for operation over the 112 nm to 250 nm range.

When only photons above 330 nm are allowed to irradiate the spore deposit, the inactivation rate of the three types of Bacillus endospores tested is significantly less (Sect. 5.1.6).

3.4 Setting the gas pressure for maximum emission intensity from the NO$_\gamma$ molecular system

We just saw that we should be looking for a maximum of emission intensity from the NO$_\gamma$ system. The upcoming emission intensities were recorded perpendicularly to the chamber axis through the observation window with an optical fiber directed at the fused silica window, probing a 300 mm depth (width of the chamber). These data were corrected for the spectral response of the spectrophotometer (including the fiber) and the transmission of the fused silica window.
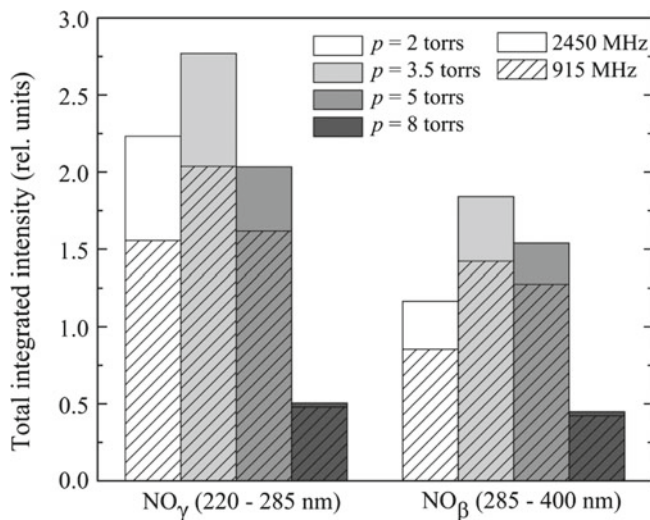
Figure 7 shows the relative emission intensity of the NO$_\beta$ and NO$_\gamma$ molecular systems, integrated over their respective wavelength range, at four different pressures and two microwave field frequencies with 200 W absorbed power in the 50 L afterglow chamber (Fig. 8) with $x_d =$ 820 mm. The N$_2$-O$_2$ gas mixture contains 0.21% O$_2$ (maximum UV intensity conditions) and the N$_2$ flow is 1.4 sLm. The integrated emission intensity of the NO$_\gamma$ system is higher than that of NO$_\beta$ at the three pressures considered, as predicted by calculations [12]. The UV intensity from both the NO$_\gamma$ and NO$_\beta$ systems goes through an absolute maximum at a pressure of 3.5 torr ($\approx$470 Pa) in the chamber at both 915 and 2450 MHz.

3.5 Kinetic pathways leading to the NO$_\gamma$ molecular-system emission

The transition from the upper energy level NO(A$^2\Sigma^+$) to the NO(X) ground energy level yields the NO$_\gamma$ molecular-

Fig. 7. Relative emission intensity of the NO$_\beta$ and NO$_\gamma$ molecular systems, integrated over their respective wavelength range, at four different operating pressures and two microwave field frequencies with 200 W absorbed power in the 50 L afterglow chamber (Fig. 8) with $x_d = 820$ mm. The N$_2$-O$_2$ gas mixture contains 0.21% O$_2$ (maximum UV intensity conditions) with a 1.4 sLm N$_2$ flow rate. The integrated emission intensities are corrected for the spectral response of the spectrophotometer and the transmission of the fused silica observation window.
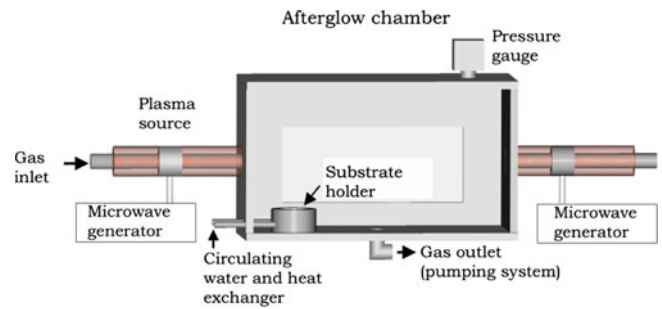

Fig. 8. Schematic view of one of our plasma sterilizer/disinfector units. Gas discharge is sustained by microwaves at 915 MHz (surfatron) or 2450 MHz (surfaguide) [23], either in a single discharge tube or simultaneously in two discharge tubes (x_d is set in the range 150–220 mm or exactly at 820 mm). The volume of this parallelipipedic enclosure is 50 L with inner dimensions 61 × 26 × 30 cm^3. The main frame is made from aluminum and the observation windows (for spectroscopy studies) are in fused silica. The inner diameter of the discharge/connecting tube is 25.5 mm. See text for further details.

system emission. It is observed in both the N$_2$-O$_2$ discharge and its flowing afterglow, in the torr range (150–700 Pa). It was assumed in previous publications [19] to have been created within both the discharge and afterglow, by the following kinetic route:

$$N_2(A^3\Sigma_u^+) + NO(X^2\Pi) \rightarrow NO(A^2\Sigma^+) + N_2(X). \quad (2)$$
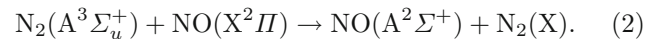
However, since the N$_2$(A) density decreases rapidly in the late afterglow (Sect. 3.1), there results a fast depletion of the density of the NO(A) level. Assuming this kinetic pathway only, the calculated emission intensity of the NO$_\gamma$ system in the late afterglow comes out two or three orders of magnitude lower (depending on the N$_2$-O$_2$ mixture composition) than that of the NO$_\beta$ system (see [20]). Experimentally however, the emission intensity from the NO$_\gamma$ system is significantly higher than that from the NO$_\beta$ system (Fig. 7). To cope with this discrepancy, Kutasi et al. [12] introduced another creation pathway for NO(A) (and for NO(B) also), a reaction formerly suggested in [21], namely:

$$N(^4S) + O(^3P) + (N_2) \rightarrow NO(A^2\Sigma^+) + (N_2), \quad (3)$$
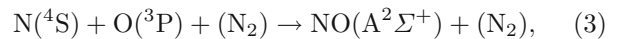
where the parentheses around N$_2$ indicate that it can either be a 2- (i.e., without the participation of N$_2$) or a 3-body reaction. The NO(A$^2\Sigma^+$) state in relation (3) can, in effect, be obtained through two different sets of intermediate reactions [21]. The first set starts with:

$$N(^4S) + O(^3P) \leftrightarrow NO(a^4\Pi) \leftrightarrow NO(C^2\Pi, v = 0), \quad (4)$$
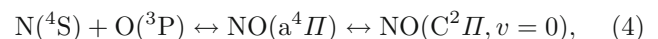
and is followed by an electronic (downward) transition due to quenching by N$_2$ molecules:

$$NO(C^2\Pi) + N_2 \rightarrow NO(A^2\Sigma^+) + N_2, \quad (5)$$
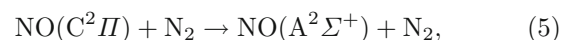
while the second set calls for cascade radiation from the NO(C$^2\Pi$) state (4), such that:

$$NO(C^2\Pi) \rightarrow NO(A^2\Sigma^+) + h\nu, \quad (6)$$
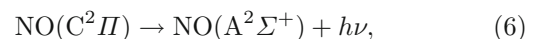
this second sequence (Eqs.(4) and (6)) constituting a two-body reaction. In summary: the creation of the NO(A) state in the discharge is predominantly due to reaction (2) while in the late afterglow, due to a reduced N_2(A) concentration, it is reaction (4), followed by either reaction (5) or reaction (6), which becomes the dominant source of NO(A).

The calculated corresponding probability that N and O atoms form NO excited molecules through collisions (reactions (4) and (5) as a three-body interaction) is a few times 10^{-10} (details in footnote[12]). This process is, in the end, efficient because of the relatively long lifetime of these atoms (beyond at least 2 ms for O atoms and more than 100 ms for N atoms, as shown in Fig. 3b). These long-lived N and O atoms can therefore diffuse, for example, into holes and crevices before ending in the $NO(A^2\Sigma^+)$ state, which immediately afterwards, generates a photon (see further in Fig. 25). In this way, the whole surface of complex-form objects is, finally, subjected to UV irradiation. This is not the case when using UV lamps since their photons travel unidirectionally (Sect. 1.1).

4 Experimental arrangement and operating conditions of the sterilizer/disinfector

4.1 The N_2-O_2 discharge flowing afterglow system, a remote-plasma sterilizer/disinfector

Figure 8 is a schematic representation of one of our sterilizer/disinfector units, this one being possibly operated either with a single microwave-sustained plasma source or two.[13] The species generated within the discharge tube(s) are carried, by the incoming gas flow, into and throughout the 50 L afterglow chamber before being evacuated through the pumping outlet located at mid-axial position on the bottom of the chamber, as shown in Figure 8.

---

[12] The reaction rate for the formation of NO molecules through the (two-body) collisional interaction of N and O atoms is approximately 1.2×10^{-17} cm^3 s^{-1} [12] and the density of atoms (say O as the target) in the few torr range ($\approx$200–700 Pa) is approximately 0.5×10^{14} cm^{-3}. Therefore, the number of NO atoms created per second in the unit volume is 1.2×10^{-17} cm^3 s^{-1} $\times 0.5 \times 10^{14}$ cm^{-3} = 6×10^{-4} s^{-1}. The collision frequency between an N and an O atom being approximately 3.6×10^6 s^{-1}, the probability of forming a NO molecule is then 6×10^{-4} s^{-1}/3.6×10^6 s^{-1} $\simeq 1.7 \times 10^{-10}$. Calculation result for a three-body NO reaction is within the same order of magnitude.

[13] Figure 12b, further on, shows that past a certain microwave power value, say 200 W, the increase in UV intensity slows down with increasing power: this is due to the increase of the discharge gas temperature, which above a certain level, lowers the N_2 dissociation rate [22]. This is why we have been running two plasma sources with 250 W each, instead of a single one with 500 W. Comparison of the spore inactivation rate achieved with a single 500 W plasma source with that of two 250 W plasma sources is, however, not straightforward, since the gas flow, set for axial uniformity, needs to be doubled with two plasma sources and the O_2 content modified as well.

A primary-vacuum pump is utilized for that purpose. The flow rates of the discharge gases (N_2 and O_2) are set individually with mass flow controllers, and gases are merged before inputting into the discharge tube(s). The N_2 gas flow entering each discharge tube is adjusted for uniformity of the UV radiation along the chamber axis (x coordinate), given the gas pressure in the chamber, which in the absence of O_2, is usually set between 3.5 and 5 torr ($\approx$470–670 Pa). When two plasma sources are used simultaneously, the gas flow is at 1 sLm in each tube. Details of the substrate holder are presented in Figure 13 below.

Plasma is currently sustained in fused silica or Pyrex® tubes through the propagation of an electromagnetic surface wave launched by a surfatron, a Ro-box or a surfaguide [23]. This wave utilizes as its propagating medium the plasma and the dielectric tube enclosing it. The incident and reflected microwave powers of each plasma source are monitored with a bi-directional power coupler and a power meter to determine the power absorbed by the discharge.

As a first approximation for scaling and comparison purposes of sterilizer/disinfector chambers of different volumes, we have expressed the total power P absorbed in the plasma source(s) relatively to the afterglow chamber volume V, defining the ratio P/V. In doing so, we consider that the amount of microwave power absorbed in the discharge tube provides given numbers of the various species, which are proportional to the absorbed power, these species being assumed to be distributed evenly within the chamber given volume (Sect. 4.1.1 below for considerations on species uniformity in the chamber). To be adequate, this scaling factor requires the chambers to be made from the same material and with approximately the same ratio of chamber-wall surface to afterglow volume. It also implies that the emission intensity increases linearly with microwave power, which is not always the case (see footnote 13). Then, provided these conditions apply, one thus expects to be able to maintain the same microorganism inactivation rates by doubling the absorbed microwave power when scaling up the 50 L chamber to 100 L. In the 50 L chambers used, during the course of our experiments, the P/V ratio was varied between a few watts per liter up to 10 W/L, keeping this ratio constant for a given study.

Figure 9 displays a plasma sterilizer similar to that in Figure 8, but of a much smaller volume (5.5 L). Note that the gas outlet is located this time on the side wall opposite that with the afterglow gas inlet, both positioned along a common axis.

4.1.1 Calculated spatial distribution of the concentration of N and O atoms and NO(A) excited-state molecules in the sterilizer/disinfector chamber. Measured axial variation of the NO_γ emission intensity

Figures 10a, 10b, 10d and 10e show the calculated contour maps, in a vertical plane comprising the axis defined by the connecting tube from the plasma source (Fig. 2), of the concentration of $O(^3P)$ and $N(^4S)$ atoms in a 50 L
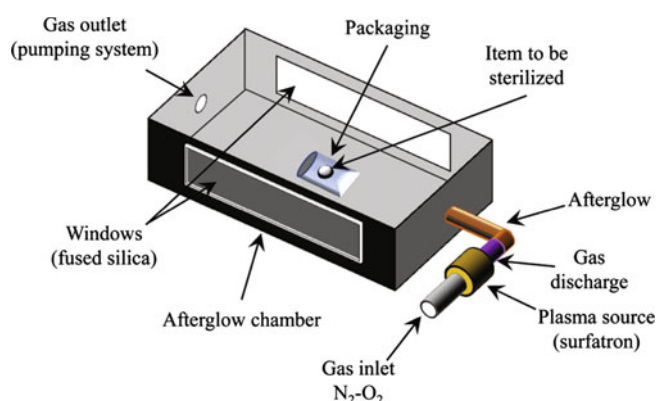
Fig. 9. Plasma sterilizer/disinfector system similar to that in Figure 8, but approximately 10 times smaller in volume (38 × 18 × 8 cm³: 5.5 L). The pumping outlet is located on the wall opposite that with the afterglow species inlet, both positioned along a common axis. The tube connecting the plasma source to the chamber entrance has an elbow-like shape to reduce its bulkiness (x_d is approximately 250 mm). The (single) packaged item is laid on the bottom of the chamber and at the center of it, with the pouch open side directed against the incoming flow from the discharge. The inner diameter of the discharge tube is 4.8 mm. This device was mostly operated at 2450 MHz.

afterglow chamber supplied from a N_2-O_2 discharge sustained at a field frequency of 2.45 GHz with 0.3% added O_2 (maximum UV intensity conditions) at a pressure of 5 torr (≈670 Pa) in the chamber. The gas inlet to the chamber is represented by an inward arrow (west side)

and the gas outlet from it by an outward arrow. Both pumping outlet locations tested, bottom and east side of the chamber, are considered in this calculation. The density distribution of the N atoms varies significantly across the chamber when the pumping outlet is on the east side, i.e. directed along the gas flow entering the chamber; the density distribution of O atoms is relatively more uniform. When the pumping outlet is located at 90° from the direction of the entering flow, it "forces" the incoming flow to turn towards the pumping orifice and, at the same time, "slows down" any directed outflow from the connecting tube, thereby favoring diffusion of the species in the chamber: a west gas inlet with a bottom gas outlet rather than an east gas outlet provides better spatial uniformity of both N and O atoms.

Figures 10c and 10f further display calculated contour maps in the afterglow chamber of the concentration of the NO(A) excited-state molecules, which constitute the upper energy level of the transition down to the NO(X) ground-state level that generates the NO_γ molecular system (Sect. 3.5). The density distribution of the NO(A) molecules in the chamber with bottom pumping is also predicted to be more uniform compared with east-side pumping. In the latter case, as a matter of fact, there are important local variations throughout the chamber. For instance, at $z \approx 15$ cm (chamber bottom plane), the NO(A) concentration varies from 0.1 (10^6 cm⁻³) at $x = 10$ cm to 2 (10^6 cm⁻³) at $x = 55$ cm, i.e. a possible change in UV intensity by a factor of 20! Since the microorganism inactivation rate is expected to vary by that same figure, such a situation is unacceptable for uniform
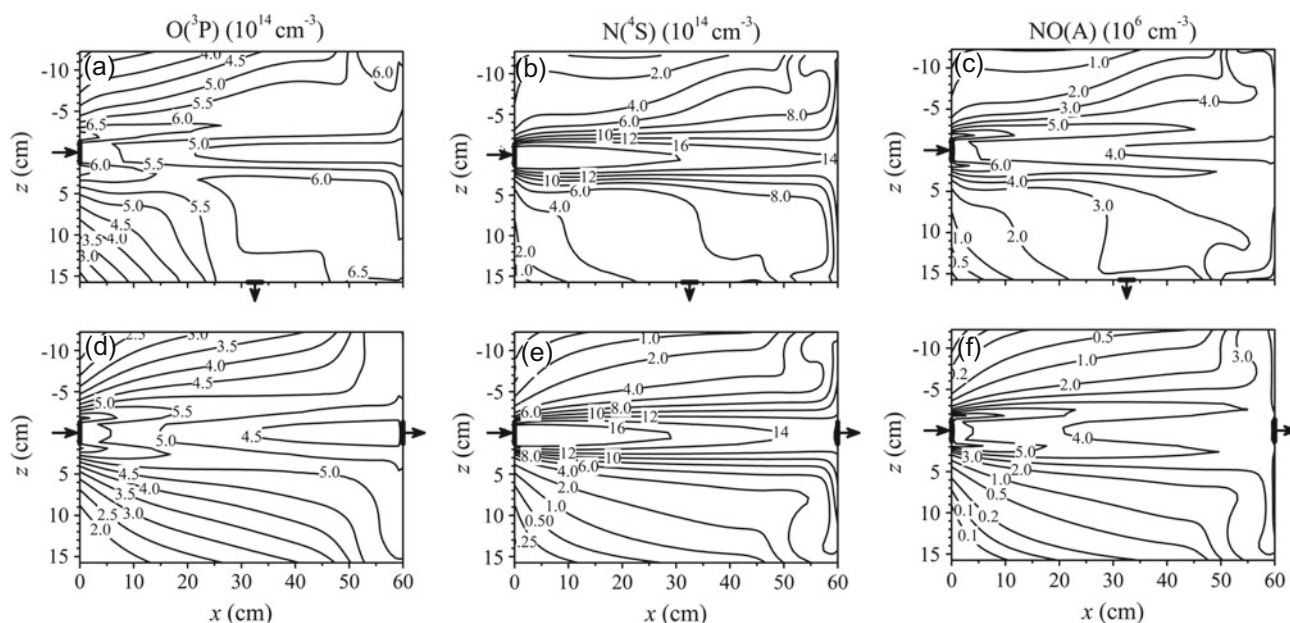

Fig. 10. Calculated contour maps of the concentrations of O(³P) and N(⁴S) atoms and NO(A) molecules in the afterglow chamber, at 10 ms elapsed time (Fig. 3), in a vertical plane comprising the axis defined by the connecting tube entering the chamber (Fig. 2). The N_2-O_2 discharge is sustained at 2.45 GHz with 0.3% added O_2 (maximum UV intensity conditions) and the gas pressure in the chamber is 5 torr (≈670 Pa). The gas inlet is represented by an inward arrow (west side) and the gas outlet by an outward arrow. Both cases of pumping outlet locations actually tested, bottom (a–c) and east side (d–f) of the chamber, are depicted (calculations by Kutasi et al. according to the code developed in [12]).

batch processing. It is thus strongly suggested, once more, to have the pumping outlet located perpendicularly to the incoming afterglow flow, and, furthermore, avoid positioning MDs too close to the entrance port, say at $x < 10$ cm.

Measured axial variation of NO_γ emission intensity in the 50 L chamber. According to the calculations presented in Figure 10, obtaining species uniformity within the small-volume chamber in Figure 9 where the gas inlet and pumping outlet are directed along the same axis ($z = 0$) is unlikely. This is confirmed experimentally (data not presented). This fact was not known at the time that this chamber was built. However, given the application intended, i.e. processing a single MD at a time, non-uniformity within the chamber is not really a concern. In fact, the gas flow was optimized to achieve maximum UV intensity at the center of the chamber, where the packaged MD to be processed is located. An advantage of this small-volume sterilizer/disinfector is that much less microwave power is needed than in the 50 L chamber for achieving a comparable inactivation rate, opening the way to small-size transistorized microwave power sources (instead of bulky magnetron tube generators).

Figure 11 displays the variation of emission intensity of a band head of the NO_γ molecular system as a function of axial position x in the 50 L chamber (pumping outlet at 90 ° from the gas inlet: Fig. 8) at three different heights z and for two frequencies of the microwave field sustaining the discharge. The gas flow rate is initially set to obtain the best possible uniform axial profile on the tube axis ($z = 0$). While the UV intensity on the chamber entrance side ($x \approx 0$) differs significantly at the three heights probed,[14] these axial profiles tend to merge into a single one, within the uncertainty bars, when approaching the opposite front wall. This effect can be thought as resulting from the bouncing back of the diffusing N and O atoms on the chamber wall opposite the entrance (probability of surface recombination of N and O atoms on aluminum is usually less than 1% [24]).

In Figure 11, the (average) ratio of the emission intensity from a given band head recorded (as in Sect. 3.4) at 2450 MHz over that at 915 MHz is close to 1.35 (similar ratios are observed in Figs. 21 and 22 further on). This outcome from a given band head is in agreement with Figure 7 where the emission intensity is integrated over the whole NO_γ molecular system, where the discharge sustained at 2450 MHz also yields an intensity ratio approximately a factor of 1.35 greater than at 915 MHz (3.5 torr pressure). Calculations made assuming a NO(X) density close to 10^{11} cm^{-3} indicate that the afterglow medium thus probed over a 300 mm depth is actually optically thin.

---

[14] The flowing afterglow entering the chamber gives rise to a visually observable (yellow-orange) beam-like shape, this beam having approximately the diameter of the connecting tube (25 mm) and extending on half the chamber length. Such an effect is clearly predicted by calculations, as can be seen in Figure 10b in the case of N atoms for $z = 0$, and it tends to attenuate off the axis at $z = 5$ and 10 cm, as confirmed experimentally in Figure 11.
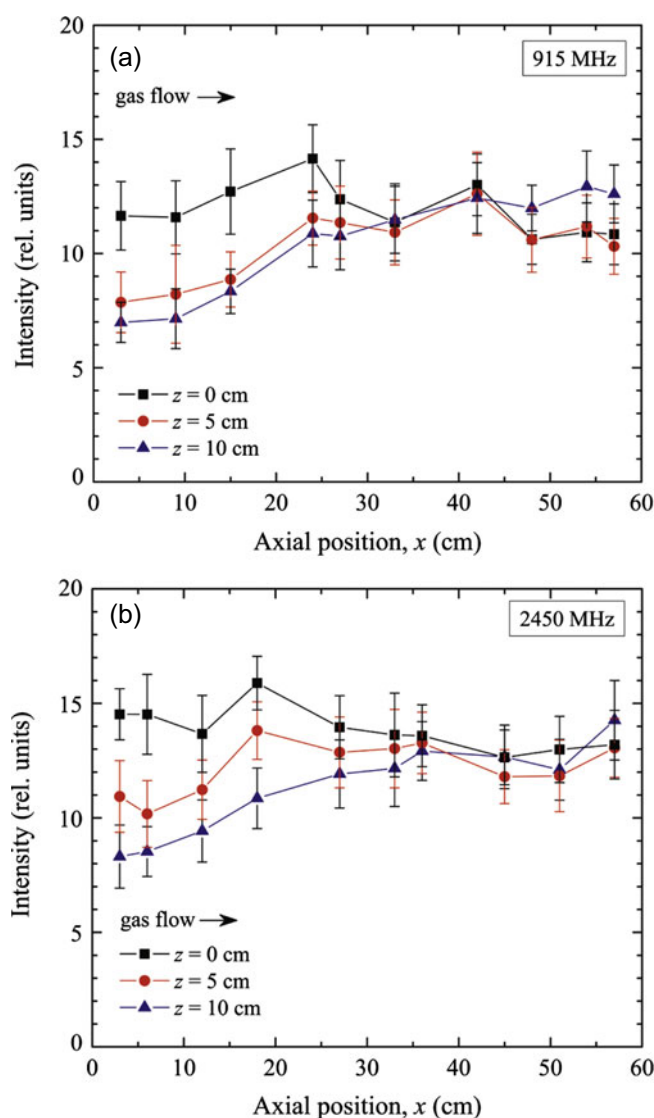

Fig. 11. UV intensity from a NO_γ band head (304 nm) as a function of axial position x at three different heights z from the tube axis ($z = 0$) in the 50 L chamber (with a single plasma source) at the discharge sustaining field frequency of (a) 915 MHz and (b) 2450 MHz, for the same given absorbed power (200 W). Pressure in the chamber is 3.5 torr ($\approx$470 Pa) with a N$_2$ and O$_2$ gas flow rates of 1.4 sLm and 3 sccm, respectively. Connecting tube distance is $x_d = 820$ mm. The gas inlet is on the left side of the figure and the gas pumping outlet is on the bottom of the chamber (at $z = 15$ cm for $x = 30 \pm 2$ cm).

4.1.2 Influence of the discharge field-frequency on UV intensity for a given absorbed microwave power

For a given absorbed microwave power, the degree of dissociation of N$_2$ molecules into N atoms increases with the discharge frequency [22]. As a result, the formation of NO* excited molecules in the N$_2$-O$_2$ flowing afterglow should also increase with frequency. Figure 12a, recorded in the small-volume chamber of Figure 9, shows such an increase by a factor of 6 and 7 when raising the frequency from 433 and 915 MHz to 2.45 GHz (the O$_2$ percentage in the
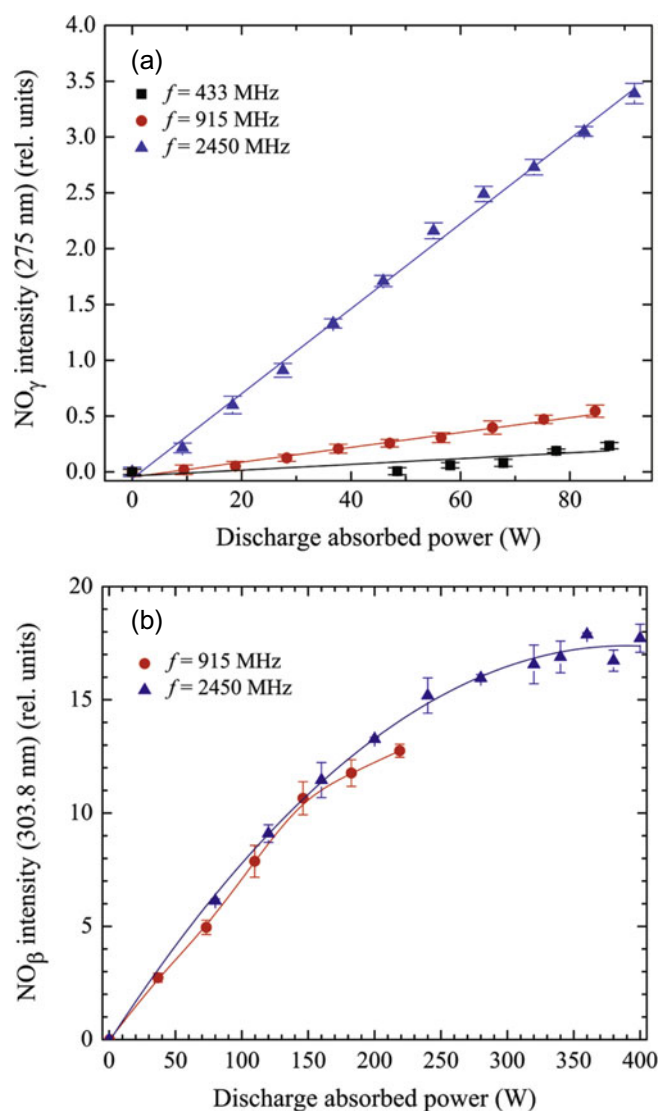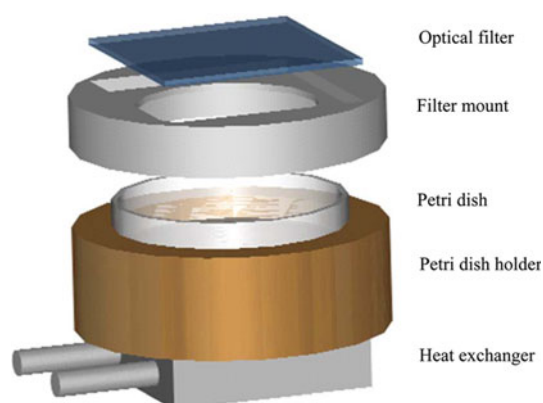
Fig. 13. Exploded view of the temperature-controlled Petri dish holder and high-pass optical filter mount. In this configuration, the Petri-dish frame is fully encased. The optical filter plate (window), whenever in place, fits freely on top of the filter mount, reducing the access of some of the afterglow gaseous species to the inside of the Petri dish. The substrate holder is located on the bottom of the afterglow chamber, close to the chamber entrance, as shown in Figure 8.

Figure 12 also indicates that the UV intensity increases linearly with microwave power at values below 150 W, then starts slowing down (see footnote 13 for an explanation).

4.1.3 A heat-controlled substrate holder accommodating a Petri dish, which can be closed by different high-pass filters at specific optical wavelengths

The polystyrene Petri dishes (Sarstedt, 55 mm diameter, 14 mm height), on which the spores to be inactivated have been deposited and let dried, fit firmly (good thermal contact) within a temperature-controlled substrate holder made from brass (Fig. 13), the latter resting on the bottom ($z = 150$ mm) of the afterglow chamber, as shown in Figure 8. The inoculum in the Petri dish surface is then situated at $z = 129$ mm from the discharge axis. Its temperature can be set, for parametric study, anywhere in the 4–80 °C range through circulating water coming from a heat exchanger (Neslab). When the substrate holder is not heat controlled, the temperature at the end of a 30 min process does not exceed 35–40 °C.

Various high-pass optical filters, which allow UV radiation to go through above a given minimum wavelength (cut-off wavelength), can be successively positioned over the Petri dish, as shown in Figure 13. In such a configuration, the filter considerably reduces the concentration of reactive species (such as ions and metastable-state molecules) entering the Petri dish since most of them recombine/deactivate on obstacles (in the present case a very narrow aperture[15]), in contrast to N and O atoms, which

---

[15] The filter-window resting on the filter mount does not ensure gas-tight sealing of the Petri dish: it allows achieving pumping down or restoring atmospheric pressure in the chamber without actually breaking the window.

Fig. 12. Measured UV intensity as a function of the power absorbed in the discharge at different (authorized) industrial scientific medical (ISM) frequencies. (a) NO_γ band head at 275 nm at a pressure of 5 torr ($\approx$670 Pa) in the small-volume chamber (Fig. 9 with $x_d = 250$ mm); (b) NO_β band head at 304 nm at a pressure of 3.5 torr ($\approx$470 Pa) in the 50 L chamber with a single plasma source (Fig. 8 with $x_d = 820$ mm). The O_2 percentage in the N_2-O_2 mixture has been adjusted for maximum UV intensity.

N_2-O_2 mixture was tuned at each frequency for maximum UV intensity, namely 0.25% at 433 MHz and 0.37% at 915 and 2450 MHz). The UV intensity increase from 433 and 915 MHz to 2450 MHz in the small chamber is enhanced due to the fact that the gas flow rate had been set for maximum UV intensity at the pouch location. Figure 12b, in contrast, shows a very slight increase in emission intensity on a given head band when raising the frequency from 915 MHz to 2450 MHz in the 50 L chamber. Nonetheless, integrating the emission intensity over the whole NO_β system shows that it is 1.3 times higher at 2450 MHz (data for 3.5 torr in Fig. 7).
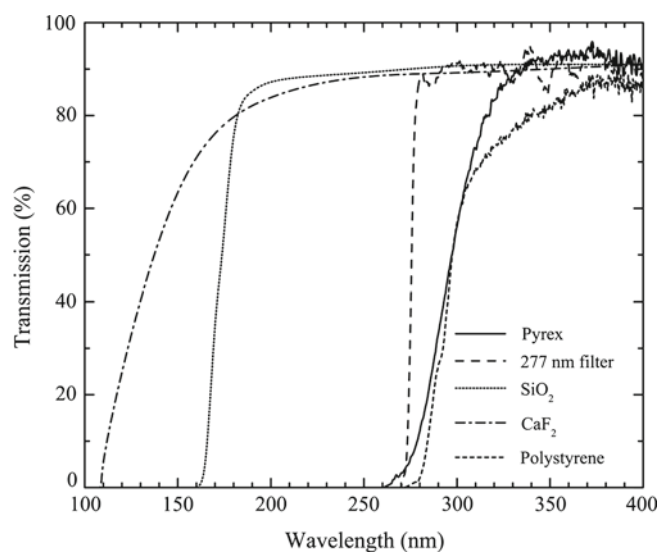
Fig. 14. Percent transmission of the optical filters used as a function of wavelength. The CaF_2 and SiO_2 windows have a 5 mm thickness while thickness of the other filters is close to 1 mm. The wavelength at half-maximum transmission percentage of CaF_2 and Pyrex-polystyrene filters is 130 and 300 nm, respectively.

(almost) freely enter the Petri dish. The spores deposited in the Petri dish are thus mainly inactivated by the UV photons from the chamber that go through the filter. However, the UV photons formed within the Petri dish as a result of the N and O atoms interacting to produce NO* excited molecules can also contribute to inactivation, but to a lesser extent. The percent transmission of these optical filters is displayed as a function of the (VUV-UV) wavelength in Figure 14. The value reached at their plateau lies between 85 and 90% of full transmission. Note the particularly sharp rise just above cut-off of the 277 nm and SiO_2 filters. Pyrex and polystyrene (PS) plates having approximately the same wavelength response, we currently use the cap of PS Petri dishes as a Pyrex optical filter.

4.2 Optical emission spectroscopy recording

Vacuum UV (VUV) and UV spectrophotometers were successively used to record the spectral characteristics of the flowing afterglow in the chamber: (i) a 1 m focal length grating-spectrometer (McPherson 225) was utilized to cover the portion of the VUV spectrum extending from 112 nm[16] to 180 nm as well as the initial portion of the UV band up to 250 nm; (ii) a 320 mm focal length grating spectrometer (Jobin-Yvon HR320), equipped with a Hamamatsu R636 photomultiplier tube, was employed to examine the 200 to 400 nm spectral range; its spectral response was determined using a calibrated deuterium lamp (Oriel).

---

[16] This lower limit is the cut-off wavelength of the CaF_2 and MgF_2 vacuum sealing windows at the spectrometer entrance slit and on the photomultiplier tube.
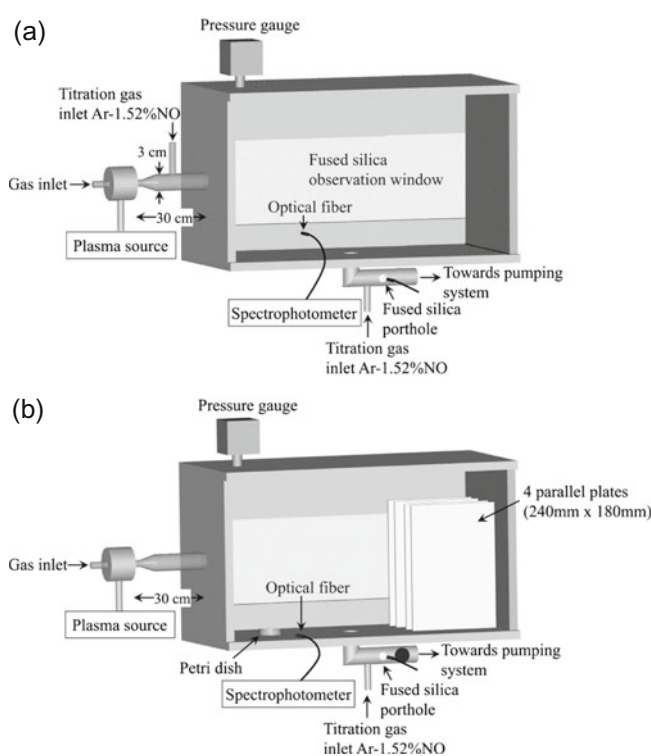

Fig. 15. Open view of the 50 L sterilizer/disinfector: the chamber-wall structure (with its fused silica window) on the lateral side nearest to the reader has not been drawn for clarity. The drawing shows: (a) the position of the NO titration gas inlets (one at the chamber entrance and one along its pumping outlet) on the 50 L flowing afterglow system. The fused silica porthole on the pumping outlet can also be used to determine the remaining UV intensity at that point while a movable optical fiber can be utilized to record, through the large fused silica observation window, the UV intensity at different locations in the chamber, in particular above Petri dishes; (b) the position of the rectangular plates (up to four) used to determine the loss of N and O atoms as a result of surface recombination on given materials. The Petri dish here is located on the entrance side of the chamber, ahead of the plates.

Figure 15a shows how the NO titration technique is implemented on the 50 L afterglow system to obtain the absolute concentration (density) of N and O atoms. The NO gas can be introduced either at the chamber entrance inlet (on the connecting tube) or along its pumping outlet, and the spectroscopic observations made within the chamber through the fused silica observation window or through the fused silica window on the porthole situated on the aluminum pumping outlet. The method used to infer these concentrations is described in [25].

To assess quantitatively the decrease of the concentration of N and O atoms due to surface recombination on specific materials, up to four rectangular plates of the same given material, with dimensions $240 \times 180 \times 2$ mm, can be set parallel to each other, separated by a 40 mm spacing provided by an aluminum holder resting on the chamber "floor". These plates are positioned at the chamber extremity opposite to the entrance of the flowing

10001-p13

afterglow into the chamber, as shown in Figure 15b. A Petri dish can be located close to the chamber entrance side, lying on the chamber bottom along the discharge tube axis. Operating pressure, in this experiment, was 2 torr ($\approx$270 Pa), the discharge was sustained at 2450 MHz and the connecting tube distance x_d was 300 mm. The N and O atom concentrations reported in this case are those measured at the pumping outlet of the chamber.

4.3 Variation of the emission intensity of the NO$_\gamma$ molecular system as a function of the percentage of O$_2$ added to N$_2$ and of the connecting tube distance x_d

In early publications, we limited our observations/ measurements of the UV emission intensity from the N$_2$-O$_2$ flowing afterglow to that originating from the NO$_\beta$ system, mistakenly considering that the NO$_\gamma$ system was varying exactly in the same way as a function of the added O$_2$ percentage ([26] is the last of our papers with such a misinterpretation). Furthermore, as discussed in Section 3.2, it is the UV photons of the NO$_\gamma$ system, not those of the NO$_\beta$ system, that are essentially responsible for the inactivation of our reference spores: we thus need to focus on the NO$_\gamma$ system.

Figures 16a and 16b display the emission intensity of a given band head of both the NO$_\beta$ and NO$_\gamma$ molecular systems, respectively, as functions of the percentage of O$_2$ added to N$_2$ in the flowing afterglow (50 L chamber, as in Fig. 8 with two plasma sources). The emission intensity of both molecular systems goes through a maximum at an O$_2$ percentage close to 0.3. In the case of the NO$_\beta$ system, the emission intensity drops definitely at the noise level above 3% added O$_2$,[17] in contrast with the NO$_\gamma$ system. The latter emission intensity comes close to the noise level for O$_2$ around 2.4% but then increases, slightly, above 3% O$_2$ to reach, at 10% O$_2$ and beyond, a constant level of approximately 10^{-2} of the maximum intensity. Such a spectrum remains quite faint, as shown in Figure 16b, and actually requires, to be detectable, a large enough microwave power absorbed in the discharge (at least 500 W when using the 50 L afterglow chamber).

Although the intensity of the NO$_\gamma$ band head at 10% added O$_2$ is approximately 60 times lower than at maximum UV intensity, spore inactivation is nonetheless observed to take place through the UV irradiation that it generates (Sects. 5.1.2 and 5.1.3) and with the same inactivation efficiency provided exposure time at 10% added
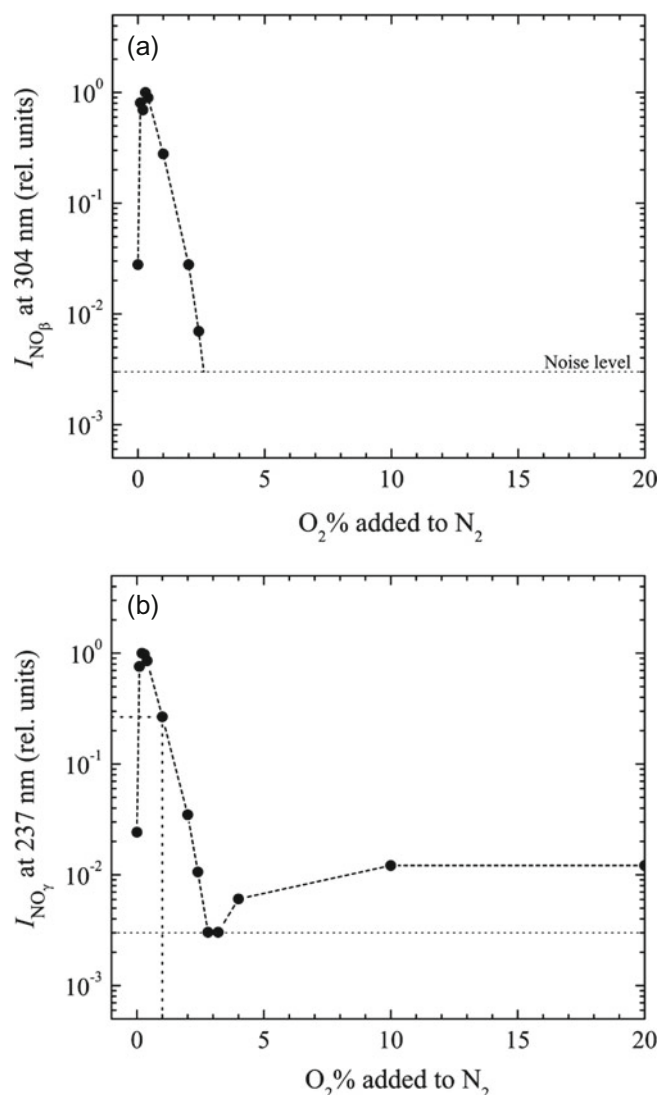
---

[17] In fact, complete extinction of the visible blue light emission coming from the afterglow (these band heads of the NO$_\beta$ system are in the 380–430 nm range) occurs as the O$_2$ percentage reaches approximately 3% while for higher O$_2$ percentages, the afterglow visible light turns green.

Fig. 16. Emission intensities recorded in the flowing afterglow (a) of a band head (304 nm) of the NO$_\beta$ system and (b) of a band head (237 nm) of the NO$_\gamma$ molecular system as functions of the O$_2$% admixed to N$_2$ (at 1 sLm N$_2$ in each tube, 5 torr ($\approx$670 Pa) and 10 W/L at 915 MHz). The maximum intensity of each band head is normalized to unity.

O$_2$ percentage is extended by such a factor of 60 to gather, in the end, a given total number of photons (i.e., the same fluence: Sect. 5.1.2 further on).

It is noteworthy that, according to the kinetic model developed in Section 3.5, both the NO$_\gamma$ and NO$_\beta$ molecular systems should be simultaneously present at reduced pressures. In the present case, at 10% added O$_2$, in lieu of the NO$_\beta$ system in the spectrum, we observe band heads of the second positive system of the N$_2$ molecule, as can be seen in Figure 17.

Figure 18 shows, unexpectedly, that the UV intensity in the chamber is almost 50% higher when the distance of
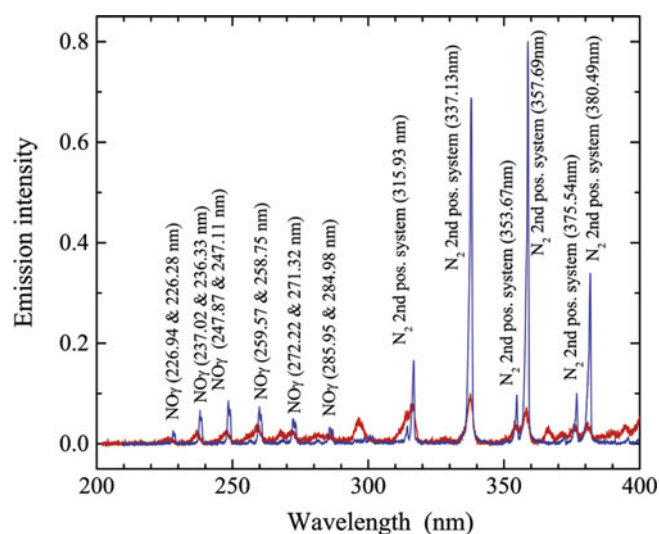
Fig. 17. In red, actual spectrum observed at 1 sLm N_2 and 10% added O_2. In blue, for identification purposes: (i) from 200 nm up to 280 nm, the NO_γ system spectrum recorded at maximum UV intensity ($\approx 0.3\%$ added O_2), but afterwards reduced in intensity for display purposes. It allows to show that the band heads at 10% O_2 from 227 to 270 nm come out as part of the NO_γ system; (ii) beyond 310 nm, the spectrum recorded in a N_2 discharge matches with that at 10% O_2 added to N_2. Operating conditions: 5 torr (≈ 670 Pa) in the 50 L chamber and 500 W absorbed power at 915 MHz.
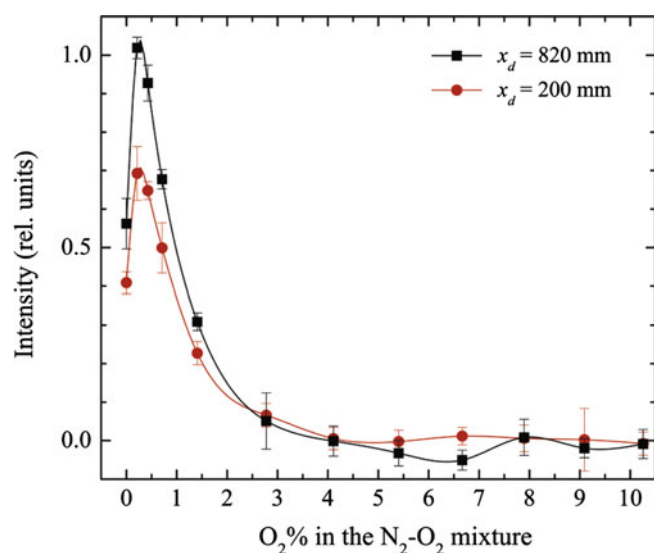

Fig. 18. Relative emission intensity from a NO_γ band head as a function of the O_2 percentage in the N_2-O_2 mixture for two distances x_d of the connecting tube. Operating conditions: 915 MHz with 100 W absorbed power, N_2 flow rate of 1.4 sLm at a 3.5 torr (≈ 470 Pa) pressure. The spectrophotometer optical fiber was directed at $z = 10$ cm and $x = 30$ cm.

the connecting tube to the chamber, x_d, is the largest. We hypothesize that species from the early afterglow participate in generating, essentially, more N atoms than when x_d is 200 mm.

4.4 Surface recombination of the N and O atoms on various materials in the N_2-O_2 discharge flowing afterglow and its influence on the reduction of the NO_γ emission intensity

The recombination of O and N atoms on surfaces (chamber walls, items to be sterilized and packaging materials) reduces the number of NO excited molecules generated in the afterglow chamber, leading to a decrease in the UV emission intensity of the NO_γ molecular system, hence to an increase in the time required to reach sterility or a given level of disinfection.

4.4.1 Recombination of N and O atoms on Teflon, aluminum, stainless steel and copper surfaces as a function of the percentage of O_2 added to N_2

The experimental arrangement described in Figure 15b is used to determine the concentrations of N and O atoms remaining at the pumping exit when the four plates are in position in the chamber as compared with their concentrations in the empty chamber. Figure 19 shows that adding Teflon plates (sheets) barely reduces the concentrations of N and O atoms. However, when aluminum plates are present, the decrease in concentrations becomes significant while it turns out to be much higher with (304 grade) stainless steel plates. Copper comes out as the most recombining material of them all.

The difference in the recombination rates of N atoms on different materials for a given $O_2\%$ tends to vanish as the percentage of added O_2 exceeds approximately 1% (Fig. 19a). In contrast, the difference in the O atoms concentration on the various surfaces grows with the increase in the percentage of added O_2, which indicates a constant recombination rate for oxygen atom with added O_2 percentage (Fig. 19b). This suggests that past 1% added O_2 essentially only the O atoms recombine (as O_2) on surfaces: they predominantly occupy the vacant sites on surfaces, as they are more reactive than N atoms [27,28].

4.4.2 Influence of surface recombination of the N and O atoms on the emission intensity of the system NO_γ

Figure 20 shows that the largest difference in the observed UV intensities depending on the material considered is recorded close to the percentage of added O_2 yielding the maximum of UV intensity. Comparison of Figures 19a and 19b suggest that the lowering of the maximum of UV intensity results from the more or less important loss of N atoms by surface recombination on these different materials.

The reduction in UV emission intensity due to surface recombination on the various materials examined above lowers the inactivation rate of our reference bacterial endospores, as we shall see in Section 5.1.6. The loss of O and N atoms on the material of the packaging pouches is investigated in Section 5.4.1.
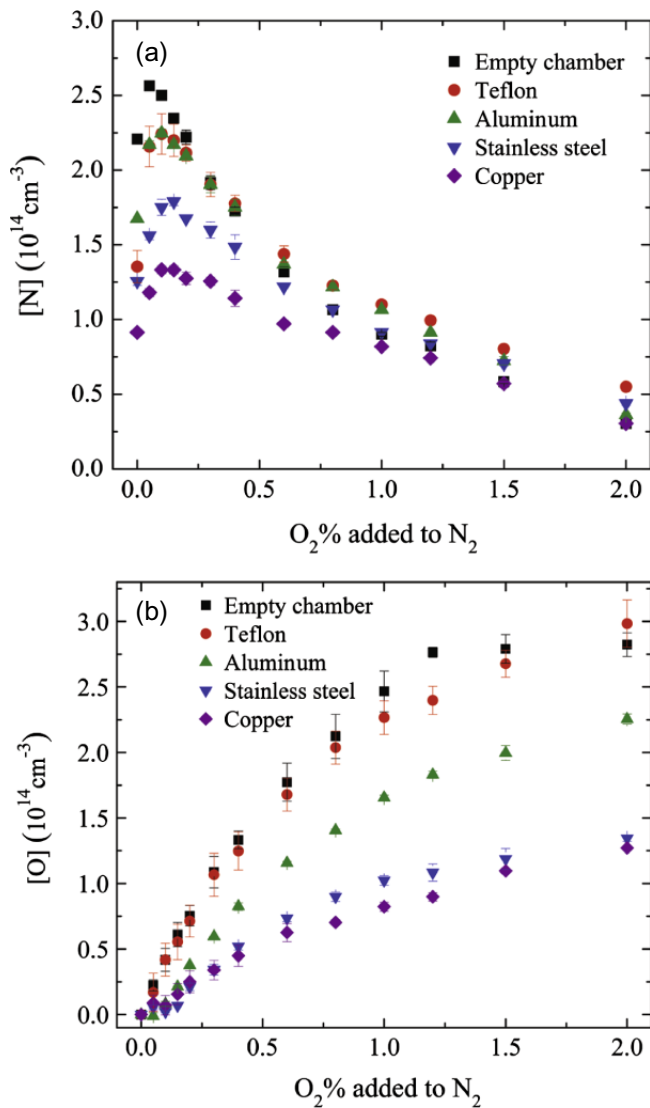
Fig. 19. Variation of (a) the N-atom concentration and (b) O-atom concentration as a function of the percentage of O_2 added to N_2, as measured at the pumping outlet of the afterglow chamber, when successively introducing into the chamber different sheets of materials, positioned as described in Figure 15b. Operating conditions: discharge sustained in a 6 mm i.d. Pyrex tube at 2.45 GHz with 100 W absorbed power, at a 2 torr pressure ($\approx$270 Pa) in the 50 L chamber with a 0.9 sLm N_2 gas flow [24,29].

A final note on the influence of a high surface-recombination rate on uniformity of the UV intensity along the chamber. As a rule, it is possible to adjust the N_2 gas flow rate to achieve axial uniformity of the UV emission intensity, which relies on species diffusion. However, when the four copper plates are introduced in the chamber, it becomes impossible to establish satisfactory uniformity: the rate at which the N and O atoms disappears (locally) on surfaces is so high that it prevents diffusion from playing its uniformizing role.
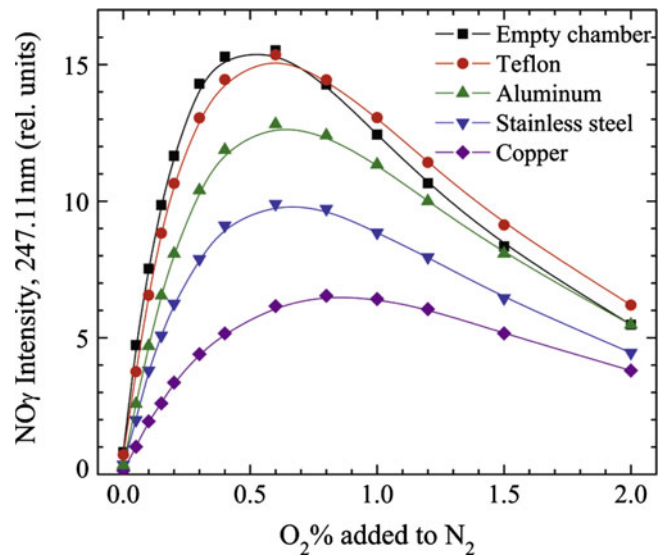

Fig. 20. Variation of the UV intensity (recorded on the 247.11 nm band head of the NO_γ system) in the 50 L chamber as a function of the percentage of O_2 added to N_2 in the presence of plates of different materials as compared with the empty vessel. Operating conditions as in Figure 19 [24,29].

4.4.3 Influence of the presence of metallic objects at a given location in the chamber on the axial uniformity of UV emission intensity

The main point developed in this section is the fact that the loss of N and O atoms occurring through surface recombination, even though this loss is localized somewhere in the chamber, is "shared" within the whole chamber volume because of the highly efficient diffusion of these atoms.

As a first example, consider the configuration of Figure 15b where the Petri dish is situated at $x \simeq 150$ mm and the plates extend from $x = 400$ mm till the chamber wall. The emission intensity of a given band head of the NO_γ molecular system recorded above the Petri dish decreases as the plates are added on the opposite side of the chamber, such a decrease following the increase of the plate surface-recombination coefficient (data not shown [24]). This prompted us to make axial measurements of the UV intensity in the chamber.

Figure 21a shows the variation of the axial UV intensity of a NO_γ band head at three different heights z in the chamber when an aluminum block (50 mm $\times$ 50 mm $\times$ 100 mm) rests on the bottom of the chamber (see inset for its location), as compared with the empty chamber in Figure 21b. It is noteworthy that the presence of the aluminum block does not affect locally the axial profile: in other words, it is not possible from the recorded axial profile to determine where the block is actually located as a function of axial position. As a matter of fact, the recombination of N and O atoms on the aluminum block turns out to reduce uniformly, i.e. by the same factor, the axial UV intensity at a given height, once again without affecting much its axial profile. This indicates that diffusion
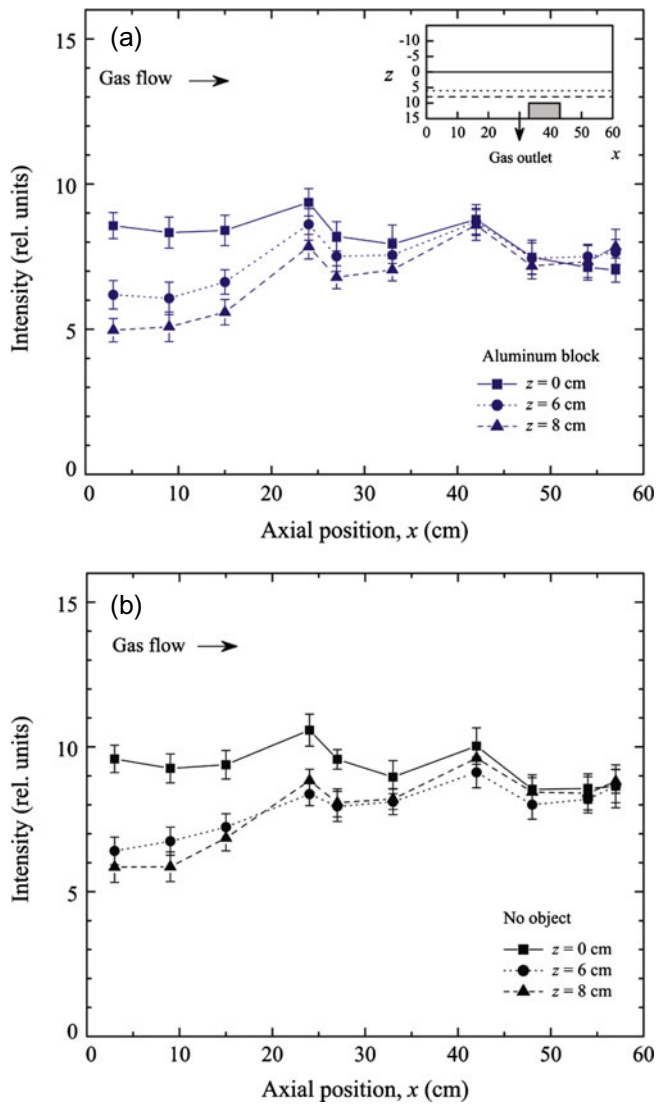
Fig. 21. Axial variation of the (relative) intensity of a NO_β band head (304 nm) at three values of the height z in the chamber: (a) with an aluminum block in the chamber ($z = 8$ cm is 2 cm above the surface of the aluminum block); (b) in the empty chamber. Operating conditions: discharge sustained at 915 MHz with 200 W absorbed power (single plasma source) in the 50 L chamber at a pressure of 3.5 torr ($\approx$470 Pa) with N_2 and O_2 gas flow rates of 1.4 sLm and 3 sccm, respectively. Connecting tube distance is $x_d = 820$ mm. The gas inlet is on the left side of the figure and the gas pumping outlet is on the bottom of the chamber at $z = 15$ cm and $x = 30 \pm 2$ cm.

of the N and O atoms is very efficient in re-establishing uniformity, recalling that surface recombination is local.

Figures 22a and 22b show the axial profile in the presence of a brass full cylinder and a copper hollow cylinder, respectively. Surface recombination on these materials is higher than on aluminum, hence a lower UV intensity. The axial profile is more or less the same, with and without the object. Once again it appears impossible to determine where the objects are located by looking at the axial variation of the UV intensity: any local depletion of the main
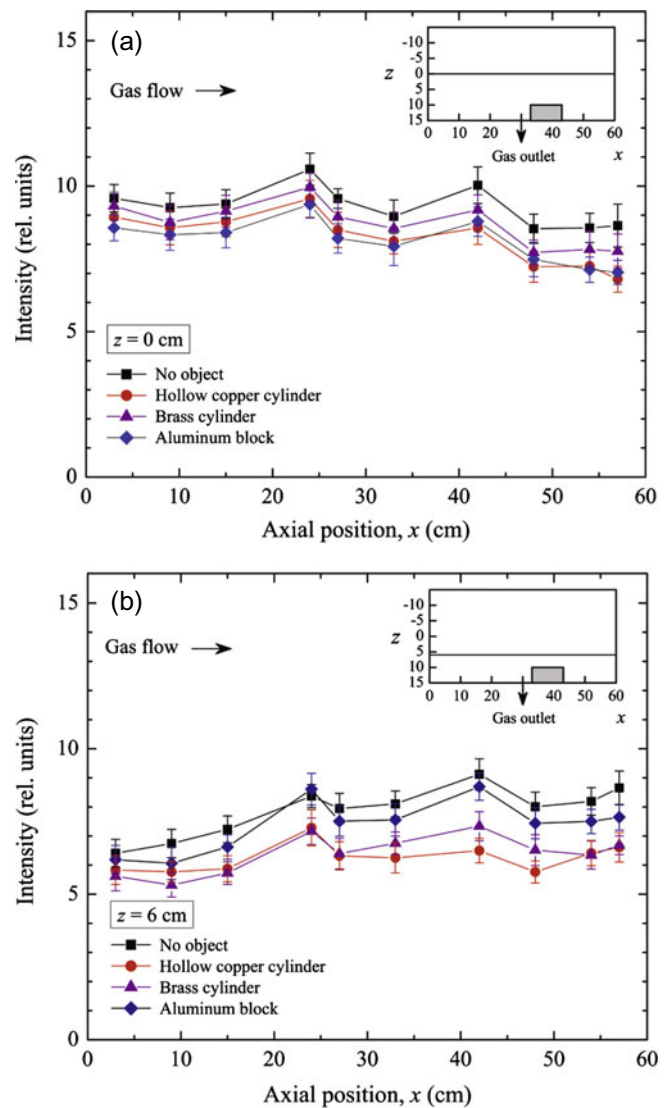
Fig. 22. Axial UV emission intensity in the presence of an aluminum block, a brass full cylinder and a copper hollow cylinder: (a) at $z = 0$ cm; (b) at $z = 6$ cm. Operating conditions as in Figure 21.

species (N and O atoms) through surface recombination is compensated by the action of diffusion.

4.5 Microbiology experimental protocols

Bacterial spore study. It involves three successive steps:

(i) Preparation of the required spore suspension (number of spores in a given dilution and volume) from stock suspension, mostly of *B. atrophaeus* bacterial endospores, their deposition (number of spores in a given volume) in Petri dishes (usually made from polystyrene) and drying of the deposits at ambient temperature in the dark.

(ii) Exposure of the spore dried deposits to the flowing afterglow under various operating conditions.

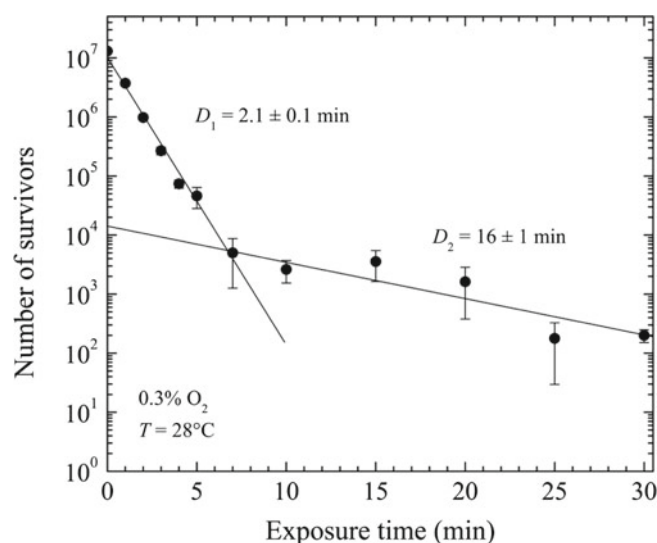10001-p17

Fig. 23. Survival curve for 10^7 *B. atrophaeus* spores exposed to the flowing afterglow from a 915 MHz microwave discharge in a N_2-O_2 gas mixture (0.3% O_2 added to N_2 for maximum UV intensity). The pressure in the 50 L sterilization/disinfection chamber is 5 torr ($\approx$670 Pa) under a 1 sLm N_2 flow in each of the two discharge tubes (Fig. 8). The connecting tube distance $x_d \approx 150$ mm. Total absorbed microwave power is 500 W, i.e. a P/V ratio of 10 W/L. The Petri dish is kept at 28 °C whitin the temperature-controlled substrate holder (Fig. 13). The full lines are best fit to the data points and the uncertainty bars (non symmetrical on a log scale) are standard deviations.

(iii) Spore recovery and colony-forming unit (CFU) counting, leading to a survival curve (logarithm of CFUs as a function of exposure time to the biocidal agent, for example, as in Fig. 23). Details of the recovery procedure can be found in [30].

Although it is customary to lay 10^6 spores when focusing on achieving sterility, on most occasions we deposited 10^7 spores for two main reasons:

(i) To increase their stacking and thus have a closer look at the second phase of the inactivation kinetics (see further Sect. 5.1.1 for the definition of phases);
(ii) To avoid determining if sterility had been achieved by looking for zero spore left, while it is much safer, statistically speaking, to check the SAL criterion with ± 10 spores left in the end.

Tests were conducted to ensure that the various steps involved in the inactivation process prior to igniting the discharge, for instance (sudden) pumping down of the process chamber to reach a few mtorr ($\approx$10–30 Pa) of vacuum and exposure to microwave field alone, had no influence on *B. atrophaeus* spore viability. In addition, the Petri dishes were kept at three given temperatures (12, 52 and 68 °C) while being subjected to a N_2-0.3% O_2 gas mixture (no discharge on) flowing at 2 sLm under a

5 torr ($\approx$670 Pa) pressure for as long as 30 min without the viability of the spores and their deposited number being affected [31].

Pyrogen study. Pyrogens are bioactive molecules, which, as their name indicates, are fever-inducing substances that can even lead to a septic shock whenever they enter the bloodstream or tissues. The most pathogenic ones are found in the outer cell walls of gram-negative bacteria and are released upon bacterial cell lysis.[18] In gram-negative bacteria (e.g. *E. coli*, *Pseudomonas* species), we encounter lipopolysaccharides (LPS) and, in gram-positive bacteria (e.g. *B. atrophaeus*, *S. aureus*), lipoteichoic acids (LTA).

Commercially available purified LPS and LTA molecules, as well as bacterial endospores, were deposited into 96-well polystyrene-tissue culture plates (Costar® 3595, tissue culture treated, nonpyrogenic, polystyrene, sterile). In order to expose the samples to the flowing afterglow of a low-pressure N_2-O_2 discharge, they all need to be dried beforehand, which is achieved overnight at ambient temperature in the dark. The culture plates are placed at the center of the 5.5 L afterglow chamber (Fig. 9) and exposed for 2 h to the flowing afterglow. After their exposure, the plates are kept 24 h at ambient temperature in the dark and rehydrated (with 20 μL ultra-pure sterile pyrogen-free water) to comply with the volumes stated in the test protocol. Then the assay is conducted according to the reference lot comparison test method, using the PyroDetect System. We conducted five assays at different times, using four different PyroDetect kits (EMD-millipore), two different LPS standards as well as different bacterial spore stocks and deposits. The results presented are pooled from all experiments.

Prion protein study. Experiments on prion proteins subjected to plasma are relatively new and not yet standardized. The reader is referred to our full paper [32] for a thorough and detailed presentation of the protocol.

Operating conditions of the flowing afterglow system for prion protein study: the sterilization/disinfection system used in this prion assay is the same as in Figure 8, namely a 50 L chamber but with a single discharge tube. Typically, the gas flow rates are fixed at 1 sLm for N_2 and 8 sccm for O_2 (0.4% O_2 in the mixture) and the pressure set at 8 torr ($\approx$1070 Pa) in the chamber. The discharge is sustained at 433 MHz with an absorbed power of 300 W, which translates into 6 W/L in the afterglow chamber. The gas temperature therein is well below 40 °C, except very close to the flowing afterglow entrance into the chamber. The samples are placed inside the chamber, on a stand located at mid-axial distance and along the discharge tube axis, i.e. at $x \approx 300$ mm, $z = 150$ mm (Fig. 2 for coordinates).

---

[18] Cell lysis (cell disruption) generally results from the destruction of the cells from the inside out due to a weakening of the cell wall, which is subjected from the interior to a high osmotic pressure.

5 Spore inactivation with the N$_2$-O$_2$ flowing afterglow: characteristic representation of the inactivation process and specific properties of our method

5.1 Survival curves

A survival curve, as already mentioned, is usually a logarithmic plot of the number of viable microorganisms as a function of exposure time to a given biocidal agent. It characterizes the response and rate of inactivation of given microorganisms to specific biocidal agents.

5.1.1 Shape of survival curves

Figure 23 shows a typical survival curve resulting from exposure of 10^7 *B. atrophaeus* endospores to the discharge afterglow from a N$_2$-O$_2$ gas mixture with 0.3% added O$_2$ to N$_2$ (maximum UV intensity conditions) at 5 torr ($\approx$670 Pa) under a 1 sLm N$_2$ flow in each discharge tube (Fig. 8 system). The microwave power delivered at 915 MHz in each discharge tube is 250 W, i.e. a total P/V ratio of 10 W/L for this 50 L chamber.

We observe that the survival curve is bi-phasic, i.e. comprised of two distinct linearly decreasing segments on this logarithmic plot. The decimal time D (time required for the number of survivors to decrease by a log) of the second segment of the survival curve, D_2, is much longer than that of the first phase, D_1: for that reason, the second phase is often called tailing. The first phase is believed to correspond to lethal (irreversible, i.e. non-repairable) lesions induced by UV photons from the gaseous phase on isolated spores or on the top ones on a stack, while the second phase is thought to relate to spores that UV photons cannot access as efficiently because these spores are either within a stack, aggregated, located in cavities or crevices, or covered by some bio-product/debris (Fig. 1). Such an explanation for the second phase assumes that the population of the *B. atrophaeus* spores is not affected by phenotypic variations and that it does not comprise a group of bacteria more resistant to UV irradiation.

Figure 24 is a schematized and simplified representation of spore gathering destined to show the limited accessibility of UV radiation to the DNA of non-isolated spores: in contrast to isolated spores and top ones on a stack, aggregated and stacked spores are exposed to a reduced photon flux (sometimes to no photons at all) from the surrounding gaseous phase, depending on how the incoming photons get absorbed on their way to their "target".[19]

Figure 25 illustrates the possible case of N and O atoms infiltrating, through diffusion, in-between spores in a stack

Fig. 24. Schematized representation of: (a) an isolated spore with its genetic material (DNA) surrounded by various protecting coats and membranes (blank part); (b) and (c) spore aggregates offering only partial direct access to UV photons from the gas phase; (d) an enclosed spore in a stack. The "drawn intensity decrease of the photon ray" as it penetrates spore material suggests that the UV photon is absorbed by "peripheral" spores before it reaches the DNA material of the most "hidden" spore, hence a comparatively reduced photon flux on that spore, and thus a longer required time to achieve a given number of lethal lesions on the DNA strand.
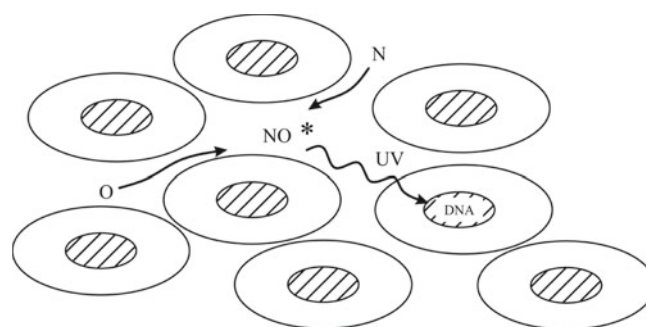
Fig. 25. Schematized representation of how N and O atoms, through diffusion, can infiltrate in-between spores (more on this possible diffusion process in Sect. 5.4.4) and form a NO* excited molecule, then emitting a UV photon that reaches the DNA of a hidden spore in a stack.

and forming there a NO* excited molecule[20] emitting a photon that goes through the DNA of an enclosed spore, otherwise not readily accessible to UV photons coming from outside the stack. Clearly, such a low-probability mechanism in terms of its occurrence, but a reality because of the high diffusiveness of the N and O atoms, requires a longer time to gather the lethal dose of photons needed to inactivate the "hidden" spore than for an isolated spore or a spore on top of a stack.

---

[19] The measured optical absorption in the 200–330 nm range across a *B. atrophaeus* spore lies between 10% and 15% of the incident UV radiation. Since the typical dimensions of *B. atrophaeus* spores are 1.3 μm (length) by 0.7 μm (width), this suggests that very few photons should go through three to four spores in a stack and then reach and damage the DNA material of a fifth spore underneath.
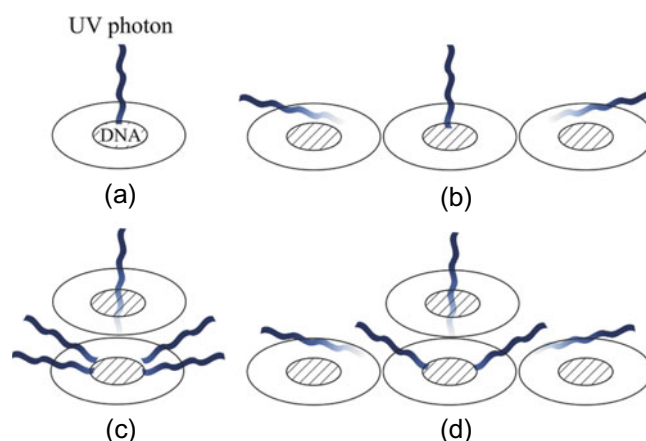
[20] The formation of NO* molecules through the interaction of N and O atoms alone, a two-body reaction, is possible (reactions (4) and (6)), but it can also involve the presence of a third body, namely N$_2$ (reactions (4) and (5) in Sect. 3.3). The probability of forming a NO* molecule is of the order of 10^{-10} (Sect. 3.5).

A remark about spore stacking: SEM micrographs (not presented) show that deposition of spores using a pipette in a single shot leads to a variety of sheltered spore assemblies, located mainly at the periphery of the deposit. The complexity of such a given assembly of spores, in terms of its architecture, increases with the number of spores it comprises. The more complex these assemblies, the less reproducible they are from one independent spore deposit to another. As a result, there can be important statistical variations from one sample to another in the time required to inactivate well-"hidden" spores, which are the very last ones to be inactivated. Hence, passing a straight line through the number of survivors (on a log scale) to try defining the second phase, as in Figure 23 for instance, must be considered as a rough approximation as far as the last few viable spores are concerned.

Further remarks on the nature of the second phase of survival curves. Rossi et al. [33] agree with us on the fact that the second phase is related to stacked spores, but they call on both UV irradiation and etching of the spores for a faster inactivation than with our less aggressive UV approach only. They set a 95% O_2 content in the N_2-O_2 mixture, therefore achieving a high etching rate with a much reduced UV intensity (in the 200–300 nm range), but sufficient to provide a high combined inactivation rate, in fact complete sterilization within 5 min of *B. atrophaeus* spores. In contrast, Akishev et al. [34] suggest that the second phase (stage as they call it) on the survival curve is related to a different type of lesions than in the first phase.

5.1.2 Modeling survival curves and the concept of fluence (dose)

Adapting Cerfs model to bi-phasic survival curves. Cerf proposed to express the decrease in the number of viable microorganisms with time as a first-order rate, with a unique term, in the form [35]:

$$N(t) = N(0)10^{-t/D}, \qquad (7)$$

where D, as already mentioned, is the time required to reduce the number of viable spores by a factor of 10 (1 log) following their exposure to a given biocidal agent. Notwithstanding the preceding remark concerning the second phase of survival curves, we shall assume, as a first approximation, that its inactivation rate can also be represented as a first-order rate (Sect. 5.3). Since photons are, in the present case, the biocidal agent, we write the inactivation rate explicitly as k_iI where I is the UV radiation intensity and k_i, the reaction coefficient (sensitivity), which depends on the type of microorganism and UV wavelength range considered. We then have for a bi-phasic survival curve:

$$N(t) = N_{0\text{-}1} \times 10^{-k_1It} + N_{0\text{-}2} \times 10^{-k_2It}, \qquad (8)$$

where $k_1I = 1/D_1$ and $k_2I = 1/D_2$ are the slopes of phases 1 and 2 on the survival curve, respectively. In this

mathematical representation, N_0, the total number of viable microorganisms at time $t = 0$, can be thought of as resulting from the sum of the initial population densities to be distributed over the first and second phase, respectively:

$$N_0 = N_{0\text{-}1} + N_{0\text{-}2}. \qquad (9)$$

Here, $N_{0\text{-}1}$ sums up not only isolated spores, but also the top ones in stacks, while $N_{0\text{-}2}$ relates to spores shielded from UV radiation by other spores, such as in the case of aggregated and stacked spores, or spores possibly buried in debris. The solid curve in Figure 26 has been drawn from relation (8), the required parameters being extracted from the fitting of the survivor data points in Figure 23. These parameters are displayed in Table 1. The intercept with the Y-axis of the second phase segment defines $N_{0\text{-}2}$: the extrapolated value of $N_{0\text{-}2}$, in the present case, is approximately 8000 (i.e., only 0.08% of an initial deposit of 10^7 spores) and, therefore, $N_0 \approx N_{0\text{-}1}$.

Table 1 shows that the inactivation rate k_2I of the second phase is approximately 10 times smaller than that for isolated spores or top ones in the case of stacked spores; the overall time required to reach sterility is definitely controlled by the second phase.

The concept of fluence (dose). Survival curves resulting from the exposure of given microorganisms to UV
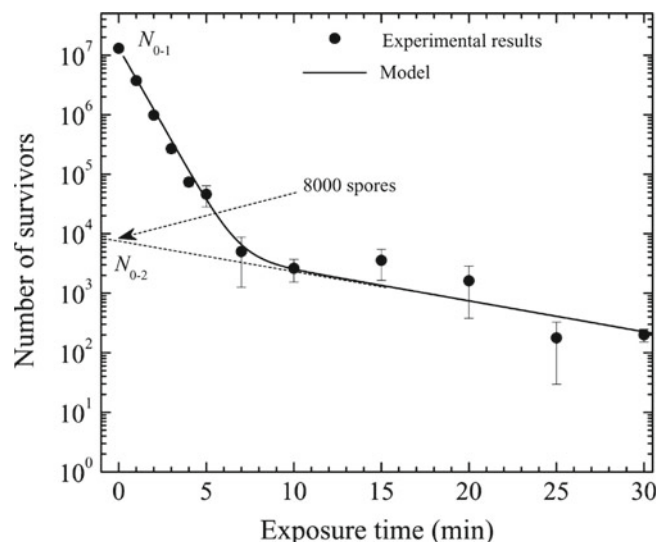

Fig. 26. The solid line on this survival curve is plotted from the modeling expression (8), in which we used the characteristic parameters displayed in Table 1. The data points are originally those of Figure 23. The dotted line is an extrapolation to exposure time zero, indicating the number of stacked spores yet non-inactivated as the second phase begins.

Table 1. Values of the characteristic parameters of relation (8), as obtained from fitting them to the experimental points in Figure 23.

$N_{0\text{-}1}$	k_1I (s^{-1})	$N_{0\text{-}2}$	k_2I (s^{-1})
1.3×10^7	0.52	8000	0.053

irradiation at set intensity levels can be brought into a unique survival curve provided the number of survivors is plotted as a function of UV intensity I times exposure time t, i.e. fluence (photon dose), instead of exposure time, as we demonstrate below.

Figure 27a shows the survival curves for *B. atrophaeus* spores obtained under three different values of UV irradiation intensity, plotted, as usual, as functions of exposure time. The different UV intensities were obtained by varying the percentage of O_2 added to N_2: 0.3% added O_2 yields maximum UV intensity from the NO_γ molecular system, normalized thereafter to unity, 1% O_2 corresponds to a relative intensity of 0.3 and 10% O_2 is $\approx 10^{-2}$ times the value at maximum intensity . These three distinct survival curves can be merged into a single one provided exposure time in the abscissa of Figure 27a is replaced by fluence of the UV photons as shown in Figure 27b. Strictly speaking this fluence value is relative since the UV intensity at maximum intensity has been normalized at unity ($I_{max} = 1$).[21] The unique curve in Figure 27b fits the data points obtained at the three different UV intensities in a particularly outstanding way in the case of the first phase.[22] This is a strong indication that the UV photons are predominantly controlling spore inactivation, whatever the UV intensity levels considered here. This is noteworthy since the density of O atoms increases by approximately a factor of 10 (see Sect. 5.2.1) when the percentage of added O_2 is raised from 0.3% up to 10%: the inactivation rate is apparently not significantly affected by the erosion (etching) of the spores as a result of a larger density of chemically reactive O radicals combined with a much larger exposure time to these radicals than at 0.3% added O_2.

The least-square fit of the second phase on the fluence plot (Fig. 27b), when accounting for the uncertainty bars, is also particularly convincing. It thus again supports, as for the first phase, the predominant role of UV photons on the inactivation process. As we have already written, we are assuming that the second phase is related to "hidden spores", for which we have suggested (Fig. 25) their possible inactivation by UV photons coming out from the interaction of N and O atoms infiltrated, through diffusion, in-between the stacked spores. Since the intensity of the photons generated in-between spores should obey the same dependence on the actual percentage of O_2 added to N_2 in the probability of forming NO^* excited molecules as those from the surrounding gas phase, it seems difficult to

---

[21] A survival curve can thus be plotted either as a function of (exposure) time or, in a more universal way, as a function of fluence. In the first case, the radiation intensity I is constant and $k_1 I$ and $k_2 I$ are the slopes of phases 1 and 2 on the survival curves, $k_1 I$ and $k_2 I$, characterizing the respective inactivation rate. In the second case where the plot is made as a function of the fluence, namely the product It, the slopes of phases 1 and 2 are then simply k_1 and k_2, the reaction coefficients.

[22] In other words, the number of inactivated spores depends upon the total number of photons (the dose) that has reached them, independently of the time it has taken to achieve such a dose.
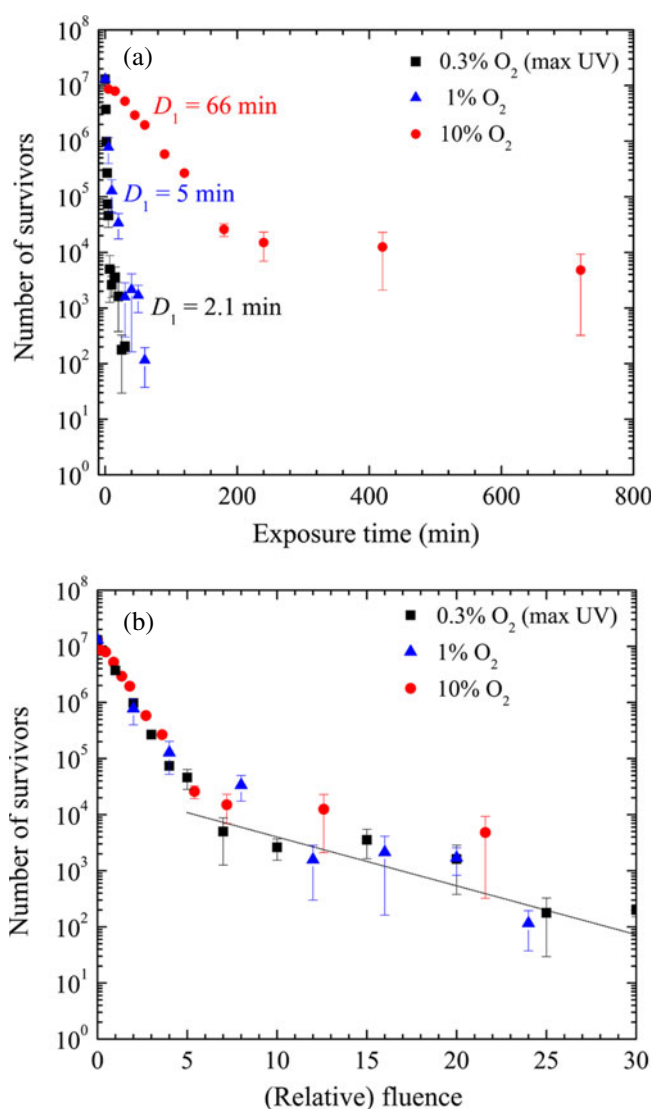

Fig. 27. (a) Survival curves of *B. atrophaeus* spores following their exposure to the N_2-O_2 flowing afterglow at three different UV intensity levels obtained by setting the O_2 admixture percentages to N_2 at 0.3%, 1% and 10%. The D_1 time values for phase 1 are indicated; (b) same survivor data counts as in Figure 27a, but plotted as functions of fluence instead of exposure time. Data extracted from [31] at a substrate temperature of 28 °C.

determine the respective contribution, to the inactivation process, of the NO^* excited molecules formed in the gas phase (outside the stacks) from those formed in-between the stacked spores.

How fluence affects the shape of survival curves. To further illustrate the large, but only apparent, diversity of survival curves when plotted as functions of exposure time (instead of fluence), we look at Figure 28a where three levels of UV intensity are virtually considered, namely full intensity, and then 25% and 10% of it. The shape of the three survival curves, calculated from expression (8), is truly much different one from the others, but in fact these three separate curves, when plotted as a function
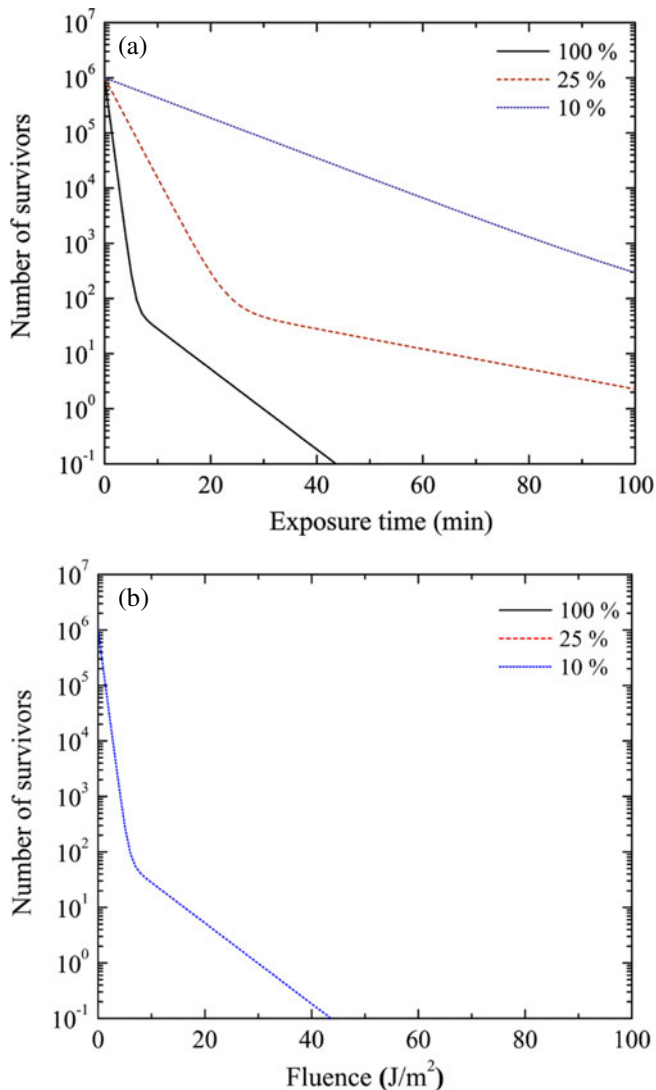
Fig. 28. Calculated number of survivors plotted from relation (8), at three different values of assumed UV intensity: (a) as a function of exposure time; (b) as a function of UV fluence, which then yields three perfectly superposed curves.

of fluence, can be turned into a unique one, as shown in Figure 28b. In that respect, the curve at 10% full intensity in Figure 28a could be considered as a zoomed view of the very beginning part of Figure 28b.

5.1.3 Spectral range of the sporicidal action of UV photons on B. atrophaeus spores

To determine the sporicidal efficiency of the UV photons as a function of their wavelength, we have successively laid four high-pass optical filters on top of the Petri dish, using the filter mount described in Section 4.1.3 (Fig. 13). As mentioned in that section, almost full optical transmission of these filters can be assumed above their cut-off wavelengths, which are 112 nm, 180 nm, 277 nm and 330 nm. At the same time, this arrangement hinders the flow of gaseous species that would otherwise freely enter
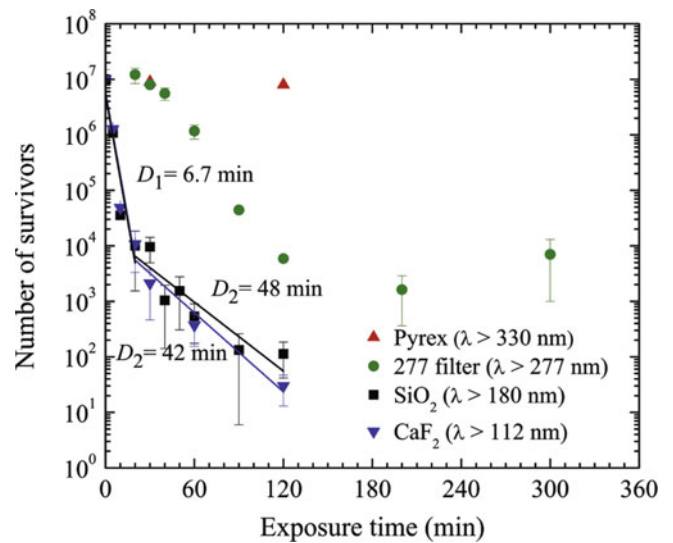

Fig. 29. Corresponding survival curves for *B. atrophaeus* spores deposited on a Petri dish successively covered by four different optical filters using the arrangement in Figure 13, and immersed in the flowing afterglow of a N_2-O_2 discharge. The spore deposit in the Petri dish is located at $z = 105$ mm from the discharge tube axis (Fig. 2), at the chamber entrance (Fig. 8). The Petri dish was maintained at 28 °C, other operating conditions being as in Figure 23.

the Petri dish. Figure 29 shows the four corresponding survival curves obtained for *B. atrophaeus* spores. We note the following:

(i) The use of a CaF_2 window (>112 nm) among the set of high-pass filters considered leads to the highest mortality;

(ii) The SiO_2 high-pass filter (>180 nm) yields a barely lower mortality compared to that recorded with the CaF_2 filter;

(iii) The 277 nm high-pass filter results in a much lower inactivation rate and yields a survival curve with an initial shoulder (lag time)[23];

(iv) With the Pyrex window (>330 nm), close to the full initial number of viable spores is recovered even after a 2 h exposure. This latter result additionally supports the fact that the afterglow particles (e.g., O atoms) do not significantly contribute to spore inactivation if we assume that the filter plate does not ensure a gas-tight sealing of the Petri dish.

These observations support the already generally accepted statement that photons above 300 nm (due to too low their energy) have a significant reduced biocidal action (more on this topic in Sect. 5.1.6 further on). The fact that the level of inactivation does not vary much when capping

---

[23] The absence of spore mortality at the beginning of a survival curve, prior to the first phase and designated as a "shoulder" or lag time, is indicative of an acting repair mechanism: although lesions to the DNA are produced by UV photons the minute they start to be irradiated, the lethal dose (sufficient number of lesions) is only reached at the true beginning of the first phase.

the Petri dish successively with the 112 and the 180 nm high-pass filters indicates that most of the inactivation of *B. atrophaeus* spores is achieved above 180 nm. This is consistent with the combination of the action spectrum of *B. atrophaeus* and the emission spectrum of the NO_γ molecular system, as displayed in Figure 6.

5.1.4 Influence of the operating field-frequency on survival curves

As mentioned earlier, numerical calculations (Sect. 4.1.1) showed that an afterglow chamber having its gas pumping outlet directed along the axis of the gas inlet provides poor uniformity of the active species throughout the chamber as compared to a configuration where the gas pumping outlet is at 90° with respect to the gas inlet: this can be seen by comparing Figure 10f with Figure 10c in the case of the NO(A) concentration. From that moment on, we ceased using the 5.5 L chamber described in Figure 9, which was operated at 2.45 GHz, and equipped instead a 50 L chamber, having its pumping outlet at 90° with respect to the gas inlet, with a 915 MHz surfatron on one tube and a 2.45 GHz surfaguide on the other tube (Fig. 8) for sustaining alternately a surface wave discharge at either frequency [36]. Furthermore, also based on calculations, we chose to use a connecting tube length x_d that was long enough (820 mm) to ensure a pure late afterglow
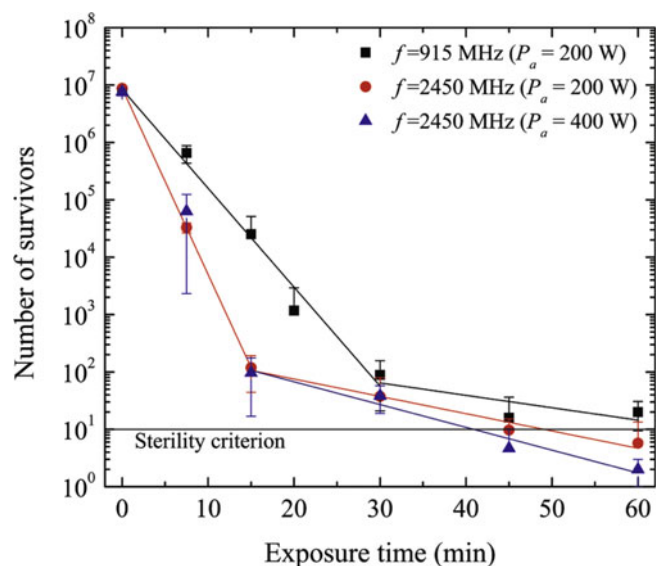

Fig. 30. Survival curves for 10^7 *B. atrophaeus* spores exposed to the flowing afterglow from a N_2-O_2 microwave discharge sustained either at 915 MHz or 2450 MHz, in a 26 mm i.d. tube in the 50 L chamber (Fig. 8). Operating conditions were optimized for maximum UV intensity (N_2-0.2% O_2 at 3.5 torr ($\approx$470 Pa)) and axial uniformity (1.4 sLm N_2 flow) under conditions of a pure late afterglow ($x_d = 820$ mm). Absorbed microwave power is either 200 W at both frequencies or 400 W at 2450 MHz, i.e. a P/V ratio of 4 and 8 W/L respectively. The safety assurance level of 6 logs is reached after 60 min at 2450 MHz.

Table 2. Decimal times corresponding to the survival curves in Figure 30.

		D_1 (min)	D_2 (min)
915 MHz	200 W	5.8 ± 0.4	$46(+130/-20)$
2450 MHz	200 W	3.1 ± 0.1	33 ± 4
2450 MHz	400 W	3.1 ± 0.1	25 ± 4

within the whole process chamber. The survival curves obtained under these operating conditions, at both 915 and 2450 MHz with 200 W absorbed power ($P/V = 4$ W/L), are shown in Figure 30. In addition, the survival curve obtained at 2450 MHz with twice the power, i.e. 400 W, is also displayed.

Regarding the results obtained at 200 W at both 915 and 2450 MHz, the following features are noteworthy:

(i) D_1, the decimal time of the first phase, is within uncertainty bars twice shorter at 2450 MHz than at 915 MHz for the same absorbed power (Tab. 2), while the average intensity ratio for the whole NO_γ spectral range is in fact only 1.35 times higher at 2450 MHz (Fig. 7);

(ii) Assuming the UV photon flux to increase almost proportionally with absorbed power when provided by two plasma sources sustained with 250 W each (Fig. 12b and footnote 13), the UV emission intensity at 500 W $= 2 \times 250$ W should be higher by a factor of 2.5 when compared to that at 200 W. This implies that the D_1 time of 5.8 min in Figure 30 (Tab. 2 at 200 W) should drop by the corresponding power ratio to 2.3 min, while the observed D_1 time is actually 2.1 ($\pm$0.1) min (at 28 °C) in Figure 23;

(iii) In the present set of experiments, four Petri dishes were exposed simultaneously, located on the "floor" of the afterglow chamber along the discharge axis, two on each side of the pumping orifice (at $x = 100, 240, 370$ and 510 mm: chamber full length is 610 mm). The uncertainty bars related to the data points are particularly small (slightly smaller than at 915 MHz), suggesting a more uniform inactivation rate than in Figure 23;

(iv) The extrapolated value $N_{0\text{-}2}$ for the second phase in Figure 30 is much lower ($\approx$200 spores) than in Figure 26 ($\approx$8000 spores). We attribute this decrease partially to the fact that the larger x_d value in Figure 30 ensures a 1.5 higher UV intensity than in Figure 23, as shown in Figure 18.

Concerning the two survival curves for 2450 MHz plotted at 200 and 400 W in Figure 30, Table 2 indicates that their D_1 value is the same at both 200 and 400 W, with a slightly shorter D_2 time at 400 W. Referring to the variation of UV intensity as a function of microwave power in Figure 12b, we would have expected a higher inactivation rate at 400 W by at least a factor of 1.35. The only real advantage of raising the power from 200 to 400 W in the present case is achieving a safer margin on the SAL criterion.

10001-p23

5.1.5 Bacillus atrophaeus, the endospore most resistant to inactivation by the N$_2$-O$_2$ discharge flowing afterglow used as bio-indicator (BI)

As a rule, research groups working on sterilization/disinfection use bacterial endospores as bio-indicators (BI) to characterize the inactivation efficiency of their apparatus since these are known to be the most resistant types of microorganisms. However, given a plasma system, it is not yet always clear which is the most resistant spore among the set of usual (non-pathogenic) spores available. To resolve this matter, three of them have been exposed to the N$_2$-O$_2$ discharge flowing afterglow system, Figure 31 displaying their survival curve under our operating conditions. *Geobacillus stearothermophilus* is much more easily inactivated than *B. atrophaeus* (formerly *B. subtilis*): the initial number of *G. stearothermophilus* spores is reduced by 7 logs in 60 min while approximately one log less (5.9 logs) is reached with *B. atrophaeus*. However, *B. atrophaeus* and *B. pumilus* spores present a similar number of viable spores after a 60 min exposure. Nonetheless, *B. atrophaeus* having the longest decimal time for its first phase is retained as the most resistant BI. This choice is further influenced by the fact that *B. atrophaeus* is the most commonly used spore as BI for testing sterilizing/disinfecting systems based on UV radiation [16], as is the case with the present N$_2$-O$_2$ flowing afterglow.

Exposing these spores in the 50 L chamber, instead of the 5.5 L one as was done for the present Figure 31, would have resulted in smaller uncertainty bars, as can be seen by comparing the survival curves for *B. atrophaeus* in Figures 30 and 31 for a 2450 MHz discharge flowing afterglow.
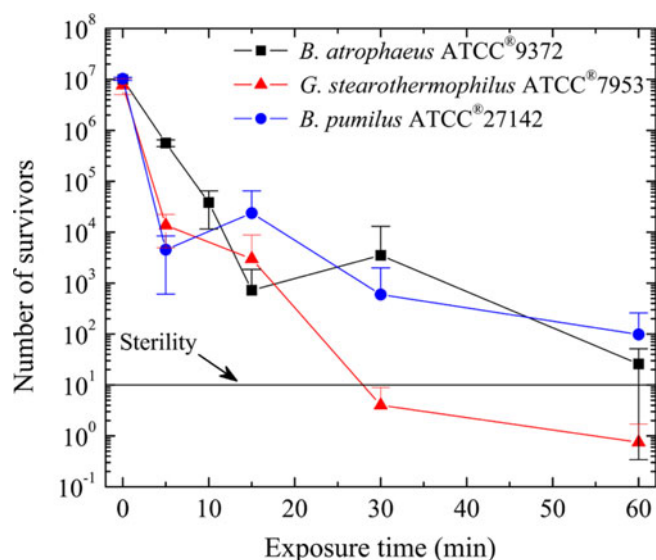

Fig. 31. Survival curves for three different (non-pathogenic) endospores subjected to the N$_2$-O$_2$ flowing afterglow from a discharge sustained at 2.45 GHz with 120 W absorbed power in N$_2$ at 800 sccm and comprising 3 sccm of O$_2$ (0.37% O$_2$ in the N$_2$-O$_2$ mixture). The pressure in the 5.5 L chamber (Fig. 9) is 5 torr ($\approx$670 Pa).

Table 3. Percentage of the spores inactivated after a 15 min exposure to the N$_2$-O$_2$ discharge flowing afterglow, when the spore deposit in the Petri dish is free from any filter as compared to the Petri dish being successively capped with a given high-pass filter. 99.99% correspond to the total number of spores inactivated without any filter atop the spore deposit. Since the high-pass filters hinder the flow of metastable-state atoms/molecules and ions, if any, from the gas phase to the spore deposit, spore inactivation can then be essentially attributed to UV photons. In the specific case of *B. atrophaeus* the larger uncertainty bars are strongly dependent on the initial number of spores in the deposit, which varies. Operating conditions are as in Figure 31.

	B. pumilus	*B. atrophaeus*	*G. stearothermophilus*
No filter	99.99 ± 0.01	99.99 ± 0.01	99.99 ± 0.01
$\lambda > 112$ nm	99.97 ± 0.06	96 ± 6	99.97 ± 0.04
$\lambda > 180$ nm	99.9 ± 0.2	96 ± 5	99.97 ± 0.04
$\lambda > 277$ nm	96 ± 2	92 ± 8	99.9 ± 0.1
$\lambda > 330$ nm (Pyrex)	48 ± 10	89 ± 5	75 ± 6

5.1.6 Corresponding inactivation wavelength range for the three types of spores tested in Sect. 5.1.5

Table 3 shows that approximately 50% of the deposited *B. pumilus* spores are still viable when the photon wavelength is higher than 330 nm (Pyrex high-pass filter) while, in contrast, 89% of the *B. atrophaeus* spores are then inactivated. Full mortality of the *G. stearothermophilus* spores extends at longer wavelengths than for the two preceding spores, decreasing suddenly somewhere in-between 277 and 330 nm. These results clearly indicate that the efficient inactivation of different species of spores benefits from broad-wavelength UV emission, which is in fact what is provided by the N$_2$-O$_2$ flowing afterglow through essentially its NO$_\gamma$ and NO$_\beta$ molecular systems (Sect. 3.2, Figs. 4 and 6).

5.1.7 Influence on the inactivation rate of B. atrophaeus spores due to the reduction of the N and O atom concentrations in the afterglow chamber as a result of their surface recombination on given materials

Table 4 displays the decimal time of the first phase of the survival curve of *B. atrophaeus* spores as a function of the nature of the recombining plates introduced in the afterglow chamber (see Sect. 4.4). The Petri dish location with respect to the plates is indicated in Figure 15b.

Somehow unexpected, the spore inactivation rate is higher (lower D_1 time) when the Teflon plates are present than in the empty chamber. This contrasts with the fact that according to Figure 20 the UV intensity at maximum is quite the same in the empty chamber and with the Teflon plates in.[24] A possible, partial, explanation can

---

[24] The D_1 values obtained in the empty chamber and with the aluminum plates present in the chamber are the same within uncertainty bars.

Table 4. Decimal time of the first phase of the survival curve of *B. atrophaeus* endospores exposed to the flowing afterglow of the N_2-O_2 discharge in the presence of a group of four plates of a given material in the chamber (Sect. 4.4) as compared to the empty chamber. Operating conditions: discharge sustained at 2.45 GHz with 100 W absorbed power, which converts into $P/V = 2$ W/L in the 50 L chamber, where the gas pressure is 2 torr ($\approx$270 Pa) [24].

	D_1 time (min)	Added O_2% for max. UV
Empty chamber	12.0 ± 0.5	0.6
Group of 4 plates		
Teflon	9.9 ± 0.7	0.6
Aluminum	10.7 ± 1.4	0.8
Stainless steel	12.8 ± 1.0	0.8
Copper	17.1 ± 1.0	1.0

Table 5. Observed surface temperature on the tested plates after an hour of exposition to the N_2-O_2 flowing afterglow with the percentage of added O_2 set for maximum UV intensity. Operating parameters as in Table 4.

Teflon	50 °C
Aluminum	35 °C
Stainless steel	50 °C
Copper	35 °C

be related to the heating of the plates due to surface recombination (an exothermic reaction): Table 5 shows that the Teflon surface reaches a temperature of 50 °C after an hour of exposition to the flowing afterglow. It suggests that the temperature of the gas phase could increase when the recombining plates are in position as compared to the empty chamber: even though the temperature also rises on the walls of the empty chamber, gas heating is more important with the plates in since the recombining surface area is then 50% greater. In such a case, the temperature of the spores deposited in the Petri dish would also reach higher values, compared to the case of the empty chamber, increasing the inactivation rate, as documented in Section 5.3. In contrast to the experiments reported in Section 5.3, the temperature of the Petri dish in the present series was not controlled, the temperature rising freely with time, before reaching a plateau.

5.2 Assessing the influence of the species specific to the early afterglow and to the late afterglow of the N_2-O_2 discharge on polymer damage and spore erosion

As discussed in Section 3.1, the early afterglow of a N_2-O_2 discharge is comprised of N_2^+, N_4^+ and NO^+ ions together with $N_2(A)$, $N_2(a')$ and $O_2(^1\Delta_g)$ metastable-state molecules. These species by themselves, and some of them in combination with UV photons (photoexcitation), can lead to a significant erosion of polymers (and to structural damage to microorganisms) and, as such, they might have a detrimental effect on the processed MDs. This is why it

is essential to reduce as much as possible the concentration of these adverse particles by striving to achieve, at least, a predominant late afterglow if not a pure late afterglow. In a pure N_2-O_2 late afterglow (implying elapsed traveling time of particles from discharge exit greater than 10 ms, largely achieved with a connecting tube distance $x_d = 820$ mm), calculations predict, besides N and O atoms, the presence of essentially $O_2(^1\Delta_g)$ metastable-state molecules (Fig. 3a), which are known to be highly reactive. Together with O atoms, these species seem to be essential for achieving some specific processes with our afterglow system (see Sect. 6).

5.2.1 Damage related to species from the early afterglow

Damage to a polymer (polystyrene). To evidence the action of early afterglow species and localize them within the afterglow chamber, we examine the level of damage inflicted to microspheres of polystyrene of approximately the same size (with less dimensional dispersion) as our reference spores. Polystyrene microspheres, contrary to spores, are of a uniform composition throughout, which facilitates interpretation of their erosion. In particular, erosion of the microspheres is expected to be linear with exposure time, in contrast to what happens with spores due to variations in their composition (e.g., coats) as etching progresses [37].[25] The microsphere approach is, therefore, of particular interest to get reliable erosion data when the O_2 content is small, say below 1%, and strongly dependent on small variations of the added O_2 percentage and position in the chamber. This study is furthermore indicative of the possible level of damage that could be experienced by polymer-based MDs, depending on their position in the chamber, when subjected to our sterilization/disinfection technique.

Figure 32 shows a set of micrographs from scanning electron microscopy (SEM) of polystyrene microspheres subjected for 2 h to a 2.45 GHz N_2-O_2 discharge afterglow. The percentage of admixed O_2 was set at 1%, in a 2 sLm N_2 gas flow, to achieve maximum UV intensity at 2 torr ($\approx$270 Pa). The top pairs of micrographs in Figure 32 are for a tube connecting the plasma source to the chamber entrance of length $x_d = 170$ mm, while the middle pair is for $x_d = 240$ mm. In the left columns, the microspheres are located at the discharge axis, close to the chamber entrance ($z = 0$, $x = 15$ mm: see Figure 2 for coordinates, chamber full length is 600 mm) and, in the right column, the microspheres are at the same distance from the chamber entrance ($x = 15$ mm), but below the axis, at $z = 50$ mm, with the "floor" of the chamber situated at $z = 150$ mm. The bottom micrograph in the set of figures corresponds to unexposed microspheres.

For $x_d = 170$ mm, the microspheres located on the axis are disrupted while, comparatively, only weakly eroded off

---

[25] In that respect, Crevier [37] presented results of erosion of *B. atrophaeus* spores as functions of exposure time under 10% O_2, displaying three different etching rates: 2 nm/min from time zero to 30 min, 17 nm/min from 30 to 40 min and 0.4 nm/min above 40 min (data not presented).
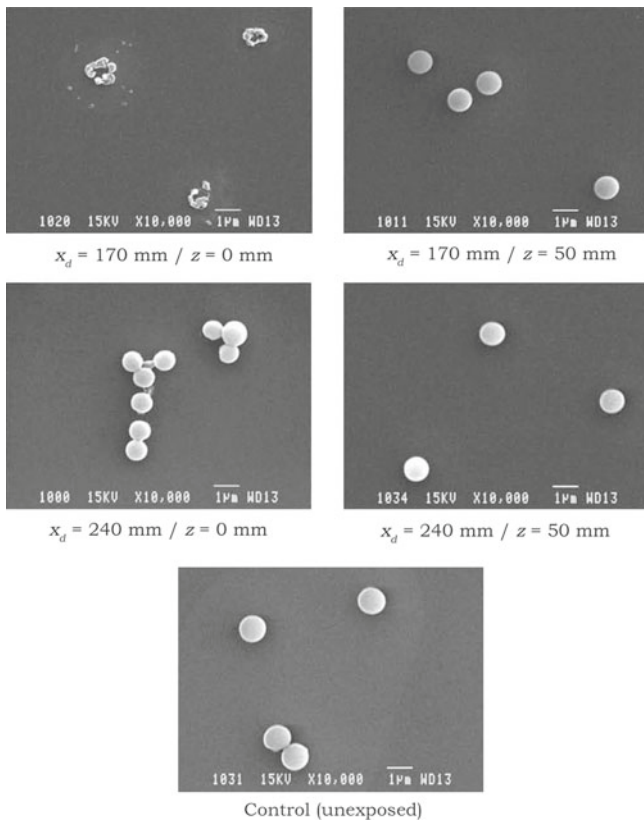
Fig. 32. SEM micrographs of polystyrene microspheres deposited on glass plates (from a water suspension and left to dry) and subjected for 2 h to a 2.45 GHz 100 W ($P/V = 2$ W) N_2-O_2 discharge afterglow in the 50 L chamber. The percentage of admixed O_2 was set at 1% to achieve maximum UV intensity at 2 torr ($\approx$270 Pa) in the chamber under a 2 sLm N_2 gas flow. The first and second rows of micrographs are for $x_d = 170$ mm and 240 mm, respectively, which is the length of the tube connecting the plasma source to the chamber entrance. In the left columns, the microspheres are located at the discharge axis, close to the chamber entrance ($z = 0$, $x = 15$ mm: see Fig. 2 for coordinates, chamber full length is 600 mm) and, in the right column, the microspheres are below the axis but at the same distance from the chamber entrance ($z = 50$ mm (bottom of the chamber at $z = 150$ mm), $x = 15$ mm). The single micrograph in the third row corresponds to unexposed microspheres [26].

axis. In contrast, with $x_d = 240$ mm, the microspheres located on the axis retain their initial shapes, although they are heavily eroded as compared to those located off axis. Table 6 provides a quantitative evaluation of the microsphere erosion. It indicates that, to avoid damaging the devices to be sterilized, these should not be located on the axis unless the plasma source distance x_d is large enough.[26] The spatial distribution of the level of damage by the early afterglow species in the chamber corresponds, in fact, to the slightly divergent cylindrical beam drawn in Figure 2. This beam is represented as dying out within

---

[26] From calculations (after [12]), ensuring a "pure" late afterglow in the chamber requires x_d to be longer than 600 mm: we have actually set x_d at 820 mm.

Table 6. Measured diameter of the polystyrene microspheres as a function of their position in the chamber, following their exposure to the N_2-O_2 afterglow under conditions of Figure 32 (statistics on 15–20 microspheres) [26].

x_d (mm)	x (mm)	z (mm)	Diameter (μm)
170	15	0	Disrupted
	15	50	0.93 $\pm$0.01
240	15	0	0.84 $\pm$0.02
	15	50	0.95 $\pm$0.01
Unexposed (control)			1.05 $\pm$0.01

the chamber as functions of the axial distance x from the chamber entrance and distance z from the discharge axis down the chamber. The late afterglow dominates outside this beam flow, as we already mentioned.

A further way of reducing the presence of possible early afterglow species would be to "break the beam" (depicted in Fig. 2) by installing a fused silica plate a few mm away from the aperture of the chamber entrance and perpendicularly to it, or any other kind of beam deflector: ions would possibly recombine on it into neutral particles and metastable-state molecules probably de-excite as they hit the plate, while most N and O atoms would bounce off such a fused silica surface (on which surface recombination loss is less than 1%) and go on diffusing throughout the chamber.

Damage to spores. Figure 32 has provided strong indications that species from the early afterglow are involved in the erosion of the polystyrene microspheres, since this phenomenon is observed to decrease both off-axis and far away from the chamber entrance. Indeed, this behavior agrees with the assumed beam-like dispersion of these species, depicted in Figure 2, as they flow into the chamber. Figure 33 shows that, within experimental uncertainties, there are no real differences in the O-atom concentration obtained with either length x_d of the connecting tube, while the concentration of the species involved in erosion (besides N and O atoms) is known to decrease as the length x_d of the connecting tube increases (assume a longer elapsed time in Fig. 3a).

Although the percentage of added O_2 at maximum intensity is low ($\approx$0.3–1%), it nonetheless corresponds to some 10^{14} atoms cm^{-3}, as indicated in Figure 33. The concentration of the O atoms increases approximately linearly as the percentage of added O_2 is raised past 1% up to 5% (Fig. 33) and, in fact (not shown), up to 10%: the O-atom concentration at 10% O_2 is at least 10 times that at 0.3%. The question then naturally arises as to a more significant contribution of O atoms to erosion at such a higher concentration. To assess such a possible effect of these radicals, knowing that they diffuse throughout the chamber (Sect. 4.1.1), we have recorded the damage incurred by spores at 10% added O_2 as a function of position in the chamber.
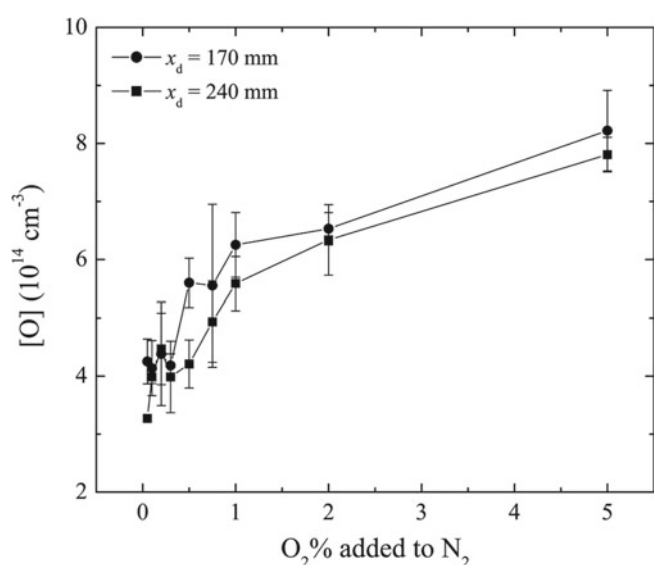
Fig. 33. Concentration of O atoms as a function of the percentage of O_2 added to N_2 in the 50 L afterglow chamber, as measured by NO titration with the NO gas introduced through the gas inlet located at the chamber entrance, as shown in Figure 15a. Operating conditions: 2 sLm of N_2 at a pressure of 2 torr ($\approx$270 Pa) in the chamber before any addition of O_2, discharge sustained at 2450 MHz with an equivalent power density in the afterglow chamber of 2 W/L [26].

Figure 34 shows SEM micrographs of *B. atrophaeus* spores taken after a 2 h exposure to the N_2-O_2 flowing afterglow of a 915 MHz discharge ($P/V = 6$ W/L) with 10% added O_2; the pressure in the 50 L chamber is 5 torr ($\approx$670 Pa) and the distance x_d from the surfatron gap to the chamber entrance lies approximately between 100 mm and 150 mm.[27] The Petri dish into which the spores are deposited is positioned at an axial distance $x = 100$ mm from the chamber entrance and at different heights z downward the discharge axis (see Fig. 2 for coordinates). The damage to spores in Figure 34, essentially a reduction in size due to erosion, varies spatially in the same way as the erosion of the polystyrene microspheres at 0.3% added O_2: damage is at its maximum on the axis and it decreases away from it. Having increased the percentage of added O_2 from 0.3% to 10% has not qualitatively modified the spatial variation of erosion [38]. We therefore conclude that the O atoms, which are assumed to be uniformly distributed within the chamber as a result of diffusion (case of a chamber with bottom pumping outlet: Fig. 10a), are not responsible, at least not alone, for the observed damage.

We end this section by plotting through the same beam-like shaped region, the spore width, confirming that its erosion rate, at a given distance from the chamber entrance, indeed decreases with the height z of the Petri dish. The average width of an unexposed *B. atrophaeus* spore is 700 nm [3], comprising an inner coat in the

---

[27] In the first sets of experiments performed in our laboratory (<2003), no special attention was paid to the plasma source distance to the chamber entrance. In fact, it was too short ($x_d < 150$ mm) to ensure a pure late afterglow.
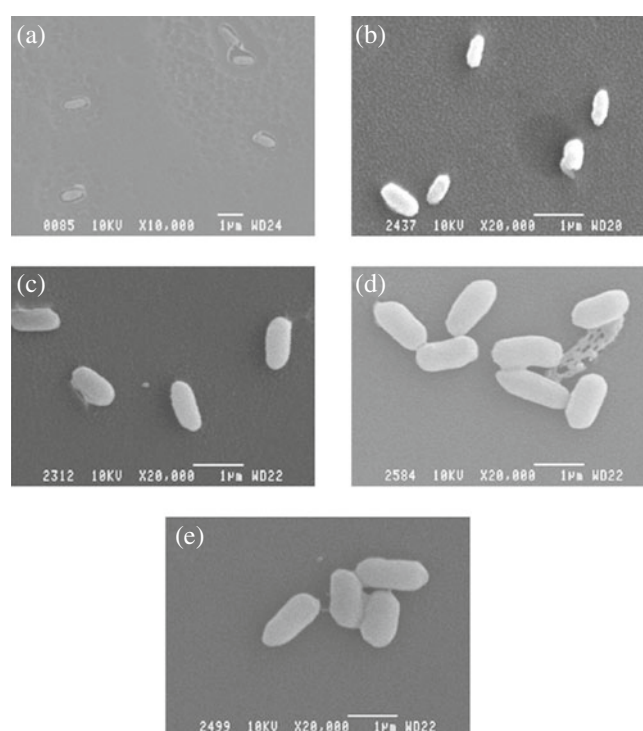

Fig. 34. SEM micrographs of *B. atrophaeus* spores taken after a 2 h exposure to the flowing afterglow from a N_2-O_2 discharge with 10% added O_2 in a 50 L chamber with $x_d \approx$ 100–150 mm, at an axial distance $x = 100$ mm from the chamber entrance and at different heights z: (a) 15 mm ; (b) 28 mm ; (c) 41 mm; (d) 54 mm; (e) 67 mm (bottom of the chamber is at $z = 150$ mm). The discharge is sustained in a 26 mm i.d. tube at 915 MHz with a power of 300 W ($P/V = 6$ W/L) [38].

20–40 nm range and an outer coat in the 40–90 nm range. Figure 35 shows that spore erosion is strong close to the tube axis ($z = 0$), the spore width in fact being trimmed down to more than half its original value (region 1), while for 30 mm $< z <$ 54 mm (region 2), the erosion rate significantly slows down with increasing z, and finally for $z > 54$ mm (region 3), this rate is relatively low. The weak decrease of the spore width in region 3, which in fact should extend up to the spore actual width (700 nm), could correspond to the successive etching of the outer and inner coats of the spore.

5.2.2 Level of damage inflicted to packaged and unpackaged spores in the late afterglow as a means of determining the respective role of the N and O atoms and of the $O_2(^1\Delta_g)$ metastable-state molecules composing it

To enforce our strategy of a sterilizer/disinfector that would not damage MDs, we need to set operating conditions such that the process chamber is predominantly, if not only, filled by species in the late afterglow mode, namely N and O atoms accompanied by $O_2(^1\Delta_g)$ metastable-state molecules. Figure 3a shows that $N_2(A)$ and $N_2(a')$ metastable-state molecules should still be present along the connecting tube in the late afterglow mode
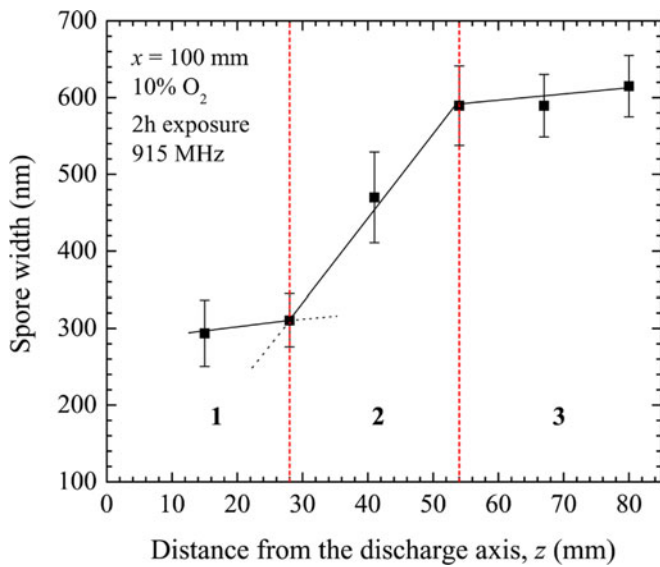
10001-p27

Fig. 35. Variation of *B. atrophaeus* spore width as a function of height z from the discharge axis (divided in three erosion rate regions), at an axial distance $x = 100$ mm from the chamber entrance, under operating conditions of Figure 34 [38]. The width of unexposed *B. atrophaeus* spores is approximately 700 nm.

(elapsed time greater than 10 ms), but with a concentration at least three orders of magnitude lower than in the early afterglow regime. These metastable-state molecules are furthermore going to be quite rapidly quenched in the gas phase within the chamber and vanish since they cannot regenerate, in contrast to the $O_2(^1\Delta_g)$ metastable-state molecules, which can do so by O atoms reassociation (Sect. 3.1).

As will be exposed more completely further on (Sect. 5.4), the pouch material that best withstands exposure to our N_2-O_2 flowing afterglow happens to be a non-porous polymer, such a pouch thus needing to be unsealed from the beginning till the end of the process. Nonetheless, the pouch opening can be made very small (typically 5 mm in length, <1 mm in width) and still allows the N and O atoms to enter it almost freely (the heterogeneous surface recombination of N and O atoms on the elected material is much less than 1% (Sect. 5.4)). In contrast, the $O_2(^1\Delta_g)$ metastable-state molecules apparently barely succeed in going into the pouch through such a narrow opening without being quenched. The efficiency of such a quenching is supported by the fact that the structure of spores in packaged Petri dishes is barely affected, which is not the case when they stand outside the pouch (Sect. 5.4.3). As a matter of fact, this provides us with two possible situations regarding exposure of objects in the afterglow: a packaged item is essentially subjected to UV photons only while, when unpackaged, $O_2(^1\Delta_g)$ metastable-state molecules can additionally act on it. By examining a given process under these two sets of conditions, we are able to determine whether the treatment is achieved as a result of the action of UV photons alone or whether it also requires the contribution of some reactive species, believed to be oxygen singlet, as will be exemplified in Section 6.

5.3 Raising the temperature of B. atrophaeus spores irradiated by UV photons increases their inactivation rate (heat and UV photon synergy effect)

All the so-called low-temperature sterilization techniques, which mainly rely on biocidal molecules (e.g. ethylene oxide, H_2O_2, O_3), are operated at temperatures in the 50 to 65 °C range but not exceeding much 65 °C, essentially to enhance the chemical reactivity of these molecules, thereby reducing sterilization time, still without damaging thermosensitive MDs. The temperature-controlled Petri dish holder shown in Figure 13 was used in the set of experiments that follows. It was checked that heat must be applied to the Petri dish simultaneously with UV photons to observe any increase of inactivation rate: pre-heating or post-heating independently of UV photons does not increase the inactivation rate [31].

To express the dependence of the survival curves on the Petri dish temperature, we suppose an Arrhenius-type dependence of the reaction coefficient α_T at temperature T. Consider, in general terms, a chemical reaction occurring between molecules A and B yielding a molecular product AB:

$$A + B \rightarrow AB. \tag{10}$$

The corresponding reaction rate can be expressed as

$$k_{AB} = \alpha_{AB} n_A n_B, \tag{11}$$

where n_A and n_B are the concentrations of molecules A and B.

Assuming the rate coefficient α_{AB} to obey an Arrhenius law, it is written as

$$\alpha_{AB} = A(T) \exp\left(-\frac{E_a}{RT}\right), \tag{12}$$

where $A(T)$, the pre-exponential term, usually only weakly depends on T, the temperature expressed in kelvin (K), E_a is the activation energy (J K^{-1}), R is the molar gas constant (J mol^{-1} K^{-1}). Since we wish to fit such dependence on survival curves where the ordinate is a log scale, we express it as

$$\alpha_{AB} = \ln A - \frac{E_a}{R}\frac{1}{T}. \tag{13}$$

Designating by α_{T_1}, the reaction coefficient at temperature T_1 (K), and α_{T_2}, the reaction coefficient at temperature T_2 (K) and assuming $A(T)$ not to vary over a relatively small range of T values (12–68 °C), we can write:

$$\frac{\alpha_{T_1}}{\alpha_{T_2}} = \exp\left(-\frac{E_a}{R}\left(\frac{1}{T_1} - \frac{1}{T_2}\right)\right), \tag{14}$$

where, we set

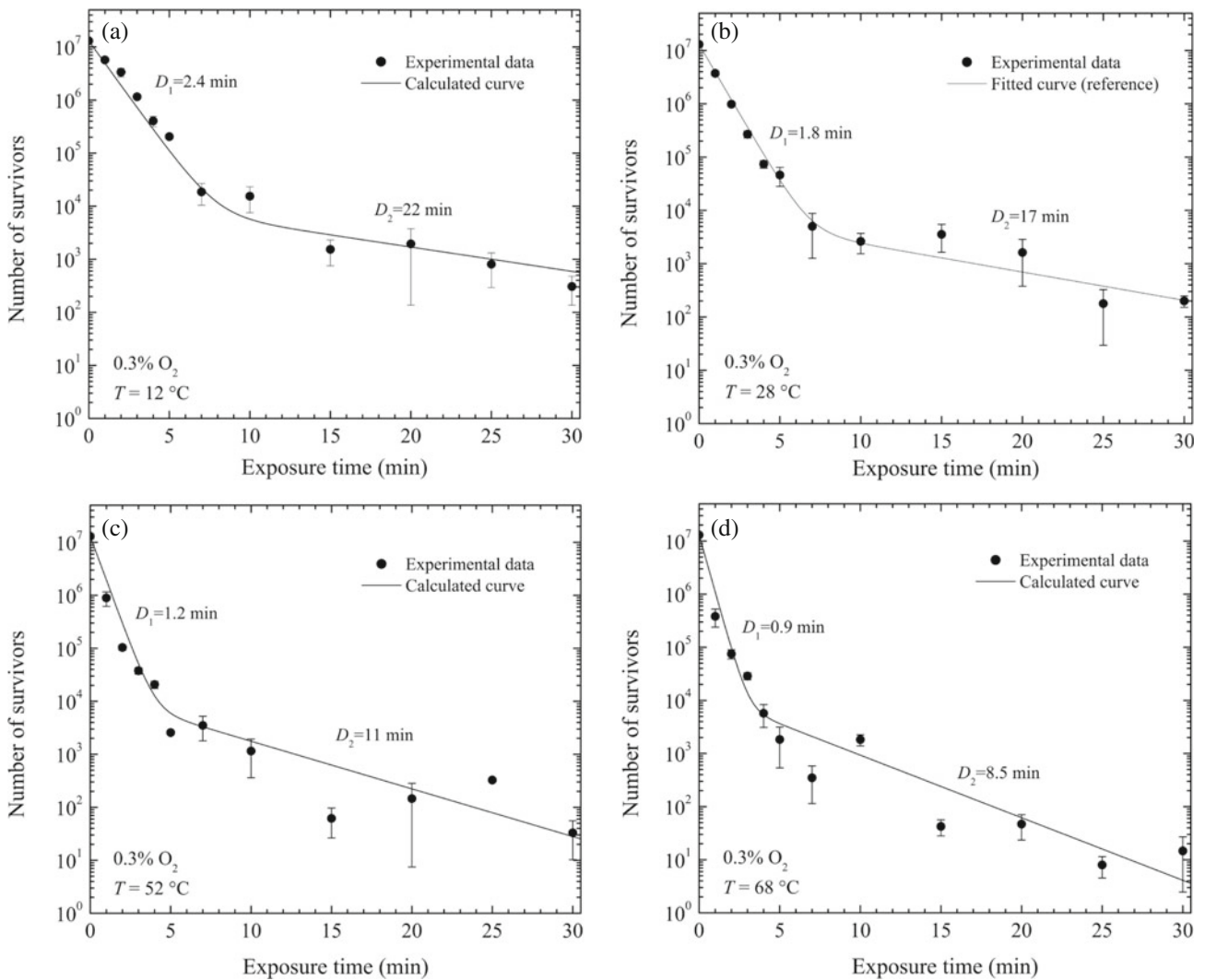$$\theta = \exp\left(-\frac{E_a}{RT_1T_2}\right), \tag{15}$$

Fig. 36. Survival curves for 10^7 *B. atrophaeus* spores exposed to the afterglow, from a discharge in a N_2-O_2 gas mixture with 0.3% O_2 added to N_2 (maximum UV intensity conditions). During the full period of UV exposure, the Petri dishes are kept alternately at four different temperatures: (a) 12 °C, (b) 28 °C, (c) 52 °C and (d) 68 °C. The location of the Petri-dish holder in the chamber is indicated in Figure 8. Other operating conditions as in Figure 23 [31]. The present D_1 and D_2 values come out from the model while in Figure 23 they corresponded to the best fit of the data points.

and T_2 is assigned the ambient temperature. Therefore, the rate coefficient at a given temperature T with respect to that at ambient (28 °C) can be represented as

$$\alpha_T = \alpha_{28} \times \theta^{(T-28)}, \tag{16}$$

where T is, this time, expressed in Celsius degrees.[28]

Figure 36 shows a set of survival curves plotted from Cerf's model (relation 8) at different Petri dish temperatures, calling on the parameter θ:

$$N = 1.3 \times 10^7 \times 10^{-0.55t\theta^{(T-28)}} + 14000 \times 10^{-0.06t\theta^{(T-28)}}. \tag{17}$$

Another aspect of this increased inactivation efficiency with T_1 can be summarized by plotting the number of

survivors following a 30 min exposure. Figure 37 shows that this number is reduced by one more log when the substrate temperature is raised from 28 °C to 68 °C. The operating conditions are those of Figure 23.

To elucidate the observed increase in inactivation efficiency with T_1, we plotted Figure 38, which represents the fluence needed for inactivating, say 2 logs[29] of *B. atrophaeus* spores as a function of the Petri dish temperature. We note that:

(i) The values of the required fluence to achieve a 2-log inactivation as functions of T_1, obtained either at maximum UV intensity or at half-maximum intensity (1% added O_2), are quite the same;

---

[28] Recall that $\exp(ap)$ where a is a real number and p a relative integer can be expressed as $\exp(a)^p$.

[29] To be exact, it is the fluence required to reduce the number of viable spores from 1.3×10^7 to 10^5.
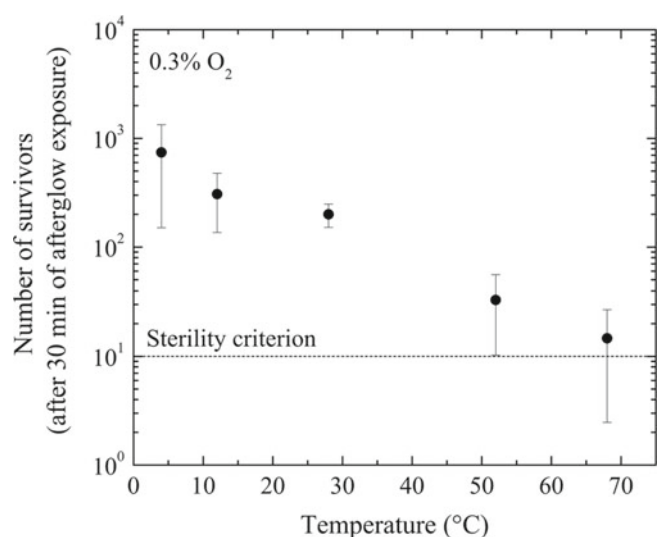
Fig. 37. Number of viable *B. atrophaeus* spores as a function of the Petri-dish temperature for a 30-min exposure to the N_2-O_2 afterglow under maximum UV intensity conditions. The data points are extracted from the set of survival curves in Figure 36, with the addition of the corresponding number of survivors at 4 °C. The 6-log sterility assurance level (SAL) criterion requires that there be less than 10 viable spores when starting from a 10^7 spore deposit [31].
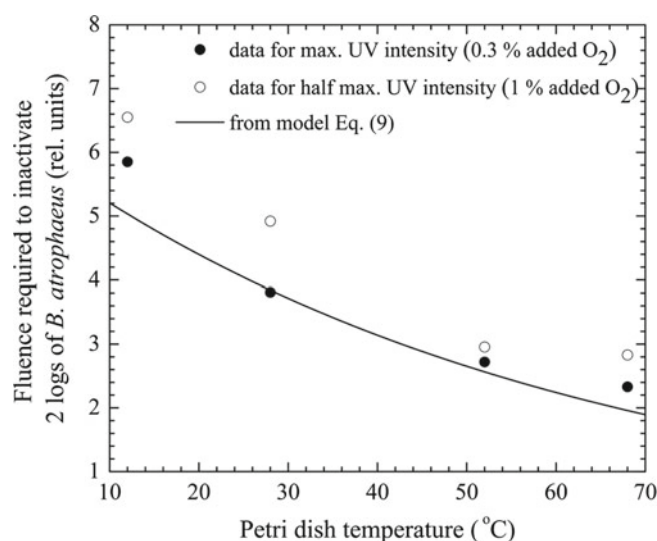

Fig. 38. Fluence required to inactivate 2 logs of *B. atrophaeus* endospores as a function of the Petri dish temperature, either at maximum UV intensity (0.3% added O_2) or at half-maximum intensity (1% added O_2). The full curve is theoretical, as plotted from relation (17).

(ii) The full curve is obtained from the model (relation (17));
(iii) The 2-log fluence value decreases approximately by a factor of 3 from 28 °C to 68 °C., i.e. less photons are required to achieve the same degree of inactivation.

Table 7. Activation energies obtained at different percentages of O_2 added to N_2 [31].

%O_2	0.3%	0.3% with filter	1%	10%
E_a (kJ mol^{-1})	12 ± 1	13 ± 2	14 ± 2	14 ± 13

As discussed in [31], the role of heat is to provide the energy required to surmount the potential barrier(s) encountered as the chemical reaction, initiated by photon excitation, proceeds. The energy barrier corresponds to molecular (conformation) rearrangement occurring after photoexcitation, as the reaction develops to reach the final chemical state creating the lethal damage to the spore DNA strands. The higher the thermal energy provided, the higher the probability of overcoming all the (small) potential barriers along the chain of events, leading to the final stage of the lesion. As a result, partially hidden spores (in a stack for example), but given additional thermal energy, can be inactivated with less incident photons, i.e. more efficiently.

A further confirmation of the validity of our modeling comes from the fact that the activation energy E_a stemming from relation (17) for spores exposed to three different (normalized) values of UV intensities namely 1, 0.5 and $\simeq 10^{-2}$ corresponding to different percentages of O_2 added to N_2, respectively, 0.3, 1 and 10% and normalized to unity at maximum intensity (see [31]), takes the same value within uncertainty bars (13 kJ mol^{-1}), as displayed in Table 7. Furthermore, when capping the Petri dish by putting atop a "CaF$_2$ window" (112 nm high-pass filter), which considerably reduces the afterglow particle flow to the spore deposit, a similar value of activation energy nonetheless comes out. This further proves that the observed heat synergy is related to UV photoexcitation exclusively, not to particles.

The value of the activation energy just deduced is approximately 13 kJ mol^{-1} (54 kcal mol^{-1}), a fairly small energy value compared with that provided by photoexcitation, which we estimate to be in the 105–110 kJ mol^{-1} ($\approx$440–460 kcal mol^{-1}) range, a usual value for many chemical reactions.

Spores exposed (for 30 min) to UV radiation in a highly oxidative flowing afterglow (N_2-10% O_2 discharge) are eroded, but the observed degree of erosion is the same whatever the temperature applied to the Petri dish. Compare Figure 39a recorded at 28 °C where the measured spore length is 1.19 ± 0.04 μm, with Figure 39c at 68 °C where it is 1.18 ± 0.04 μm (recall that the length of an unexposed *B. atrophaeus* spore is 1.3 μm). Nonetheless, the inactivation rate at 68 °C is twice that at 28 °C. This further supports our explanation as to the role of heat in facilitating lesions to the DNA in synergy with UV photoexcitation.
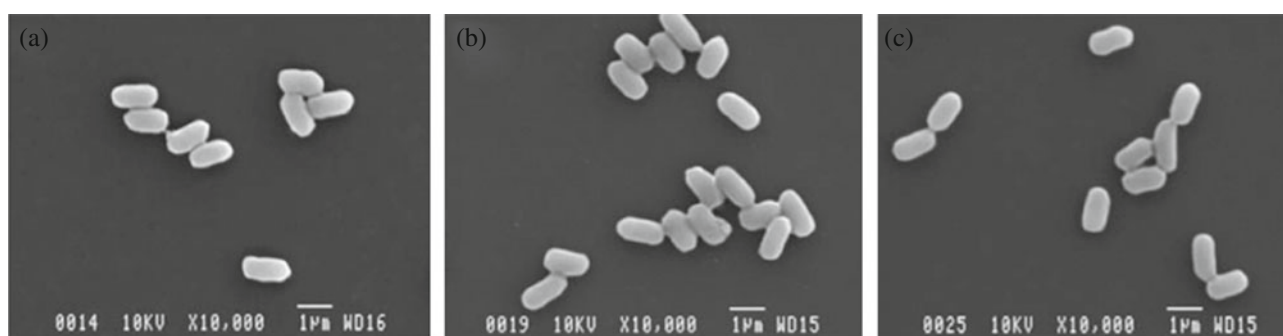
Fig. 39. SEM micrographs of *B. atrophaeus* spores (from a dried deposit) subjected for 30 min to the afterglow from a N_2-O_2 discharge with 10% O_2 added to N_2, at three different substrate temperatures: (a) 28 °C, (b) 45 °C and (c) 68 °C [31]. The position of the Petri dish in the 50 L chamber is that of the substrate holder (Fig. 8): its center is located at $x \approx 100$ mm and its base lies at 20 mm from the bottom of the chamber, i.e. at $z = 130$ mm. $P/V = 10$ W/L at 915 MHz. The connecting tube distance $x_d \approx 150$ mm.

5.4 Appraising some conventional porous packaging materials when used with the flowing afterglow of the N_2-O_2 discharge and electing a qualified one (actually non-porous)

In conventional sterilization methods (steam, ozone, chemicals), once the medical devices have been properly cleaned, they are wrapped/enclosed in adequate packaging materials, which are then closed/sealed before initiating the sterilization process: these packaging materials thus need to be porous to let the biocidal agent penetrate. In [6], three porous packagings used with conventional sterilization systems were subjected to the N_2-O_2 flowing afterglow. These were: Tyvek®, Kimguard® and SteriPouch®.[30] It was found that:

(i) Damage inherent to the afterglow exposure made all of them lose their antimicrobial barrier (water could flow through them);

(ii) The inactivation rate of spores deposited in Petri dishes that were packaged with these materials was much reduced compared with unpackaged Petri dishes;

(iii) A non-porous packaging, BagLight® Polysilk®, showed superior results:[30] no loss of the antimicrobial barrier after exposure to the N_2-O_2 flowing afterglow and a spore inactivation rate close to that obtained with an unpackaged Petri dish.

Our experiments on packaging were thus oriented, as a first step, toward a comparison of the above three conventional packaging materials with the non-porous one. Rectangular pouches were therefore made from the three conventional packaging materials to the same dimensions as that of the commercially available non-porous pouch. Since the sterilization process with the N_2-O_2 discharge afterglow is conducted under reduced-pressure conditions, a non-porous pouch can only be sealed after returning to atmospheric pressure. For that reason, the conventional material pouches as well had one extremity unsealed, the two flaps of this open end simply resting, through gravity,

on each other, providing in fact a very small aperture to the surrounding flow.[31] *B. atrophaeus* endospores served as bio-indicator (Sect. 5.1.5).

5.4.1 Exposure of packaged bacterial endospores to the flowing afterglow of the N_2-O_2 discharge

Figure 40 shows the survival curves obtained after exposure to the flowing afterglow of the N_2-O_2 discharge at 2.45 GHz, in the small-volume chamber (Fig. 9), of Petri dishes inserted into pouches of different materials (with one end open as already mentioned) compared with an unpackaged Petri dish. SteriPouch is the less efficient packaging in terms of inactivation rate with a reduction in the spore number of only one log after 60 min while it goes down by 4 logs within Kimguard and Tyvek packagings. Three of these survival curves are bi-phasic, namely they show a fast first phase and a much slower second inactivation phase [8]. Unpackaged Petri dishes and those enclosed in BagLight Polysilk pouches have the same first phase while the second phase seems even more efficient within BagLight Polysilk pouches, although the uncertainty bars of these two survival curves overlap at 60 min (each data point of these two survival curves nonetheless results from the average over nine independent experiments).[32]

Lowering of the UV intensity in the afterglow chamber due to the presence of the packaging pouch. The survival curves plotted for the different packaging materials in Figure 40 can be somehow misleading because they have not been obtained under the same incident UV intensity although the operating conditions were the same: this is because the UV intensity incident on the pouch is reduced by surface recombination of N and O atoms on the

---

[30] The description and characteristics of these packaging materials can be found in [6].

[31] Another way around, already mentioned, is to have the pouch open end thermally sealed beforehand instead and only a very small opening left (typically 5 mm in length, 1 mm in width). In this way, the pouch can be obturated at the end of the process with some appropriate sticker.

[32] In some cases, the value of the standard deviation below the average value is not shown because, on a log scale, it is so large that it would fall off the figure.
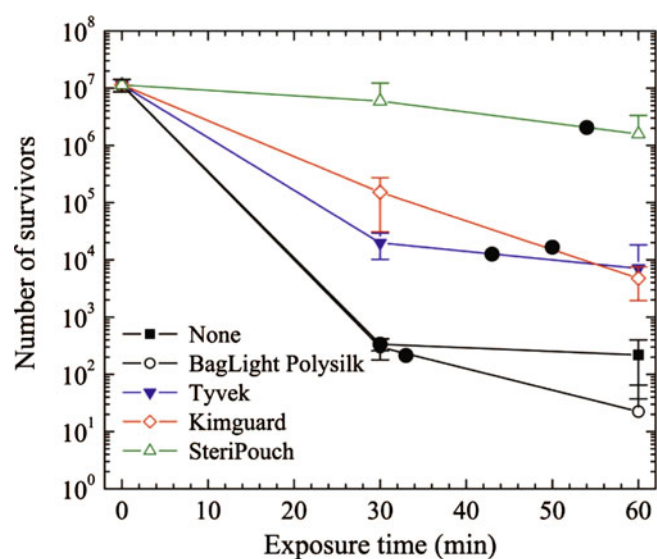
Fig. 40. Survival curves of dried deposits of *B. atrophaeus* endospores on a polystyrene (PS) Petri dish inserted in different packaging materials (with one end open) and exposed to the N_2-O_2 flowing afterglow compared to an unpackaged Petri dish. The discharge is sustained with 120 W at 2.45 GHz at a pressure of 670 Pa (5 torr) in the small-volume chamber (Fig. 9) and the flow rate of N_2 is adjusted at 800 sccm with 0.37% O_2 in the N_2-O_2 mixture (maximum UV intensity conditions in the empty chamber). The large black dot that appears on each curve corresponds to the same given dose of UV photons incident on the pouch examined, the reference dose being the number of photons collected after 30 min in the empty chamber: the way that this value is determined is described in the text accompanying Figure 41.

pouch itself. Figure 41 shows the UV intensity recorded, over the 200–400 nm spectral range[33], in the afterglow chamber above the various packaging materials relative to that in the empty chamber for the same given operating conditions. There is a decrease in UV intensity by approximately 10% with BagLight Polysilk while it reaches up to 55% with SteriPouch. In between, the photon loss is close to 30% with Tyvek and 40% with Kimguard. Adsorption of N and O atoms on these material surfaces followed by their heterogeneous recombination mainly into N_2 and O_2 molecules constitutes a loss source for these atoms, thereby reducing the formation of the NO^* excited molecules that provide the UV photons (Sect. 4.4).

The more the packaging material reduces the available UV intensity on the outside of the packaging material, the longer the time it should take to achieve a given inactivation value (e.g. 5 logs). A way of accounting for this effect is to consider the fluence or dose concept (Sect. 5.1.2). In the present case, it refers to a given total number of incident photons per unit surface on the packaging material. The fluence value (or dose) taken as reference corre-
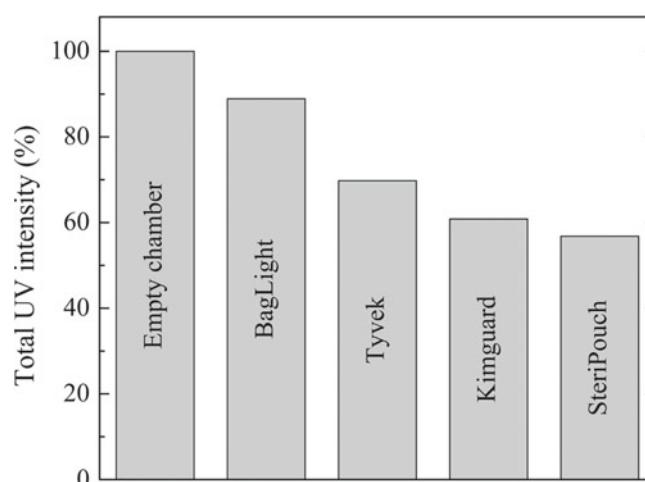
Fig. 41. Relative UV intensity (%) integrated over the 200 to 400 nm wavelength range and recorded in the afterglow chamber above the various packaging materials, as compared to the empty chamber intensity value (100%). Operating conditions are as in Figure 40.

sponds to the number of photons recorded without packaging (100%) during a 30 min exposure time (UV intensity integrated over the 200–400 nm wavelength range). The time duration required to achieve the same photon fluence incident on each packaging material can be inferred from the relative UV intensity plotted in Figure 41. Such a fluence value is marked in Figure 40 as a large black dot on the survival curve for each packaging material. The longer it takes to reach the given dose, the lower is the inactivation rate.

Optical transmission of the tested packaging materials in the UV range (200–400 nm). Optical transmission $T_I(\lambda)$ of these materials, between 200 and 400 nm, was obtained using a deuterium lamp as a continuum spectrum source together with a spectrophotometer. The value of $T_I(\lambda)$, expressed in percentage, is obtained from the ratio of the light intensity collected through the packaging material to that in absence of the packaging material. Figure 42 shows that, over the spectral range examined, the Tyvek and SteriPouch packagings are almost totally opaque to UV radiation ($\approx$1%) while Kimguard is barely more transparent ($<$4%), whereas the BagLight Polysilk material shows a 20% transparency at 200 nm, which goes up to 75% at 400 nm. It does not seem possible to draw conclusion from the survival curves in Figure 40 as to the influence of the pouch UV transparency on the inactivation rate. Consider, to this end, Tyvek and SteriPouch, which are both almost optically opaque, but show quite different inactivation rates (Fig. 40).

Erosion of the packaging materials. A low UV transparency suggests that the photons are, to some extent, absorbed in the material when crossing it and, therefore, possibly damage it. Figure 43 supports, at first sight, this assertion since the mass loss of the packaging materials considered is comparatively larger for the three conventional materials than for the BagLight material, which has the highest UV transparency. The value of the mass

---

[33] It is noteworthy that there are no changes in the nature of the emission spectrum of this afterglow, in contrast to what is observed when polymers exposed to an argon discharge, are in fact interacting with it [6].
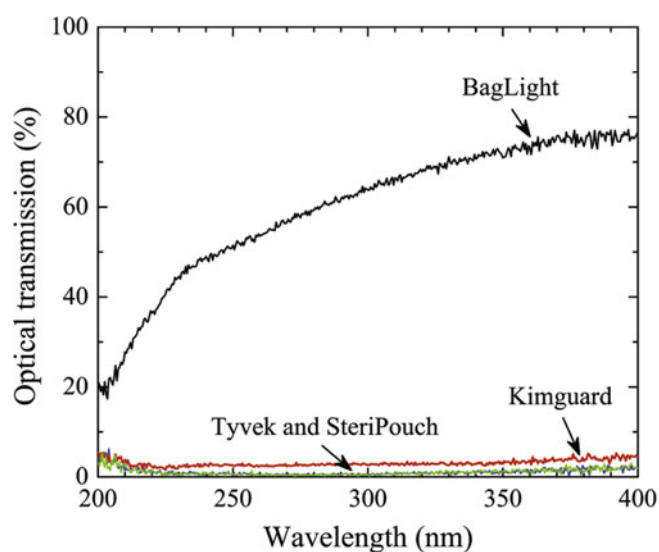
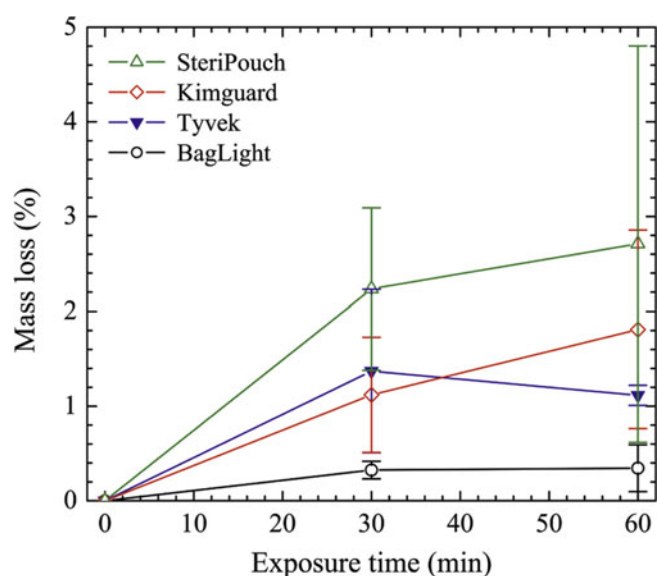**Fig. 42.** Percent relative optical transmission of the different packaging materials considered.

Fig. 43. Mass loss of the various packaging materials tested as a function of their exposure time to the N_2-O_2 discharge flowing afterglow. Operating conditions are as in Figure 40.

loss is, in fact, significant with all the porous packagings tested and it goes on decreasing in the following order: SteriPouch > Kimguard > Tyvek, while the mass loss is significantly much less with the non-porous BagLight Polysilk material.

However, there is no measurable mass loss of these same packagings when exposed to the Hg I 253.7 nm (UVC) radiation (at ambient temperature under a laminar-flow hood), which has an intensity approximately 10^5 times higher than that from the NO molecular systems in the afterglow. Therefore, we attribute such a mass loss to an erosion mechanism possibly due to the presence of $O_2(^1\Delta_g)$ metastable-state molecules together with O atoms, both

being highly reactive. These species seem to be essential for achieving some specific processes with our afterglow system, as will be demonstrated in Section 6. The difference in the degree of erosion between these packagings can be attributed to the nature but also to the configuration of these materials. It is furthermore noteworthy that as a result of their erosion in the flowing afterglow, all the porous packagings tested let water diffuse through them, thereby indicating failure of the antimicrobial barrier, which does not happen with the non-porous BagLight Polysilk packaging.

The material released from the eroded porous packagings can be expected to deposit on the spores in the Petri dish. To check for the presence of such a deposit and to determine to what extent the deposited material interacts with the spores, as a first step, we inserted a virgin Petri dish (without spores) in a pouch and subjected it to the N_2-O_2 afterglow for 60 min: the exposed Petri dish indeed showed macroscopically visible debris of the packaging material. Then, as a second step, onto this eroded material, we deposited bacterial spores: at recovery of these spores (once dried), there was no loss of viability, whatever the nature of the packaging material exposed (data not shown). The absence of sporicidal activity of the debris proves that they are not contributing to spore inactivation. In contrast, it can be surmised that the eroded material, as it deposits onto the spores, shields them from UV radiation, hindering this inactivation mechanism. This clearly demonstrates that the porous packagings tested should not be used when turning to the N_2-O_2 flowing afterglow system for sterilization/disinfection.

5.4.2 Sterilization/disinfection of a currently used metallic MD in a BagLight Polysilk packaging, as an example

Figure 44 shows that a metallic forceps, contaminated on its flat surface (see inset) with dried *B. atrophaeus* endospores, when exposed to the N_2-O_2 discharge flowing afterglow, whether packaged in a pouch or not, reaches the same high level of disinfection (4–5 logs) after one and two hours. Clearly, enclosing the forceps within a BagLight Polysilk pouch does not interfere with, nor delay, the inactivation of the bacterial spores deposited on the forceps. The nickel-plated steel surface of the forceps is responsible for heterogeneous surface recombination of N and O atoms, into N_2 and O_2 molecules, respectively, at a much higher level than on the polymer (polystyrene: PS) surface of the Petri dish.[34] This reduces significantly the formation of excited NO molecules in the chamber, hence a lower UV photon flux, which accounts for a longer process time (120 min instead of 30 min for a 5 log decrease).

---

[34] Consider Figure 20 and assume PS has a surface-recombination rate close to that of Teflon, while that for nickel-plated steel is close to stainless steel: then, we get a predicted reduction of UV intensity by a factor of $\approx 2/3$.
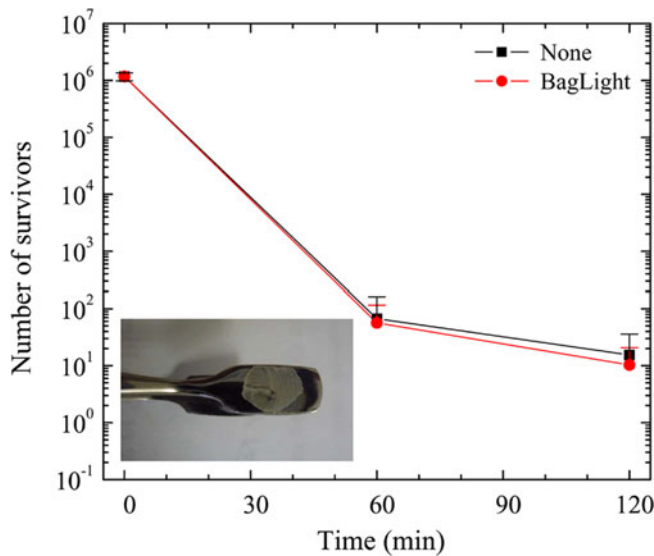
Fig. 44. Survival curves of *B. atrophaeus* spores deposited (and dried) on the flat nickel-plated steel surface of the forceps (inset) and subjected to the N_2-O_2 flowing afterglow. The forceps are exposed to the N_2-O_2 afterglow either packaged within BagLight Polysilk pouches with one extremity opened or unpackaged. Operating conditions are as in Figure 40.

5.4.3 The BagLight Polysilk pouch (with a small opening) ensures sructural integrity of spores enclosed within it when subjected to the N_2-O_2 flowing afterglow, but these are nonetheless inactivated

B. atrophaeus spores deposited in Petri dishes enclosed within this pouch with one end open (or with a tiny opening when the open end is thermally sealed) suffer little erosion (dimensional loss) and no structure weakening (breaking of the spore once rehydrated). Two different staining techniques were used to demonstrate such features.

Malachite green staining. Dried deposits of *B. atrophaeus* spores on microscope slides, unpackaged or packaged (one end open) into a BagLight pouch, resting on the bottom of the chamber around the pumping orifice, have been subjected to the flowing afterglow of a N_2-O_2 discharge sustained with 200 W in the 50 L chamber (Fig. 8) for 30 and 60 min, at both x_d distances of 200 and 820 mm for 915 MHz and at $x_d = 820$ mm for 2450 MHz. Once exposure was over, the microscope slides were flooded with malachite green staining solution, followed by a safranin counterstain [39]. Upon drying, two possibilities arise: the spores remain either colored in green, an indication that their membrane is intact, or they become red whenever the membrane has been damaged. In the present case (data not shown), the spores exposed within the pouch all remained green, while outside the pouch they all turned red (30 min) or they were no longer observable (60 min).

Dapi staining. The Dapi (4',6' diamino-2-phenylindole 2HCl solution) technique, based on fluorescence, is used
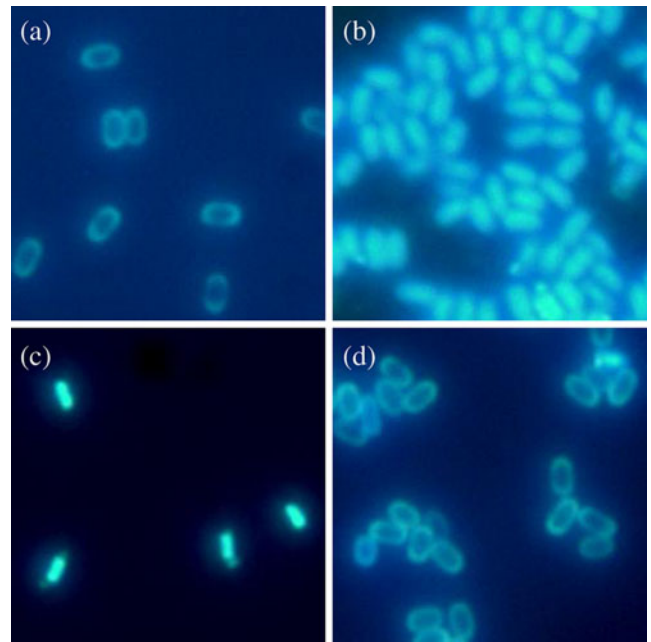

Fig. 45. Micrographs of Dapi stained *B. atrophaeus* endospores: (a) non-exposed (control); (b) autoclaved for 30 min; (c) exposed for 30 min unpackaged in the flowing afterglow of the N_2-O_2 discharge sustained with 200 W at 915 MHz at a distance $x_d = 200$ mm from the plasma source; d) same conditions as in c) but the spores are enclosed within the BagLight Polysilk (open ended) pouch.

Table 8. *B. atrophaeus* endospore length and width measured on Dapi stained micrographs.

	Dapi	x_d (mm)	Length (μm)	Width (μm)
a	non-Exposed		1.30 ± 0.02	0.78 ± 0.02
d	Exposed within	200	1.22 ± 0.04	0.70 ± 0.02
	BagLight	820	1.26 ± 0.08	0.76 ± 0.03

to evidence breaches in the spore inner membrane: when this is the case, Dapi penetrates the spore core. Then, the whole surface of the spore shows blue fluorescence. In contrast, when the membrane is intact, only the periphery of the spore is fluorescent in blue. These two situations are illustrated in Figure 45. The operating conditions are the same as for Malachite green staining. Only the photographs for $x_d = 200$ mm are displayed in Figure 45.

Comparison of the length and width of non-exposed (control) spores (a), with the length and width of spores sheltered within a BagLight Polysilk pouch (d) shows that at a distance $x_d = 820$ mm (Tab. 8) there is no significant erosion of the enclosed spores (the average length of non-exposed spores is assumed to be 1.3 μm). In contrast, non-packaged spores exposed to the afterglow suffer from an obvious loss of membrane integrity (as with autoclave).

In conclusion, the two staining methods utilized clearly show that the (open ended) BagLight pouch allows little spore erosion and, therefore, protect them against any structural damage when exposed to the N_2-O_2 flowing afterglow, without nonetheless hindering their UV inactivation. This protective feature is present even in situations where the plasma source is very close to the chamber entrance ($x_d = 200$ mm), such that species from the early afterglow may be present. It is noteworthy that it is only under such packaging that spore inactivation can be attributed solely to DNA lethal damage by UV irradiation, since otherwise breaking of the spore membrane or coat resulting from its erosion precedes, in the end, any DNA repair process.

5.4.4 More on the actual penetration through diffusion of the N and O atoms from the flowing afterglow into the pouch and the subsequent formation of NO* excited molecules therein followed by photon emission possibly within a spore stack

Comparing the number of survivors resulting from exposure to the N_2-O_2 flowing afterglow of spores in unpackaged Petri dishes with those in Petri dishes enclosed in BagLight Polysilk (with one end open) shows no significant differences (Fig. 40). This indicates, first of all, that the direction of the flowing afterglow as it enters the chamber plays no significant role: spores in unpackaged Petri dishes are mainly exposed to the direct outflow from the plasma source while the packaged ones are subjected to a "return" (diffusive) flow since the access to the open end side of the pouch is directed opposite to the incoming flow (Fig. 9). In fact, even (thermally) sealing the pouch almost completely, i.e. leaving a free open end of only 5 mm length over a total flap length of 110 mm, does not affect the observed survival curve (both first and second phase contributions). One could then argue that this is because spore inactivation exclusively results from the UV photons going across the pouch material: recall, however, that UV transmission across BagLight material is only 20% at 200 nm and 50% at 254 nm (Fig. 42), which would make a difference on *B. atrophaeus* survival curves from unpackaged and packaged Petri dishes (Fig. 40). The inactivation mechanism is, in fact, more complex since some particles from the afterglow diffuse into the pouch by its open end, as we now discuss.

To show that diffusion into the BagLight pouch is possible, we recall results from the inactivation of bacterial endospores using dry ozone (O_3 originates from the flowing afterglow of an O_2 corona discharge at atmospheric pressure) [4]. Putting the Petri dish onto which *Geobacillus stearothermophilus* spores had been deposited into the BagLight Polysilk pouch provided the same inactivation rate as in an unpackaged Petri dish. Recall that in an O_3 flowing afterglow, the biocidal species are the O_3 (reactive) molecules, not photons since no UV emission is observed.

As a matter of fact, N and O atoms from the flowing afterglow can largely enter the pouch by diffusion since their coefficient of surface recombination on BagLight material is less than 10% (Fig. 41). Thus, it seems necessary to admit that they interact, within the pouch, to form NO* excited molecules, emitting UV photons locally. Going a step further is to consider that some of these atoms "infiltrate" stacked spores (Fig. 25) before turning into NO* excited molecules, which then would contribute to UV inactivation of "well-hidden" (second phase) spores.

A further possibility of interest (although we are not sure to what extent it applies to our situation) is the dissociation of N_2 and O_2 molecules, into N and O atoms, by VUV-UV photons, as discussed in a paper by Singh et al. [40]. Their demonstration is based on a Petri dish being located in a small-volume enclosure vacuum-isolated from the N_2-O_2 afterglow chamber by a UV transparent window and filled with only N_2 and O_2 molecules at the same pressure as in the main chamber. Pumping out this enclosure reduces significantly the observed inactivation rate within (then provided solely by the UV photons crossing the window). This thus demonstrates that N and O atoms (generated in the way indicated by Singh et al.) can lead to additional UV photon emission in the pouch. However, the mechanism for obtaining N and O atoms suggested in [40] might not be applicable under our operating conditions since the dissociation of N_2 molecules by a single UV photon does not seem likely: it requires 9.76 eV, corresponding to a photon with a wavelength below 125 nm, while Figure 6 shows no emission below 150 nm. The fact of the matter is that Singh et al. [40] operate with a 20% O_2-80% N_2 mixture, which yields significant N emission intensity at 120.3 and 130.5 nm.

In conclusion, part of the UV inactivation observed within the BagLight pouch is likely to result from N and O atoms having entered the pouch through diffusion, some of these N and O atoms additionally infiltrating in-between spores in a stack before turning into NO* excited molecules emitting photons.

The coming section considers the action of the afterglow species on specific molecules and proteins, from which it will be possible to draw conclusion as to whether or not active species (assumed to be O-atoms and $O_2(^1\Delta_g)$ metastable-state molecules) participate, besides N and O atoms and UV photons, in a given process taking place in the flowing afterglow.

6 Inactivation/denaturation of pyrogenic molecules and proteins

6.1 Pyrogenic molecules

Pyrogens are bioactive molecules that, as their name tells, are fever-inducing substances, which can even lead to a septic shock whenever they enter the bloodstream or tissues where they are not normally found. The most pathogenic ones are found in the outer cell walls of bacteria and are released upon bacterial cell lysis.[18] In Gram-negative bacteria (e.g. *E. coli, Pseudomonas* species), we find lipopolysaccharides (LPS) and, in gram-positive

bacteria (e.g., *B. atrophaeus, S. aureus*), lipoteichoic acids (LTA).

Pyrogens are extremely resistant to elevated temperatures [41,42], requiring heating at 250 °C for at least 30 min. In fact, pyrogenic molecules such as LPS and LTA are not inactivated by conventional sterilization procedures (e.g., [43]). The use of non-equilibrium plasma discharges currently appears as a promising option, owing to their demonstrated efficiency in the inactivation of various microorganisms [44]. An essential literature source on the elimination of pyrogens by plasma is the series of papers by Rossi and collaborators at the Joint Research Center (Institute for health and consumer protection, European Commission, Ispra, Italy) [9,45]. Complementary results can be found in a study made under the European project BIODECON [44]. These experiments, however, do not involve the flowing afterglow of the N_2-O_2 discharge.

Commercially available purified LPS and LTA molecules, as well as bacterial endospores, were deposited into 96-well polystyrene-tissue culture plates (Costar® 3595, tissue culture treated, nonpyrogenic, polystyrene, sterile). In order to expose the samples to the flowing afterglow of a low-pressure N_2-O_2 discharge, they all need to be dried beforehand, which is achieved overnight at ambient temperature in the dark. The culture plates are placed at the center of the small-volume afterglow chamber (Fig. 9) and exposed for 2 h to the flowing afterglow at a pressure of 5 torr ($\approx$670 Pa). After their exposure, the plates are kept 24 h at ambient temperature in the dark and rehydrated (with 20 μL ultra-pure sterile pyrogen-free water) to comply with the volumes stated in the test protocol. Then the assay is conducted according to the reference lot comparison test method, using the PyroDetect System. We conducted five assays at different time periods, using four different PyroDetect Kits (EMD-millipore), two different kits of LPS standards as well as different bacterial endospore stocks and deposits. The results presented below are pooled from all experiments.

In preparing test samples, it is customary to express the quantity of LPS deposited as endotoxin units (EU) (1 EU is equal to 100 pg/mL) while, for LTA, it is by its net weight. The results are expressed as the residual pyrogenic activity, in reference to the ratio of optical density ($OD_{450 \text{ nm}}$) of the exposed sample over the non-exposed sample. Figure 46 shows such a residual pyrogenic activity for both LPS and LTA molecules following either their direct exposure to the flowing afterglow or packaged within BagLight Polysilk pouches. For both LPS and LTA, exposure is observed to be efficient only for unpackaged samples. Furthermore, the pyrogenic activity of LPS is reduced only in the case where the LPS sample content is low in contrast to LTA. Comparing the results between unpackaged and packaged samples clearly suggests that the afterglow reactive species (most probably $O_2(^1\Delta_g)$ metastable-state molecules together with O radicals) are required to achieve inhibition of the pyrogenic activity. UV photons by themselves are of not much help in that process. However, the combined action of the assumed reactive species with UV photoexcitation is not to be dismissed.
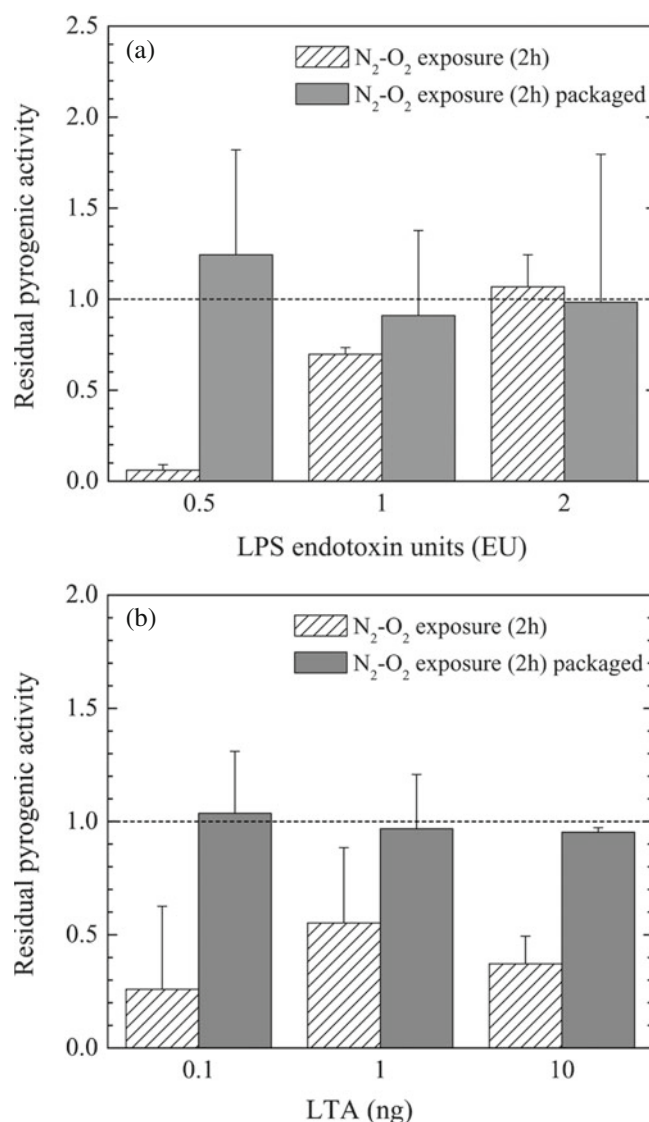

Fig. 46. Residual pyrogenic activity of a) LPS molecules (0.5, 1 and 2 EU loads) and b) LTA molecules (0.1, 1 and 10 ng loads) deposited on polystyrene-tissue culture plates after a 2 h exposure to the N_2-O_2 flowing afterglow in the small-volume chamber (Fig. 9), unpackaged and packaged in BagLight Polysilk. Pyrogenic activity is detected by Monocyte-Activation Test (PyroDetect System (Biotest), Section 4.5). The dotted line at unity refers to a non-exposed sample. The discharge is sustained at 2.45 GHz with 110 W absorbed power ($P/V = 20$ W/L) in a N_2-O_2 gas mixture containing 0.37% O_2 (maximum UV intensity conditions) with an 800 sccm of N_2 flow and at pressure of 5 torr ($\approx$670 Pa) in the afterglow chamber.

Our conclusion that the inactivation of LPS molecules requires both UV irradiation and $O_2(^1\Delta_g)$ metastable-state molecules together with O radicals, is supported by Chung et al. [46], who demonstrate that "VUV-induced photolysis and radical-induced chemical etching (oxygen and deuterium radicals) are able to damage the lipid molecular structure and reduce its endotoxic activity".

The presence of other species besides UV photons during unpackaged (direct) exposure to the flowing afterglow is further supported by the outcome of experiments with bacterial spores. Two sets of initially treated spores were considered: UVC-lamp irradiated spores, which are not damaged structurally (they remain green upon malachite staining (Sect. 5.4.3)), and autoclaved ones, which are heavily damaged. These two sets of spores were then subjected to the N_2-O_2 flowing afterglow: both these groups of spores showed a higher pyrogenic activity after having been exposed unpackaged than when packaged, more specifically 1.96 times higher for autoclaved spores and 1.66 times higher for UVC irradiated ones. This indicates that, when in direct contact with the afterglow reactive species, namely most probably $O_2(^1\Delta_g)$ molecules and O radicals, the spores are structurally damaged through erosion, leading to a larger release of pyrogenic molecules from the spore walls than from unexposed spores.

6.2 Proteins

In the preceding sections, various aspects of the inactivation of *B. atrophaeus* bacterial endospores, taken as representative of microorganisms in general, have been investigated following their exposure to the flowing afterglow system. Their inactivation process was shown to result essentially from lesions created to the DNA strands by UV irradiation. In the case of proteins, modification to their spatial conformation by the afterglow species is a possible mild or non-aggressive way (in contrast to breaking them) of making them lose their enzymatic properties, for instance. We therefore have examined to what extent the functions of the proteins can be disorganized, if not totally denatured, by their exposure to the N_2-O_2 flowing afterglow. Two types of proteins were considered: the naturally occurring lysozyme protein and the infectious prion protein having lethal outcome in mammalians. The lysozyme protein has an easily assessable enzymatic function, which allows determining almost quantitatively to what extent its enzymatic feature is affected as a function of operating conditions. The degree of inactivation of the (infectious) prion protein exposed to the afterglow is characterized ultimately by their death toll on mice.

6.2.1 Lysozyme proteins

Lysozyme belongs to a family of enzymes with antimicrobial activity, characterized by their ability to lyse such bacteria by hydrolyzing the peptidoglycan present in their cell walls. If the protein is no longer capable of inducing cell lysis of the bacteria, which implies that its enzymatic property is lost, it means that the conformation of the protein has been somewhat "destabilized" or that its active sites have been inactivated. *Micrococcus lysodeikticus* (more usually named: *M. luteus*) cells are the accepted standard for testing the lysozyme enzymatic activity. The principle of the test is that intact bacterial cells form a turbid suspension, the density of which will be reduced
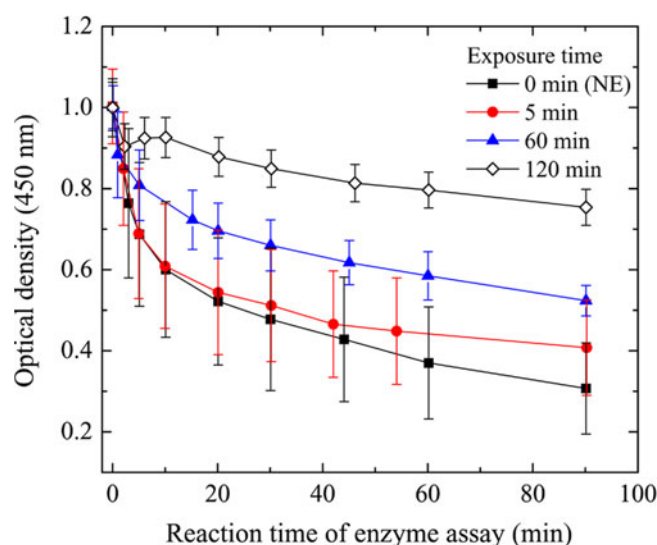

Fig. 47. Kinetic study of the enzymatic activity of the lysozyme protein (20 μg dried deposit) on *M. luteus* at three different exposure times to the N_2-O_2 flowing afterglow. Optical density is normalized to unity at time zero, which is when the bacteria are laid in the well that contains the lysozyme deposit. Operating conditions are as in Figure 46.

by the lytic activity of the enzyme. The optical density of the suspension is measured with a spectrophotometer, in the present case at 450 nm. At $t = 0$, i.e. the time at which the bacteria are laid in the well that contains the lysozyme deposit, the bacterial cells are intact and the corresponding optical density is normalized to unity.

Figure 47 shows the evolution of the optical density as a function of the enzyme reaction time as cell lysis proceeds. A non-exposed (NE) lysozyme protein, i.e. with its full enzymatic capacity, leads, after a long enough time (here 90 min), to a relatively low optical density (0.3). In contrast, when the protein has lost its enzymatic property, it can no longer induce cell lysis and the optical density of the suspension therefore remains much higher for a lysozyme (dried) deposit exposed for 2 h to the flowing afterglow, the optical density is still 0.75 after the same 90 min reaction time. The enzymatic activity decreases as a function of time in the way illustrated in Figure 47, without leading, under the present conditions, to total inactivation after a 2 h exposure time.

Figure 48 considers the cases where the well that contains the lysozyme (dried) deposit is either covered by a fused silica window (high-pass filter with $\lambda > 180$ nm) or not. It shows that the enzyme inactivation is greater when the well is fully exposed to the flowing afterglow. With the filter on, for which case it is assumed that the inactivating species is primarily the UV photon, the inactivation is much less. We thus conclude that both the particles from the afterglow ($O_2(^1\Delta_g)$ molecules and O radicals) and the UV photons are needed for an efficient reduction of the lysozyme enzymatic activity, i.e. to denature this protein.
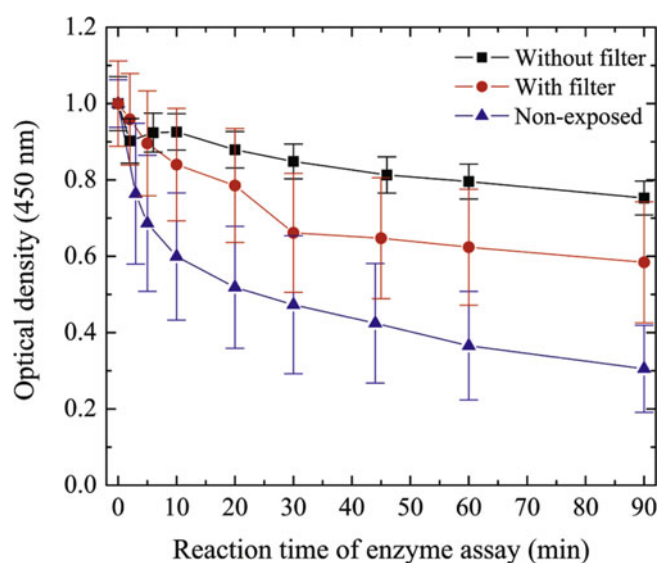
Fig. 48. Kinetic study of the enzymatic activity on *M. luteus* of the lysozyme protein (20 μg dried deposit), which has been exposed for 2 h to the N_2-O_2 flowing afterglow in a bare well or with a fused silica filter atop it. Operating conditions are as in Figure 46.

Fig. 49. Remaining reactivity level of PrP^C (non-infectious) recombinant bovine proteins (stemming from an ELISA test and read through optical density) after a 40 min exposure to the N_2-O_2 discharge flowing afterglow, compared to non-exposed ones (control) as a function of their initial concentration. Detection limit is 10 ng/mL and concentration saturation 500 ng/mL. The discharge is sustained (in a 25.5 mm i.d. single tube) at 433 MHz with an absorbed power of 300 W, which translates into 6 W/L in the 50 L afterglow chamber (Fig. 8). Connecting tube length $x_d = 200$ mm. Other operating conditions: gas flow rates at 1 sLm for N_2 and 8 sccm for O_2 (0.4% O_2 in the N_2-O_2 mixture) and chamber gas pressure set at 8 torr ($\approx$1070 Pa).

6.2.2 Prion proteins

Transmissible spongiform encephalopathies (TSEs), the Creutzfeldt-Jakob and Mad-Cow diseases being the most well known of these, are neurodegenerative disorders inevitably lethal. The infectious agent responsible for TSEs is the PrP^{Sc} prion, an abnormally folded and aggregated protein that propagates itself by imposing its conformation onto the cellular (non-infectious) prion protein (PrP^C) of the host. Normal PrP^C serves as substrate for prion replication and for prion-induced neurodegeneration [47]. Since the infectious forms of prions are transmissible and highly resistant to chemical and physical (heat) decontamination methods routinely used in healthcare, they represent a challenge for science, medicine and public health/ food systems. For example, extensive heating of prions (e.g., by autoclaving) should be avoided since it induces aggregation of the proteins, the bulk of which protects the infectious material inside it against proper inactivation [44]. To the extent that plasma species affect the conformation of the infectious prion protein, it should lead to its denaturation. In the experiments by Elmoualij et al. [32], which we are going to summarize, the infectious prion was subjected to the flowing afterglow of a N_2-O_2 discharge, which included both UV radiation and afterglow particles such as O atoms and $O_2(^1\Delta_g)$ molecules, UV irradiation alone (packaged substrates) having not been investigated in this case. The efficiency of the afterglow treatment on these proteins was examined using an in vitro assay as well as an in vivo bioassay. The reduction of the PrP^{Sc} immunoreactivity in the in vitro assays and of the PrP^{Sc} infectivity in the in vivo assays described below is considered as a direct consequence of modifications of the biological properties of the prion pro-
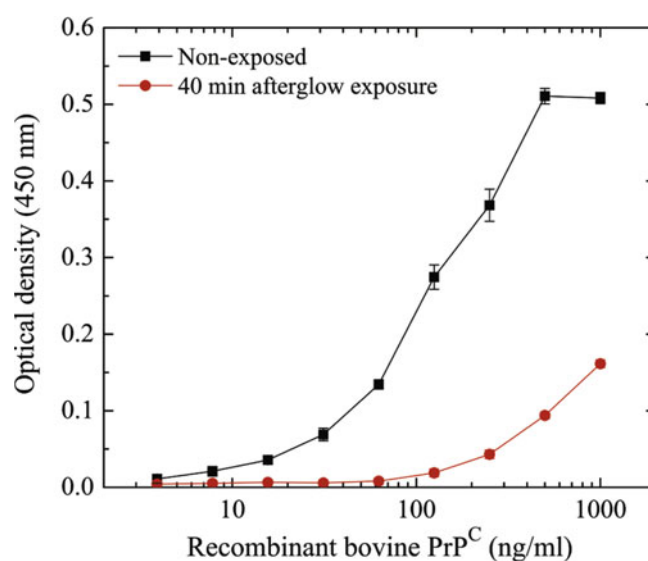
tein deposits by the plasma treatment. More specifically, the lower immunoreactivity observed is due to a loss of antigenic sites while a lower infectivity demonstrates a loss of pathogenicity of the prion proteins.

In vitro assay. As a first step (calibration experiment), results from ELISA[35] tests indicate that exposure for 40 min to the N_2-O_2 discharge flowing afterglow reduces significantly ($p < 0.001$) the immunoreactivity of PrP^C recombinant bovine protein (non-infectious protein) at concentrations ranging from 3.9 ng mL^{-1} to 1000 ng mL^{-1} (Fig. 49). The loss of immunoreactivity decreases from 93% to 61% as the concentration of PrP^C proteins deposited in polystyrene wells is increased up to 1000 ng mL^{-1}. The lower limit of detection is 10 ng mL^{-1} and the upper limit saturates at 500 ng mL^{-1}. These values are obtained by comparing ELISA test results from non-exposed proteins with exposed ones.

Then, considering a 1:1 mixture of non-infectious recombinant proteins and pathogenic prion proteins,

---

[35] Elisa stands for Enzyme-Linked Immunosorbent Assay. It is used to detect the presence of a substance, usually an antigen, in a liquid sample or wet sample. Performing an ELISA test involves at least one antibody with specificity for a particular antigen.
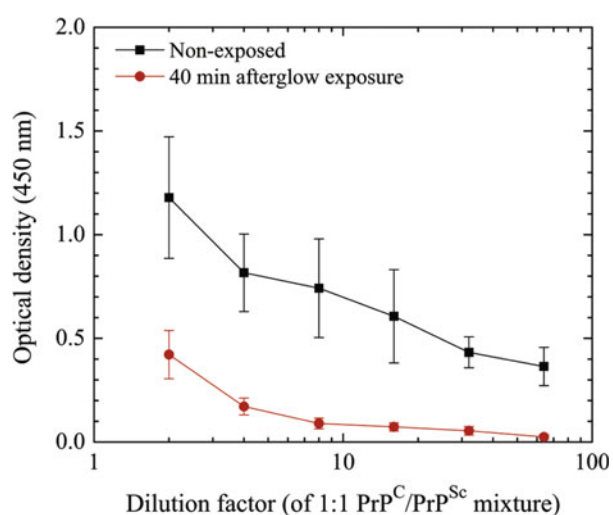
Fig. 50. Reactivity level (determined by ELISA) of the proteinic homogenate blend made from BSE-positive and BSE-negative bovine brains (1:1 mixture), coated on polystyrene surface wells at different dilutions, after a 40 min exposure to the N_2-O_2 discharge flowing afterglow as compared to non-exposed samples (control). The optical density is proportional to the remaining protein concentration (Fig. 49) and, thus, related to the immunoreactivity. Operating conditions are as in Figure 49.

Fig. 51. Kaplan-Meier survival curves of the four in vivo experimental groups (5 mice each), which were implanted with differently treated stainless steel inserts (∇: control inserts incubated with PBS only; $\triangle$: control inserts incubated with non-infectious brain homogenate; $\bigcirc$: inserts incubated with 139A infectious brain homogenate without afterglow treatment; $\square$: inserts incubated with 139A infectious brain homogenate afterwards afterglow-treated).

deposited on polystyrene substrates, ELISA shows that the N_2-O_2 discharge afterglow reduces the immunoreactivity of the non-exposed sample by approximately a factor of 3 under the present operating conditions (Fig. 50).

In vivo bioassay. Considering that in vivo bioassays are more conclusive than ELISA for infectivity monitoring and taking advantage of the fact that infectious PrP^{Sc} strongly binds to metals (as opposed to some polymers), therefore allowing (stable and reproducible) exposure of these contaminated substrates to the flowing afterglow, steel inserts were prepared under four different conditions and implanted into mice (four groups of five mice). Figure 51 presents the resulting Kaplan-Meier survival curves.[36] All mice of the group having received PBS[37] and non-infectious brain homogenates survived until the end of the experiment (555 days). In the group having received plasma-untreated 139A infectious brain homogenate, only one mouse out of five mice survived. As for the group having been implanted with afterglow-treated 139A infectious brain homogenate, four mice out of five were still alive after 555 days.

All the clinically affected mice (which included a 30% weight loss manifestation) were sacrificed (according to a

European ethical rule not to let them suffer), i.e. none of them died "naturally" but were all confirmed afterwards prion infected by immunohistolabeling. Although significant improvement of mice survival was achieved with the afterglow treatment, the loss of one animal in this group points out that residual infectivity was still present: therefore, it is possible to say that exposure to the discharge flowing afterglow contributed to reduce the level of prion protein infectivity on the contaminated stainless steel inserts implanted in the mice, but not to eliminate it. None of the mice still living when the experiment was terminated (555 days) presented clinical or histological signs of the disease in contrast to the sacrificed mice.

Clearly, higher inactivation efficiency is needed to achieve full decontamination of metal-bound PrP^{Sc} such as the stainless steel wires mimicking medical instruments. Several modifications to the present experimental protocol could be envisaged in order to increase the concentration of the active species in the flowing afterglow. As far as UV photons are concerned, this means:

(i) Increasing the operating frequency from 433 MHz to 2450 MHz: the higher the microwave frequency sustaining the discharge, the higher the dissociation degree of N_2 [22] and, thus, the higher the UV intensity for the same given absorbed power (Fig. 12);

(ii) Increasing the absorbed power in the discharge while keeping the same chamber volume increases UV intensity (and concentrations of O atoms and $O_2(^1\Delta_g)$ molecules);

(iii) Increasing exposure time increases the photon total dose;

---

[36] The Kaplan-Meier estimate of the survival function for a population is plotted as a series of horizontal steps of declining magnitude with time.

[37] PBS (phosphate-buffered saline) is a buffer solution currently used in biochemistry. It is a water-based salt solution containing sodium chloride, sodium phosphate and, in some formulations, potassium chloride and potassium phosphate. The buffer's phosphate groups help to maintain a constant pH.
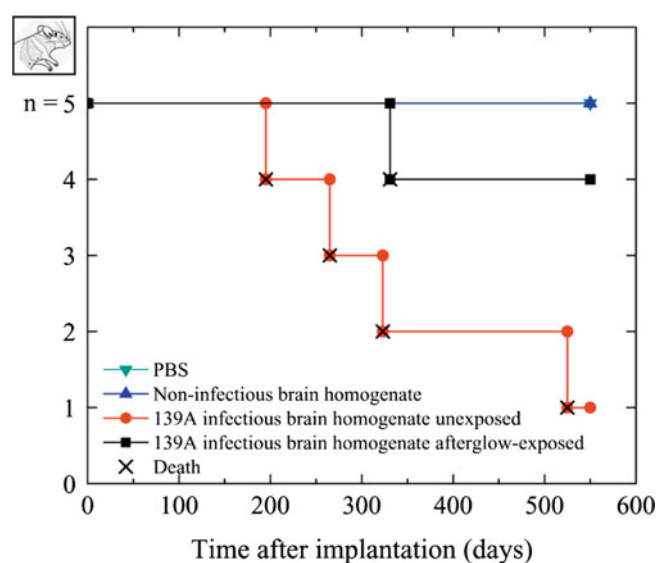
(iv) Operating at a pressure of 3.5 or 5 torr ($\approx$470 and 670 Pa) in the chamber instead of 8 torr (1070 Pa) would ensure a five to four times, respectively, higher total intensity of the NO$_\gamma$ molecular system (Fig. 7). At the time that the prion experiment was conducted, the beneficial influence of tuning the field frequency and gas pressure had not yet been determined consistently.

A final remark on the above infectious prion protein experiment is that dealing with five mice in each tested group is to be considered as a low number, asking for further studies with larger groups of animals to ensure statistical validity of the experiments. Nonetheless, the in vitro experiments presented should be regarded as a strong proof of the efficiency of the protein inactivation following its exposure to the N$_2$-O$_2$ discharge flowing afterglow.

7 Summary and perspectives

7.1 Our choice of the plasma biocidal agent and its implications

In general, sterilization/disinfection, for instance of MDs, requires considering first the process efficiency toward the inactivation of microorganisms of all kinds as well as pathogenic proteins and molecules, be these on surfaces or into crevices of MDs. Given this, one then needs to consider the level of damage inflicted to the device. In that respect, as a rule, the shorter the time required to reach a given level of inactivation, the more aggressive the process needs to be, i.e. the more damageable it is for MDs.

As far as "plasma sterilization" is specifically concerned, two different groups of biocidal agents are usually identified. In the case of the N$_2$-O$_2$ discharge flowing afterglow, these can be: (i) chemically reactive radicals (e.g., O atoms), metastable-state molecules (e.g. O$_2$($^1\Delta_g$) and N$_2$(A)) and ions (e.g., N$_2^+$, NO$^+$); (ii) UV and VUV photons. The chemically reactive species can either act separately or collaborate synergistically, inflicting more or less severe damage, through erosion (etching), to vital metabolic functions of the bacterial spores (our biological indicators). The UV and VUV photons primarily induce lesions on the genetic material (DNA, RNA), with comparatively reduced structural damage to the spores when photons are dominating the inactivation process as compared to reactive species. The UV photon alone approach is milder (less aggressive) in terms of damage, but it requires a longer processing time to reach a given level of inactivation. It implies working in the N$_2$-O$_2$ late afterglow to avoid ions and most metastable-state molecules.

According to calculations (Fig. 3), the late afterglow, besides UV photons, is comprised of N and O atoms and of metastable-state O$_2$($^1\Delta_g$) molecules. The O atoms and O$_2$($^1\Delta_g$) molecules (in combination or not with UV photons) are essential to achieve some inactivation processes. This is observed to be the case when samples comprising pyrogens or some proteins are packaged within a BagLight pouch: the level of inactivation recorded relative to a bare sample is reduced or totally absent. This is because the O$_2$($^1\Delta_g$) singlet molecules is not (much) present in the pouch since it is strongly quenched when attempting to enter the pouch through its (only slightly) open side, in contrast to N and O atoms. Pouch and no-pouch tests have in fact enabled us to determine that under our operating conditions:

(i) The bacterial spores are predominantly inactivated by the UV/VUV radiation alone;
(ii) Reducing the pyrogenic activity of LPS and LTA molecules requires the presence of reactive species that cannot freely enter the pouch, mainly the O$_2$($^1\Delta_g$) singlet molecules;
(iii) Both the particles from the afterglow (O$_2$($^1\Delta_g$) molecules and O radicals) and the UV photons are needed for an efficient inactivation of the lysozyme protein. Such a distinction was not made in the case of the inactivation process of the pathogenic prion protein because the contaminated stainless steel inserts to be implanted on mice were only processed unpackaged at that point in our investigations.

Practical consequences of our "mild" approach in terms of biocidal agents are that the sterilization/disinfection process using the flowing late afterglow is lengthy, from 30 min to 2 h, in contrast to a few min or less with direct exposure to a discharge, but structural damage to spores through erosion is observed to be lower. Damage to spores is still much less (little erosion, no membrane breach) when these are enclosed within the BagLight pouch, an indication that damage to MDs should be much lower than with direct exposure to the discharge; furthermore, the gas temperature of the afterglow is usually lower, below 35–40 °C after a 30 min exposure, which prevents damaging thermosensitive MDs.

7.2 Insight into the inactivation mechanisms based on experiments and modeling

Tuning the percentage of O$_2$ content in the N$_2$-O$_2$ mixture to maximize UV intensity was shown, from the very beginning of this research (1999), to correspond to the fastest inactivation rate of the microorganisms under such conditions (this is in fact the basis of the first patent filed by the Université de Montréal on plasma sterilization [48]). Furthermore, the notion of photon dose (total number of photons irradiating the samples) was shown to apply, which is an additional demonstration that the dominant inactivation species are really UV photons, even though O radicals and O$_2$($^1\Delta_g$) molecules are present in the late afterglow. The UV photons are provided by NO* excited molecules, formed through collisions between O and N atoms, sometimes involving N$_2$ as a third body. Using high-pass optical filters on top of Petri dishes, the NO$_\gamma$ molecular system (200–285 nm) was observed to be much more efficient than the NO$_\beta$ system (285–400 nm) for the inactivation of B. atrophaeus spores, in agreement with the literature. Since N and O atoms can enter the BagLight pouch even

though the orifice is very narrow (low rate coefficient for surface recombination of N and O atoms on such a pouch), their interaction within the pouch to form NO* excited molecules can generate UV photons that add to the photons crossing the pouch from outside. Some of the N and O atoms present in the pouch are further assumed to infiltrate around spores within a stack, where they can turn into NO* molecules that then emit a photon contributing to the inactivation of these hidden spores, which are related to the second phase of survival curves.

The increased inactivation efficiency of endospores resulting from an increase in the afterglow gas temperature was correlated to the energy required to surmount the potential barrier(s) encountered as the chemical reaction, initiated by photon excitation, proceeds toward the creation of a lesion on the DNA strand. The energy barrier corresponds to molecular (conformation) rearrangements occurring after photoexcitation, as the reaction develops to reach the final chemical state responsible for lethal damage to the DNA strand of the spore. Modeling of this temperature effect was achieved by assuming an Arrhenius-law dependence on spore temperature [31].

The modeling of the N_2-O_2 discharge flowing afterglow, proposed initially by Kutasi and collaborators [12,19,20] and extended for the purpose of the present paper, was used as a guideline to provide more insight into various phenomena. In particular, it allowed the discrimination between the early afterglow and the late afterglow in terms of reactive species (ions, metastable-state molecules, O radicals), which account for the polymer and spore erosion observed under certain conditions and locations in the afterglow chamber. Also, it helped determining how the gas inlet and outlet should be configured for best uniformity of the species in the chamber.

7.3 Advantages and limitations of the new plasma afterglow technique

Some limitations and drawbacks of our technique are common to all sterilization methods. One of the most potentially severe limitations is the undue thickness of a stack of microorganisms, since, for instance with conventional techniques, the biocidal vapor or the chemicals (as well as the UV photons of the afterglow technique) cannot reach the hindered microorganisms. All techniques can be severely weakened, or even become inoperative, when the microorganisms to be inactivated are, in addition, embedded in a large organic matrix (e.g., a blood stain, a biofilm). This is why, concerning autoclaving and chemical action, there already exists a stringent pre-sterilization cleaning process. "The most common procedure for decontamination, for example, of surgical tools consists in placing them in a mechanical washer/disinfector and subjecting them to a pre-wash at room temperature. The instruments are then cleaned by sonication with an enzymatic detergent, and finally washed and rinsed at high temperature" [44]. This procedure is followed by a careful visual check. Another concern is the overpacking of the sterilization/disinfection chambers, which is currently reported with autoclaves [49], leading to sterility failure of the processed batch.

7.3.1 Comparison of our plasma afterglow technique with conventional sterilization/disinfection methods

Plasma sterilization/disinfection of MDs, as already mentioned in the Introduction, is an alternative solution, yet to be accepted, to conventional methods, which on the one hand avoids treatments at high temperatures such as achieved with autoclaves (121 °C during 18 min or 134 °C during 5 min), which damage most polymer-based MDs, and on the other hand prevents the use of polluting and toxic chemical sterilants, which are currently utilized to ensure a process temperature below 65 °C.

In the specific case of the N_2-O_2 flowing afterglow as the plasma agent, N_2 and O_2 are non-toxic gases, therefore requiring no venting time, in contrast to most conventional chemical techniques. In that respect, coupons of the packaging material elected, BagLight Polysilk, exposed for 2 h to the N_2-O_2 discharge flowing afterglow were found not to be toxic to human cells (ANSI/AAMI/ISO 10993: 2003 protocol). Consequently, the flowing afterglow method developed is safe for both the operators and the patients. Finally, the processing time for reaching sterility with our technique should normally not require more than 2 h, which is less than with conventional low-temperature sterilization systems: ozone runs for at least 4 h while total processing time with ethylene oxide exceeds 10 h.

Besides being highly effective in inactivating microorganisms, our flowing afterglow approach can also reduce the degree of infectivity of pathogenic prion proteins and pyrogens, which cannot be done with autoclaves and most conventional chemical systems.

In contrast to conventional techniques, treatment by reduced-pressure plasmas (either by direct exposure to the discharge or to its flowing afterglow) requires vacuum pumping, in fact initially down to a base pressure of a few pascals (tens of mtorr) before admitting the discharge gases, in our case the N_2 and O_2 molecules. A direct consequence is that liquids cannot be sterilized/disinfected. Another point concerns the fact that objects to be sterilized/disinfected with conventional methods are pre-packaged (after the cleaning procedure) before being subjected to the biocidal agent, such that, once the treatment has been completed, their sterility is preserved while on shelves. The materials used with conventional sterilization methods are porous, such that the biocidal agent can penetrate the packaging, but still be effective in ensuring long-term (a few months) sterility. The most commonly used such materials were damaged when exposed to the flowing afterglow of the N_2-O_2 discharge. This was not the case with a non-porous polymer, BagLight Polysilk, which in fact does not interact with the flowing afterglow [50]. However, clearly, it cannot be sealed off before the full process is over, including returning to atmospheric pressure. The opening required in such a pouch for efficiently sterilizing the MD within it using the flowing

afterglow is extremely small, such that simple sealing techniques could be adapted on-line to close it. On-shelf storing time should then largely exceed a year according to the BagLight Polysilk pouch manufacturer.

7.3.2 Limitations and advantages of the flowing afterglow approach compared to direct exposure to a gas discharge

Choosing between these two approaches brings in the following dilemma: exposure to the discharge can successfully etch bio-burden of all kinds besides completely destroying all microorganisms, thus being fully efficient, but the discharge also interacts with various polymers (PS for instance), damaging them and at the same time interfering with the sterilization/disinfection process. The flowing afterglow provides a comparatively much "milder" process, in particular much less aggressive with polymers, but it is based on the assumption that the pre-sterilization cleaning procedure mentioned in Sections 1.2 and 7.3 is fully efficient. Such a minimal damage approach has been our main guideline when developing the present flowing afterglow technique. A clear indication that we have succeeded is the fact that when the Petri dish holding the spores is within our (slightly open) elected pouch (Sect. 5.4.3), these suffer little structural (erosion) damage and no membrane breach, although they are inactivated.

Because afterglow exposure of MDs requires a longer running time and approximately a 10 times higher gas consumption than direct exposure to the gas discharge, that part of the operating expenses related to the carrier gas (essentially N_2) is substantially higher with the afterglow process. On the other hand, for sterilizing chambers of a comparable volume, RF and microwave, power cost is lower when calling on the afterglow technique: we used from 10 to 20 W of microwave power (equivalent) per liter, while direct exposure (using RF power) requires from 60 W/L [9], sometimes even up to 140 W/L [51]. Both the direct and afterglow exposures necessitate gas pumping, but the direct exposure schemes reported [9,51] called for a lower operating pressure, specifically the 1 to 20 Pa pressure range (0.7 to 150 mtorr), requiring more expensive (and delicate) pumping systems than in the 450 to 700 Pa range (few torr domain) in the N_2-O_2 flowing afterglow.

In the course of our research, we have additionally utilized an argon microwave-sustained plasma to investigate the case of sterilization/disinfection through direct exposure to the discharge, at pressures in the 100–400 Pa range [3]. The following drawbacks were noted:

(i) MDs made from conducting materials, such as forceps for example, could screen the microwave field on one side of the object and thus prevent its full plasma immersion;

(ii) Charged particles recombine (with probability close to unity) on surfaces, thereby lowering locally the density of available plasma species. No such shading effect is observed with the flowing afterglow: this is because the recombination rate of N and O species on surfaces is comparatively very low (on aluminum surface the surface-recombination rate is less than 1%) and because of the high diffusiveness of the N and O atoms within the chamber (Figs. 21 and 22);

(iii) Metallic objects can get very hot following their Joule heating by the microwave field;

(iv) Some polymers interact with the discharge, reducing the plasma biocidal activity while, in contrast, no such shortcoming is observed with the N_2-O_2 flowing afterglow; nonetheless, with both approaches, the surface energy of most polymers was increased;[38]

(v) A very serious drawback is the detachment and release of microorganisms deposited on Petri dishes, probably under the action of ions in the argon discharge investigated: spores were found on the walls of the sterilization chamber (implying that some of these spores, still viable, went through the pumping exhaust to the "outside world"). This behavior was not experienced, following repeated checks, with the afterglow technique that we used.

Bearing all these considerations in mind, it becomes easier to determine what are the conventional applications that can be pursued and, at the same time, it enables us to propose new ones.

7.4 Possible applications of the flowing afterglow sterilizer/high-level disinfector

The N_2-O_2 flowing afterglow technique is far from being an all-purpose sterilization/disinfection system since, for example at the moment it cannot deal with endoscopes. In addition, recall that the system developed requires that the objects to be processed be dry/dried since any (contaminated) liquid left would be pumped out when initiating the process.

Besides more or less conventional uses in medicine, dentistry and pharmaceutics, such as, sterilizing implants (including casts, impressions and dentures in dentistry), tubings of all kinds and vials, the system could be employed in applications that are not allowed with autoclaving (high temperature damage) and chemical processing (toxic chemical impregnation of the objects). A possible such list includes sterilizing toys for immunosuppressed young patients, the asepsis of dehydrated food (for space and military needs, for new-born babies, spices (treated with EtO in the USA), ...), the sterilization/disinfection of synthetic food container and, economically interesting would be the conditioning of seeds for green house facilities (killing of insects, inactivating fungi, ...) and more "exotic" the decontamination (elimination of odors) of sport equipments (e.g., baseball mitts (gloves), hiking boots (shoes)) in rental shops.

---

[38] As a rule, exposure to plasma treatment modifies the surface properties of polymers [52]. Nonetheless, when for example a PS Petri dish is inserted in a BagLight Polysilk pouch, the contact angle of its surface is modified only after a 60 min exposure to the N_2-O_2 discharge afterglow [50].

7.5 Perspectives

Although many aspects of the operation of the afterglow sterilizer/disinfector are well controlled and understood, some basic research can still be envisaged related to the action of the UV photons and reactive species present in the late afterglow, which includes direct identification of the active metastable-state molecules (presumably $O_2(^1\Delta_g)$ molecules) and their concentration, identification of the kind(s) of lesions inflicted to the microorganism DNA, the extent of UV and erosion damage to various polymers, and more insight into the second phase of the inactivation rate. This latter facet concerns, in particular, the respective contribution of direct penetration of UV photon through stacked microorganisms compared to, this is our assumption, the diffusion of N and O atoms in-between microorganisms leading to the formation of NO excited molecules, which then emit a UV photon directed at a microorganism not accessible to photons originating from "outside the stack".

Economically viable solutions to the up-scaling of this afterglow sterilizer (maximum volume tested up to now is 60 L) to 200 or 500 L need to be found. Nonetheless, in our opinion, the actual system is ready for alpha-tests. As far as we know, our system is among the most advanced ones based on plasma inactivation and, probably, the best characterized, in terms of fundamental mechanisms, cold-plasma sterilizer/disinfector system reported in the literature.

References

1. W.A. Rutala, D.J. Weber, *Guideline for Disinfection and Sterilization in Healthcare Facilities* (Center for Disease Control (CDC), USA, 2008) `http://www.cdc.gov/hicpac/pdf/guidelines/Disinfection_Nov_2008.pdf`
2. E.H. Spaulding, in *Disinfection, Sterilization and Preservation* edited by C.A. Lawrence, S.S. Block (Lea & Frebiger, 1968)
3. J. Pollak, M. Moisan, D. Kéroack, M.K. Boudam, J. Phys. D Appl. Phys. **41**, 316 (2008)
4. A. Mahfoudh, M. Moisan, J. Séguin, J. Barbeau, Y. Kabouzi, D. Kéroack, Ozone: Sci. Eng. **32**, 180 (2010)
5. M. Moisan, J. Barbeau, S. Moreau, J. Pelletier, M. Tabrizian, L.H. Yahia, Int. J. Pharm. **226**, 1 (2001)
6. P. Levif, J. Séguin, M. Moisan, J. Barbeau, Plasma Process. Polym. **8**, 617 (2011)
7. M. Moisan, J. Pelletier, in *Physics of collisional plasmas* (Springer, 2012)
8. M.K. Boudam, M. Moisan, B. Saoudi, C. Popovici, N. Gherardi, F. Massines, J. Phys. D: Appl. Phys. **39**, 3494 (2006)
9. F. Rossi, O. Kylián, H. Rauscher, M. Hasiwa, D. Gilliland, New J. Phys. **11**, 115017 (2009)
10. J. Ehlbeck, U. Schnabel, M. Polak, J. Winter, T. Von Woedtke, R. Brandenburg, T. Von Dem Hagen, K.D. Weltmann, J. Phys. D: Appl. Phys. **44**, 013002 (2011)
11. V.V. Tsiolko, in *Plasma for Bio-Decontamination, Medicine and Food Security*, edited by Z. Machala, K. Hensel, Y. Akishev (Springer, Netherlands, 2012)
12. K. Kutasi, B. Saoudi, C.D. Pintassilgo, J. Loureiro, M. Moisan, Plasma Process. Polym. **5**, 840 (2008)
13. J.E. Cleaver, R.R. Laposa, C.L. Limoli, Cell Cycle **2**, 309 (2003)
14. S.B. Curtis, Radiat. Res. **106**, 252 (1986)
15. T.A. Slieman, W.L. Nicholson, Appl. Environ. Microbiol. **66**, 199 (2000)
16. K.G. Pennell, Z. Naunovic, E.T. Blatchley III, J. Environ. Eng. **134**, 513 (2008)
17. N. Munakata, M. Saito, K. Hieda, Photochem. Photobiol. **54**, 761 (1991)
18. J. Pollak, M. Moisan, D. Kéroack, J. Séguin, J. Barbeau, Plasma Process. Polym. **5**, 14 (2008)
19. C.D. Pintassilgo, J. Loureiro, V. Guerra, J. Phys. D: Appl. Phys. **38**, 417 (2005)
20. C.D. Pintassilgo, K. Kutasi, J. Loureiro, Plasma Source. Sci. Technol. **16**, S115 (2007)
21. R.W. Gross, N. Cohen, J. Chem. Phys. **48**, 2582 (1968)
22. P. Mérel, M. Tabbal, M. Chaker, M. Moisan, A. Ricard, Plasma Source. Sci. Technol. **7**, 550 (1998)
23. M. Moisan, Z. Zakrzewski, J. Phys. D: Appl. Phys. **24**, 1025 (1991)
24. D. Carignan, M.Sc. thesis, Université de Montréal, 2013
25. A. Ricard, M. Moisan, S. Moreau, J. Phys. D: Appl. Phys. **34**, 1203 (2001)
26. M.K. Boudam, B. Saoudi, M. Moisan, A. Ricard, J. Phys. D.: Appl. Phys. **40**, 1694 (2007)
27. S. Villeger, Thèse de doctorat, Université de Toulouse III, 2004

28. B. Gordiets, C.M. Ferreira, J. Nahorny, D. Pagnon, M. Touzeau, M. Vialle, J. Phys. D: Appl. Phys. **29**, 1021 (1996)

29. D. Carignan, M.K. Boudam, M. Moisan, in *Second International Conference on Plasma Medicine* ICPM-2 (San Antonio, Texas, 2009)

30. S. Moreau, M. Moisan, M. Tabrizian, J. Barbeau, J. Pelletier, A. Ricard, L. Yahia, J. Appl. Phys. **88**, 1166 (2000)

31. M.K. Boudam, M. Moisan, J. Phys. D: Appl. Phys. **43**, 295202 (2010)

32. B. Elmoualij, O. Thellin, S. Gofflot, E. Heinen, P. Levif, J. Séguin, M. Moisan, A. Leduc, J. Barbeau, W. Zorzi, Plasma Process. Polym. **9**, 612 (2012)

33. F. Rossi, O. Kylián, M. Hasiwa, Plasma Process. Polym. **3**, 431 (2006)

34. Y. Akishev, M. Grushin, V. Karalnik, N. Trushkin, V. Kholodenko, V. Chugunov, E. Kobzev, N. Zhirkova, I. Irkhina, G. Kireev, Pure Appl. Chem. **80**, 1953 (2008)

35. O. Cerf, J. Appl. Microbiol. **42**, 1 (1977)

36. T. Fleisch, Y. Kabouzi, M. Moisan, J. Pollak, E. Castaños-Martínez, H. Nowakowska, Z. Zakrzewski, Plasma Source. Sci. Technol. **16**, 173 (2007)

37. M.C. Crevier, M.Sc. Thesis, École polytechnique de Montréal, 2003

38. F. Cayla, stage de Maîtrise recherche, Université Joseph Fourier, Grenoble, France, 2003

39. G. Clark, W.J. Dougherty, F.H. Kasten, G.E. Cantwell, R.E. Coalson, J.L. Mohr, S.S. Spicer, R.L. Phillips, H. Schneider, J.W. Bartholomew in *Staining procedures* edited by G. Clark (Williams & Wilkins, 1981)

40. M.K. Singh, A. Ogino, M. Nagatsu, New J. Phys. **11**, 115027 (2009)

41. J.P. Liautard, J. Soc. Biol. **193**, 311 (1999)

42. D. Riesner, Br. Med. Bull. **66**, 21 (2003)

43. L. Moesby, E.W. Hansen, J.D. Christensen, C.H. Hoyer, G.L. Uhl, H.B. Olsen, Eur. J. Pharm. Sci. **26**, 318 (2005)

44. A. von Keudell, P. Awakowicz, J. Benedikt, V. Raballand, A. Yanguas-Gil, J. Opretzka, C. Flötgen, R. Reuter, L. Byelykh, H. Halfmann, K. Stapelmann, B. Denis, J. Wunderlich, P. Muranyi, F. Rossi, O. Kylián, N. Hasiwa, A. Ruiz, H. Rauscher, L. Sirghi, E. Comoy, C. Dehen, L. Challier, J.P. Deslys, Plasma Process. Polym. **7**, 327 (2010)

45. O. Kylián, M. Hasiwa, D. Gilliland, F. Rossi, Plasma Process. Polym. **5**, 26 (2008)

46. T.-Y. Chung, N. Ning, J.-W. Chu, D.B. Graves, E. Bartis, S. Joonil, G.S. Oehrlein, Plasma Process. Polym. **10**, 167 (2013)

47. A. Aguzzi, A.M. Callela, Physiol. Rev. **89**, 1105 (2009)

48. J. Pelletier, L.H. Yahia, J. Barbeau, Canada (priority 1999), US Patent No. 6 707 254, 2004

49. N.W. Savage, L.J. Walsh, Aust. Dent. J. **40**, 197 (1995)

50. P. Levif, J. Séguin, M. Moisan, A. Soum-Glaude, J. Barbeau, J. Phys. D: Appl. Phys. 44, 405201 (2011)

51. B. Denis, S. Steves, E. Semmler, N. Bibinov, W. Novak, P. Awakowicz, Plasma Process. Polym. **9**, 619 (2012)

52. F. Brétagnol, H. Rauscher, M. Hasiwa, O. Kylián, G. Ceccone, L. Hazell, A.J. Paul, O. Lefranc, F. Rossi, Acta. Biomat. **4**, 1745 (2008)

Jean Barbeau obtained his Ph.D. in microbiology/immunology in 1993 from the Université Laval, in Québec. He is currently full professor at the *Faculté de Médecine Dentaire* at the *Université de Montréal* where he teaches oral microbiology and immunology. His research focuses on asepsis and infection control, and comprises the study of resistance in microbial biofilms, contamination of dental instruments and sterilization. He is the director of the *Laboratoire de contrôle des infections* and is consultant for the *Ordre des Dentistes du Québec* and the *Association Dentaire Canadienne* on infection control regulation.

Mustafa Karim B. Boudam graduated from the Université Joseph Fourier (Grenoble, France) in physics (1999). He then obtained a M.Sc. (2002) and a Ph.D. (2007) from the Université de Montréal. The subject of his Ph.D. thesis concerned the influence of the UV photon-heat synergy on the inactivation of bacterial spores in the flowing afterglow of a reduced-pressure N_2-O_2 discharge and their inactivation mechanisms in an atmospheric cold plasma discharge. After a M.Sc. in medical physics (2009), he is currently working as medical physicist at the Centre Hospitalier de l'Université de Montréal (oncology).

Denis Carignan presently teaches physics at Collège de Maisonneuve in Montréal. He obtained a M.Sc. degree in physics (2013) from the Université de Montréal on the reassociation of N and O atoms on various materials in the flowing afterglow of the reduced-pressure N_2-O_2 discharge in relation with the use of such an afterglow for the sterilization of medical devices.

Benaissa El Moualij obtained a Bachelor Degree in General Biology from the University of Meknes in Morocco in 1992. Afterwards, he moved to Belgium and got successively a Master degree (1994) and a Ph.D. degree (1999) in Biochemistry from the Université de Liège. Subsequently, he joined the Human Histology team and became Scientific Director of CRPP. He is an expert in Biochemistry, Molecular Biology, Immunological techniques and in biosafety laboratory practices with high security BSL2++ and BSL3 facilities. He has been involved in many works aimed at studying the adhesion of proteins on different device surfaces as well as investigating prion proteins and other misfolded proteins involved in neurodegenerative diseases. He is a member of several scientific societies, such as the French Association of BioMaterials.

Danielle Kéroack graduated in physics from the Université de Montréal and obtained a Ph.D. in physics (condensed matter) in 1992. She worked as a Post-Doctoral Fellow at the INRS-Énergie et Matériaux (Varennes, Québec) in the research field of plasma-material interaction (Tokamak reactor). She is currently working in the Département de physique of the Université de Montréal as a professional researcher. She also holds the position of administrator of Plasma-Québec, a Québec Strategic Clusters program.

Kinga Kutasi obtained her Ph.D. in physics in 2003 from the Szeged University (Hungary). She was a Post-Doctoral Fellow at the Instituto Superior Técnico, Lisboa (Portugal) between 2005 and 2008, where she got involved in the modeling of afterglow systems based on surface-wave microwave discharges. In 2010, she has been awarded with the L'Oréal-UNESCO Women in Science national award. She is currently senior research fellow at the Institute of Solid State Physics and Optics, Wigner Research center of Hungarian Academy of Sciences, Budapest, studying different high-frequency discharge systems for biomedical applications and nanostructuring.

Pierre Levif graduated in physics from the Université de Bordeaux I and obtained a Doctorat d'État en Physique from the École Polytechnique (Palaiseau, France) in 2007. He then held a Post-Doctoral Fellow position at the Université de Montréal, Département de physique from 2007 to 2012, where he is currently doing research as a physicist and teaching. His main line research comprises plasma sterilization of medical devices in the Groupe de Physique des Plasmas with Professor Michel Moisan.

Michel Moisan graduated in physics from the Université de Montréal (UdeM) and obtained a Doctorat d'État en Sciences from the Université Paris-XI (Orsay) in 1971. He was then invited as a Post-Doctoral Fellow by the Academy of Sciences of the USSR. Assistant Professor with the Département de physique in 1976, he is currently Full Professor at UdeM. He coedited *Microwave Excited Plasmas* (Elsevier) and coauthored the textbook *Physique des plasmas collisionnels. Introduction aux décharges HF* (EDP, in English at Springer). His main line research comprises the design, development and modeling of electromagnetic (EM) field applicators to sustain plasma with RF and microwaves, including EM surface waves. He has also contributed to various plasma applications, more recently: abatement of greenhouse gases from microelectronic factories and plasma sterilization of medical devices.

Jacynthe Séguin, for the last decade, has worked as a research professional and member of Professor Michel Moisan's team, at the Université de Montréal, towards the development of a plasma sterilization system. Her contribution stemmed from important multidisciplinary research experiences acquired at various Canadian universities and hospitals, in several disciplines and environments. Her technical and teaching expertise, applied into training and supervision of undergraduate and graduate physic students in the field of microbiology, facilitated for all involved, the understanding and practical applications of many aspects of the projects.

Olivier Thellin graduated in zoology in 1994 and obtained a Ph.D. in Biomedical Sciences in 1999 from the Université de Liège (ULg - Belgium). He was then invited as a Post-Doctoral Fellow by the University of Cincinnati (Ohio, USA). Since 2002, he is a Post-Doctoral Fellow at the Université de Liège with the Service of Human Histology and the Center of Research on Prion Proteins (CRPP). His line of research as a Ph.D. student and Post-Doctoral Fellow in Cincinnati was on the impact of growth hormones, including prolactin, on immune cells. As a Post-Doctoral Fellow in Liège, he works on prion proteins, particularly as concerns its link with immune cells. His current line of research is the study of pathological biofilms in human.

Willy Zorzi, Ph.D. degree in Biochemistry in 1995, is associate Professor at the Université de Liège and executive Director of the Center of Research on Prion Proteins (CRPP), including its biosafety level 3 laboratory (BSL-3). Besides teaching, he coordinates a training center on Biosafety and Biosecurity dedicated to students, biomedical workers, researchers, biotechnologists... He achieved a 20-year career in biomedical research field especially on BSL-2 and BSL-3 pathogens, like bacterial pathogens or prion agents, addressing their detection, elimination and confinement. He is an expert member on the National Biosafety Advisory Council, member of EBSA (European Biosafety Association), expert in biological decontamination processes, in biological risk assessment and in biologistic of biohazardous goods.